Chapter 5

Meteor observations

This chapter details observations made with the Buckland Park VHF radar. It covers a selection of types of echoes which are detected, including various kinds of meteor echoes and echoes due to other causes, and a discussion on the mechanisms which produce these echo characteristics. The distinction between transverse meteors, those which reflect specularly, and down-the-beam meteors is described and an associated set of transverse meteors, aliased head echoes, is also discussed. A method for measuring the diffusion coefficient of meteor trails is discussed, and compared to the "range/angle" method for estimating the height of ablation of meteoroids. The height of detection of meteor trails is examined at different pulse repetition frequencies and compared with expected ablation heights. Measurements are made of the radial drift of meteor trails due to the background winds, and the effect and examples of fragmentation are discussed, including a Fresnel transform method for deducing the structure along a meteor trail. Following this is a discussion of the composition of meteoroids, including the possibility of "tarry" materials which cause meteoroids to ablate at greater heights than expected for stony materials.

5.1 Echo types

Before any research into the various aspects of meteor phenomena was undertaken, a large sample of meteor echoes was inspected visually in order to classify the various types of echoes observed by the radar. Examples of the different types of echoes are presented below and discussed in detail.

5.1.1 Echoes from meteors

The first example, shown in Figure 5.1, is a classical underdense meteor echo detected at 03:22:13 hours UT on the eighth of May 1999. The amplitude profile shows a fast rise and a slow exponential decay due to diffusion of the trail on which are impressed a classical Fresnel diffraction pattern. About 17 oscillations are visible in the post-t_0 amplitude record, and these also appear in the phase record (the t_0 point lies at approximately 0.65 seconds on this echo). In the unwrapped phase the oscillations

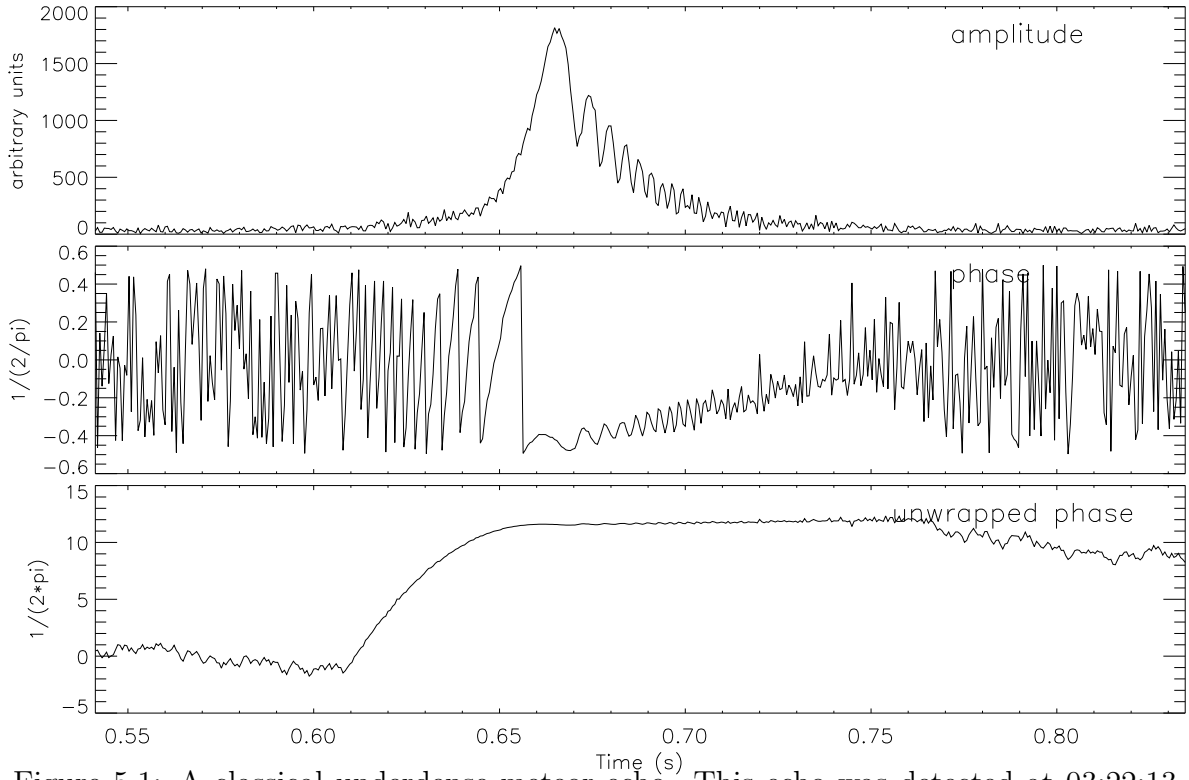

Figure 5.1: A classical underdense meteor echo. This echo was detected at 03:22:13 hours UT on the eighth of May 1999. Periodic noise reduction has been applied.

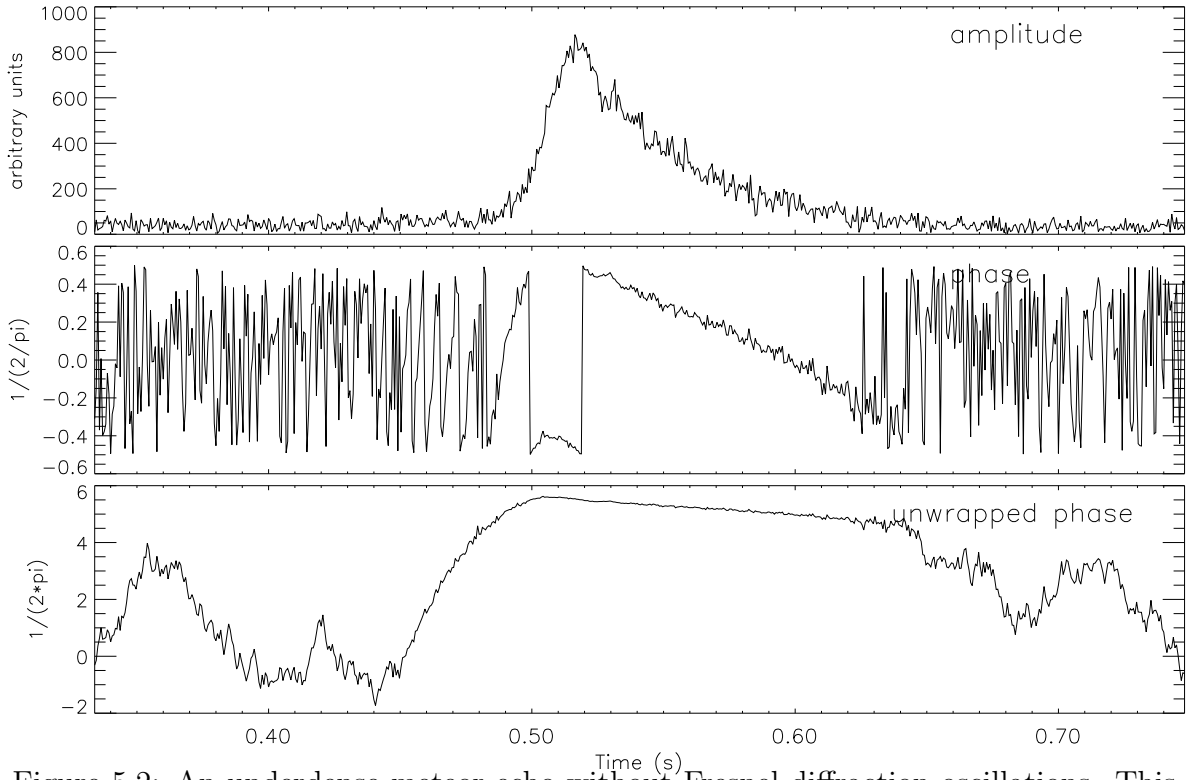

Figure 5.2: An underdense meteor echo without Fresnel diffraction oscillations. This echo was detected at 0:32:09 UT on the eighth of May 1999. Periodic noise reduction has been applied.

are less evident because the scale of the unwrapped phase panel is much greater than that of the phase panel, since many cycles of phase are represented. These post-t_0 amplitude oscillations can be used to determine the meteoroid speed (see Chapter 6). The phase information before the t_0 point is coherent long before the amplitude has risen significantly, and this data can also be used to determine the meteoroid speed. The decay in the amplitude can be measured to give the ambipolar diffusion coefficient (see Section 5.2). The post-t_0 phase also shows a steady increase between 0.65 seconds and 0.75 seconds which is interpreted as being due to the line of sight component of the drift of the ionised trail due to the local wind[1]. This "radial wind drift" can be used to measure the winds in the atmosphere (see Section 5.4).

[1]By convention, the phase is shown as a negative, increasing as the object approaches. The phase will be described as behaving in the way it is shown, thus an "increase" corresponds to motion towards the radar.

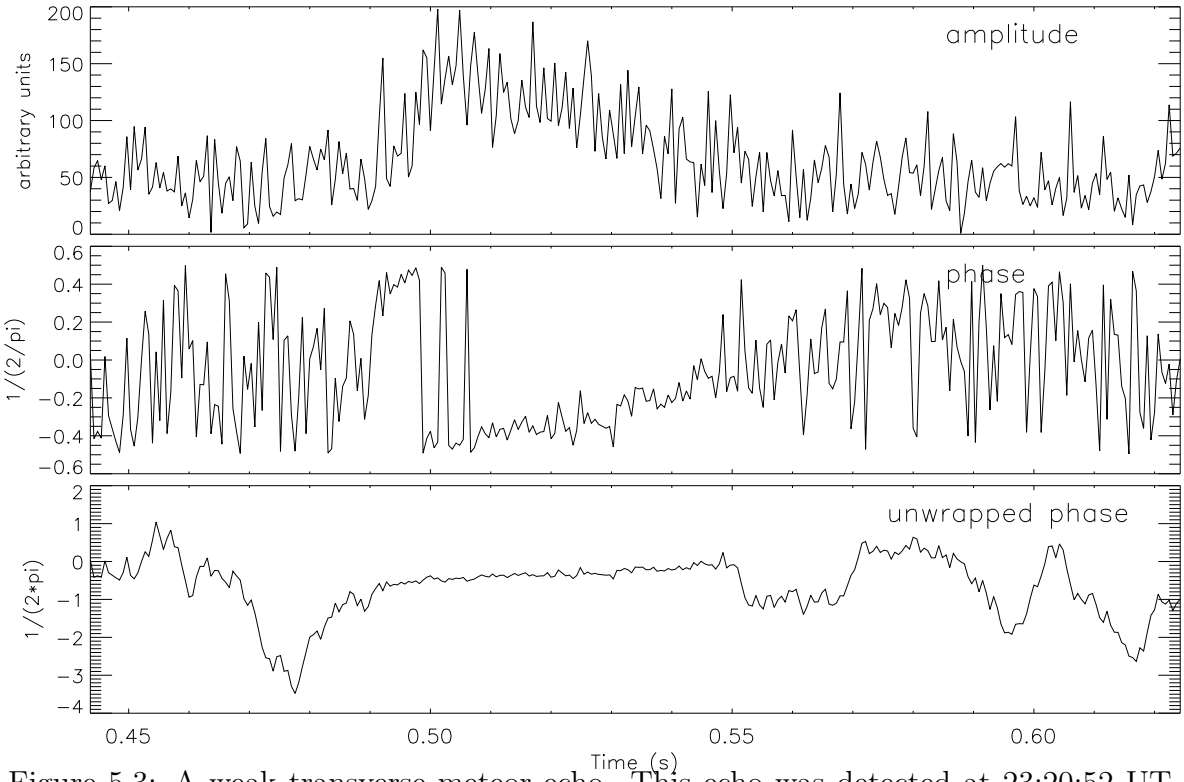

Figure 5.3: A weak transverse meteor echo. This echo was detected at 23:20:52 UT on the eighth of May 1999. Periodic noise reduction has been applied.

The method previously mentioned to measure the meteoroid speed with the post-t_0 Fresnel diffraction oscillations in the amplitude, while effective, can be difficult to apply in general, as few echoes show enough oscillations to be able to fit a curve to them. Figure 5.2 shows an example of an underdense meteor echo in which the oscillations are not evident. Note that the phase change due to the wind drift is now in the opposite direction to the previous example and that the decay due to ambipolar diffusion is not as rapid. The Fresnel oscillations have been smoothed out, and this is probably due to fragmentation. Elford & Campbell (2001) have shown by modelling the radio scattering from groups of trails produced by meteoroid fragments, that the oscillations are smeared out. Fewer oscillations are discernible as the number of fragments increases and also as the separation of the fragments in the direction parallel to the meteoroid motion increases. Further discussion on fragmentation is found in Section 5.5

The previous examples showed meteor echoes with high signal-to-noise ratios, but

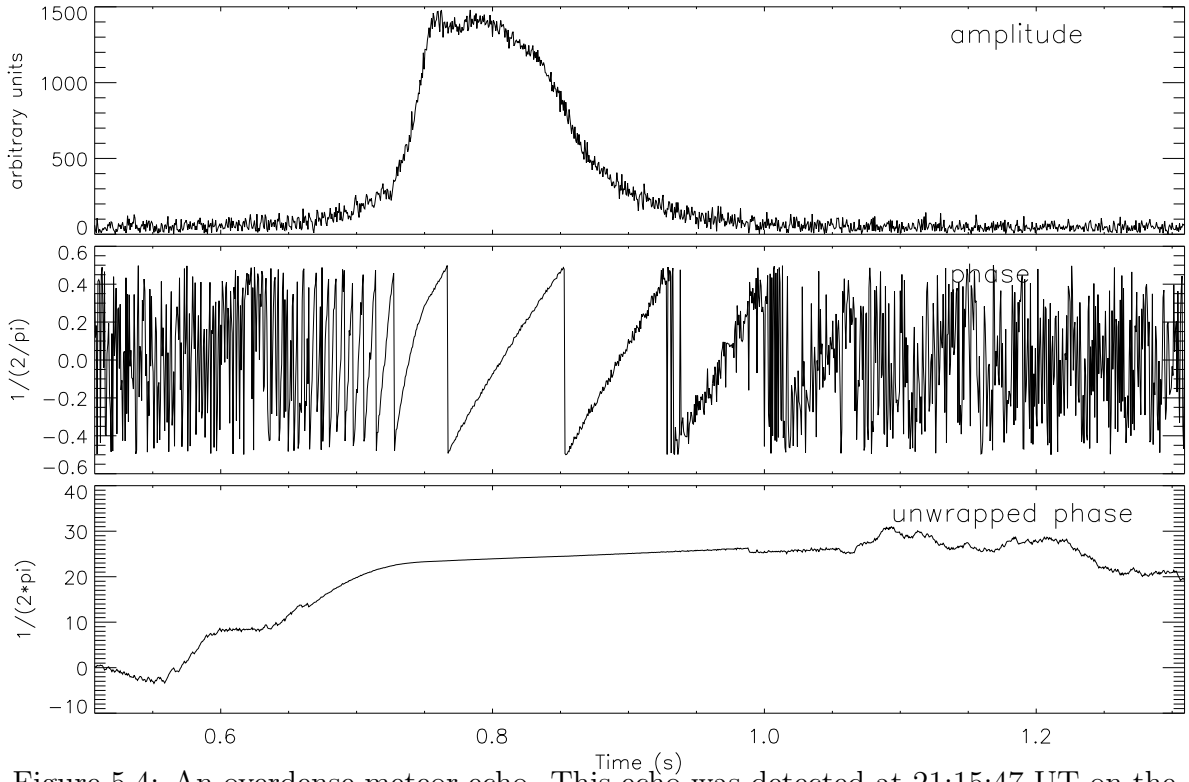

Figure 5.4: An overdense meteor echo. This echo was detected at 21:15:47 UT on the eighth of May 1999. Periodic noise reduction has been applied.

most echoes are produced by trails with lower electron line densities, and have much lower amplitude returns. Figure 5.3 shows a weak transverse echo, only a few times the noise level. Note that the maximum amplitude level is about 200 units, whereas the two previous examples have maximum amplitudes of about 1800 units and 900 units respectively. Even with this low amplitude signal the phase is still coherent, and the wind drift and pre-t_0 curve can still be seen clearly. Still smaller events are often detected by the radar, but in many cases the phase information is not coherent enough to enable wind or speed measurements.

Figure 5.4 shows an overdense transverse meteor echo. The phase characteristics are very similar to the underdense case, and the amplitude rise, from 0.65 to 0.75 seconds, is what we would expect for an underdense echo, and is very similar to that in Figure 5.1. The amplitude then remains fairly constant for about 0.05 seconds, as the amplitude of the returned signal from the overdense trail is almost independent of the electron number density. When the ionisation diffuses enough to make the trail

underdense, then the amplitude decays in the usual manner. Note that there are no apparent Fresnel oscillations in the amplitude or phase records, suggesting that this echo was caused by a meteoroid already fragmented into many pieces. The length of time that a meteor trail will remain overdense depends on the initial electron line density and the rate at which the ionisation diffuses, which in turn depends on the height of the trail, and if this is above 90 km, the orientation of the trail and the direction of the wave vector with respect to the direction of the geomagnetic field.

If we look closely at the phase record, we can see that immediately after the phase minimum, at around 0.75 seconds, the phase continues to curve, whereas we would expect the phase change here to be very small, or linearly increasing or decreasing due to wind drift. The effect is quite visible in the wrapped phase record. This curvature is only observed in overdense echoes, and can be explained in the following way:

Backscatter from overdense meteor trails behaves in the same way as scattering from a metallic cylinder. The trail will still expand due to ambipolar diffusion, but as long as the electron density is above the overdense level, then the radar will "see" a metallic cylinder. As the cylinder expands, the scattering point will move closer to the radar (further from the centre of the trail), causing a phase change. As the electron density reduces, the radio waves penetrate the trail, the "cylinder" collapses, and the scattering reference point returns to the centre of the trail. For the usually assumed uniform or Gaussian distribution of ionisation this collapse would be very rapid, which would produce a discontinuity in the phase. This is not observed, but instead the phase gradually reduces, and we must conclude that the cylinder collapses slowly. This means that the trail, while underdense in the outer regions, must still have an overdense core which reduces in size.

Another overdense meteor echo, this one displaying at least ten Fresnel oscillations is shown in Figure 5.5. As we would expect from Figure 3.4 the oscillations are present in the overdense part of the amplitude (which would act as if there were no diffusion) as shown by the line "A" in Figure 3.4, then as the underdense state is reached, the oscillations begin to behave like those shown by lines "B" and "C", being superimposed

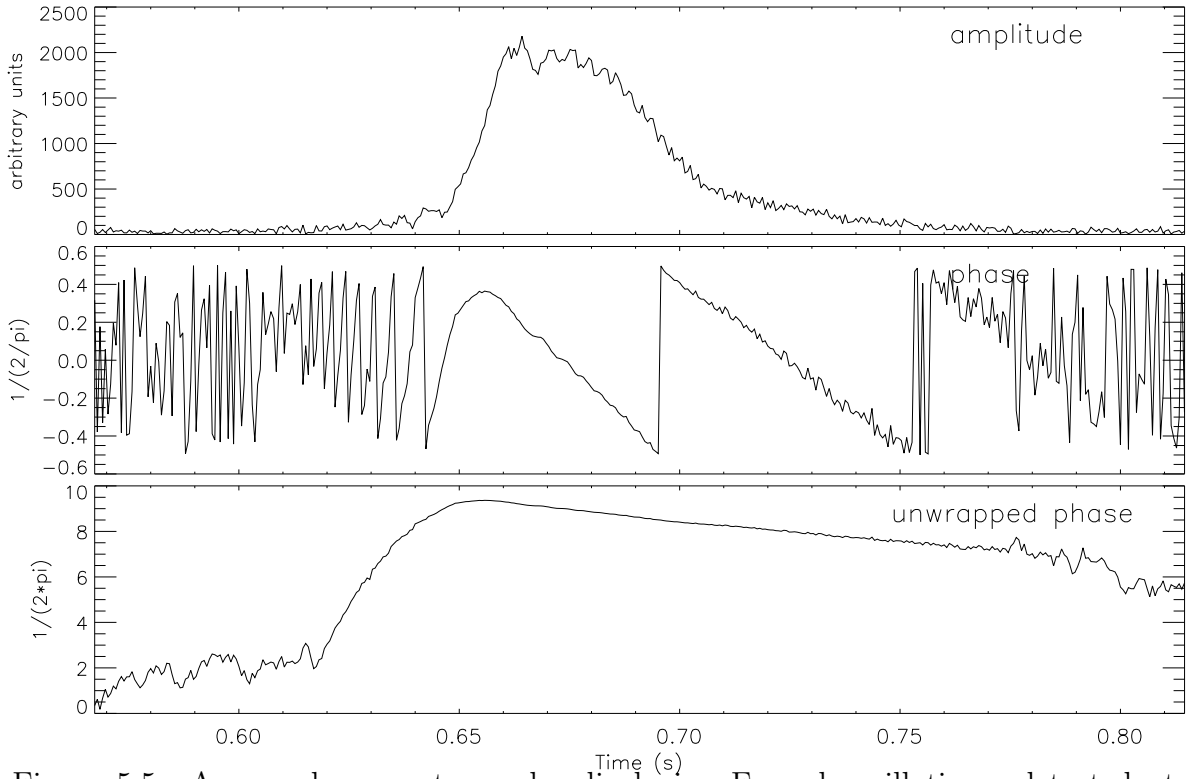

Figure 5.5: An overdense meteor echo displaying Fresnel oscillations, detected at 0:59:55 UT on the eighth of May 1999. Periodic noise reduction has been applied.

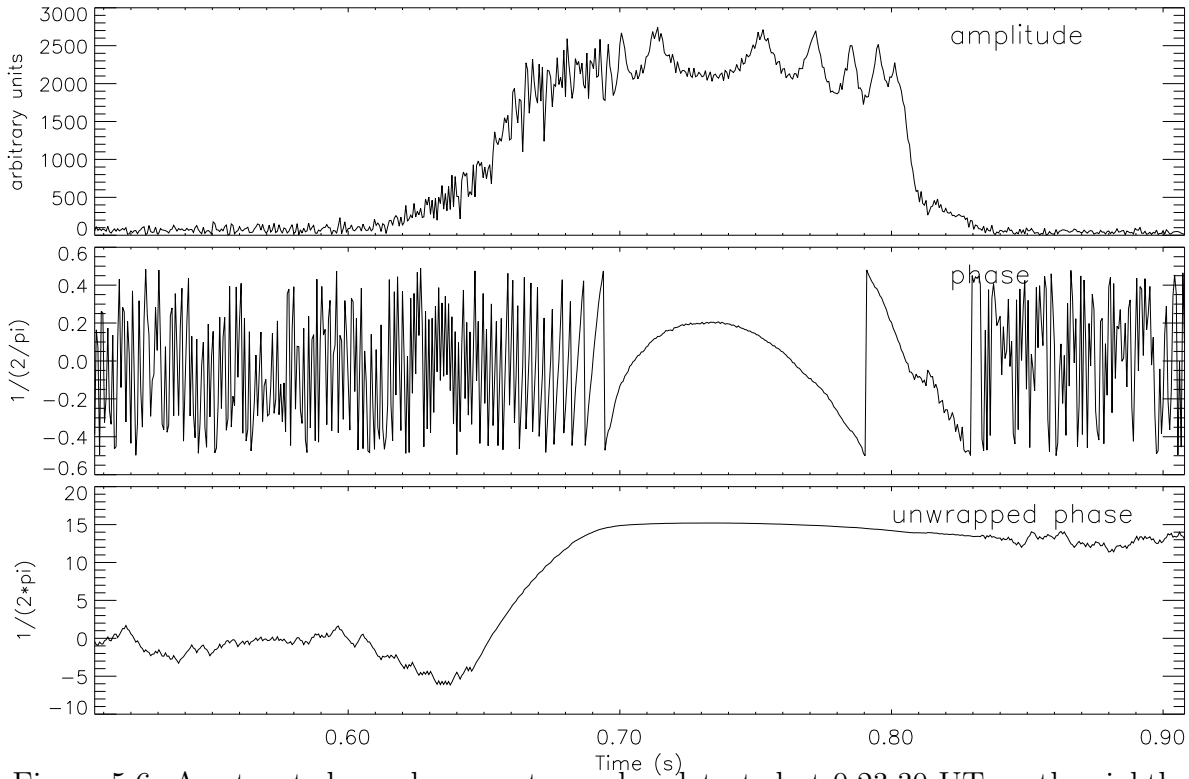

Figure 5.6: A saturated overdense meteor echo, detected at 0:23:30 UT on the eighth of May 1999. Periodic noise reduction has been applied.

over the exponentially decaying amplitude. The phase record also shows the Fresnel oscillations and behaves exactly like that of an underdense echo.

Of interest in this example are the presence of oscillations in the amplitude between 0.61 and 0.65 seconds. These oscillations are similar to those produced by McKinley (1951b) (McKinley 1961) and Nilsson (1962) by adding a phase reference signal (See Chapter 6). A Fresnel transform of this example reveals the presence of a smaller body some distance back from the main body producing the echo (See Chapter 6 for details on Fresnel transforms). The returns from this small body act as a phase reference source, producing the early oscillations, and probably making the post-t_0 amplitude oscillations visible.

Overdense echoes, because of the large amplitude of the returned signals, often produce a saturated signal. Figure 5.6 shows an echo which remains saturated for about one tenth of a second. The amplitude shows a normal rise, and flattens out as a normal overdense echo. As the trail diffuses it becomes larger in diameter, and since the electron number density is still above the overdense level, the amplitude of the return increases slowly.

As the inphase and quadrature components of the signal reach the maximum level of 2048 units, the amplitude signal begins to show the distinctive "scalloped" pattern from Figure 4.8. We are able to conclude that the true value of the amplitude is close to the maximum saturated value of about 2896 units, due to the lack of "flat spots" in the "scalloping". When the trail diffuses enough to become underdense, the amplitude decays and falls below the saturation level. Note how well behaved the phase data is while the amplitude is saturated, and the important[2] pre-t_0 phase data is unaffected, since the amplitude has not yet reached the saturation level. The extremely fast diffusion of the underdense section of this echo suggests that it occurred at a great height, and must have had an extremely large electron line density to remain overdense for over a tenth of a second. Based on the range, the echo occurred at a height of 104.7 km if it was detected in the main beam. This example shows strong

[2]Important for determining the speed of the meteoroid, see Chapter 6

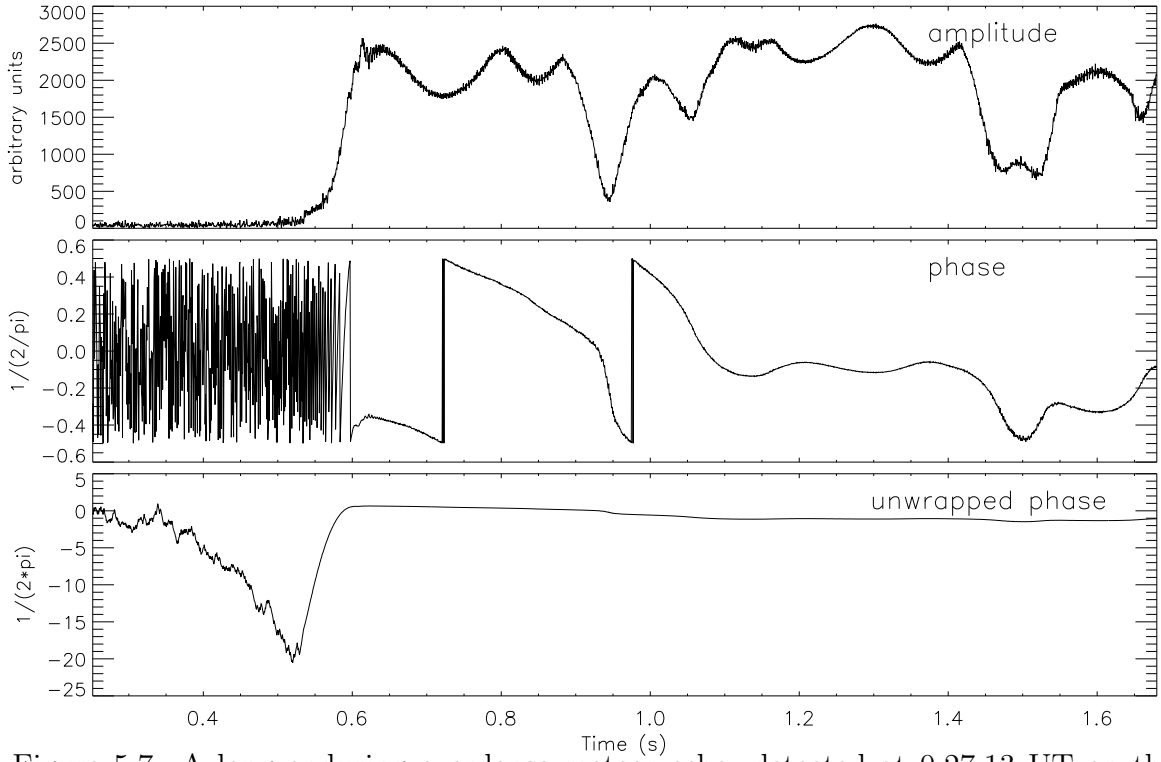

Figure 5.7: A long enduring overdense meteor echo, detected at 0:27:13 UT on the seventh of May 1999. This echo lasted for another 17 seconds. Periodic noise reduction has been applied.

curvature in the post-t_0 phase due to the expanding overdense trail and its subsequent collapse.

Many overdense trails are long lasting, and become distorted by the background wind. Figure 5.7 shows the first second of an echo which lasted for over 17 seconds. Large fluctuations can be seen in both the phase and amplitude records. These are due partly to receiver saturation, although this should have little effect on the phase, and also by the trail becoming distorted by the wind and producing multiple reflection points. Other echoes have been observed which consist solely of the trail reflections with no apparent echo during trail formation. This may be due to the trail being formed outside the radar beam and drifting into the beam. Another possibility is that these trails are formed in the beam, but initially do not satisfy the conditions for specular reflection; subsequently the trails drift and distort to give specular reflection.

The next example, Figure 5.8, appears from the amplitude times series to be an instance where two meteors have been detected in the same record, one a "classical"

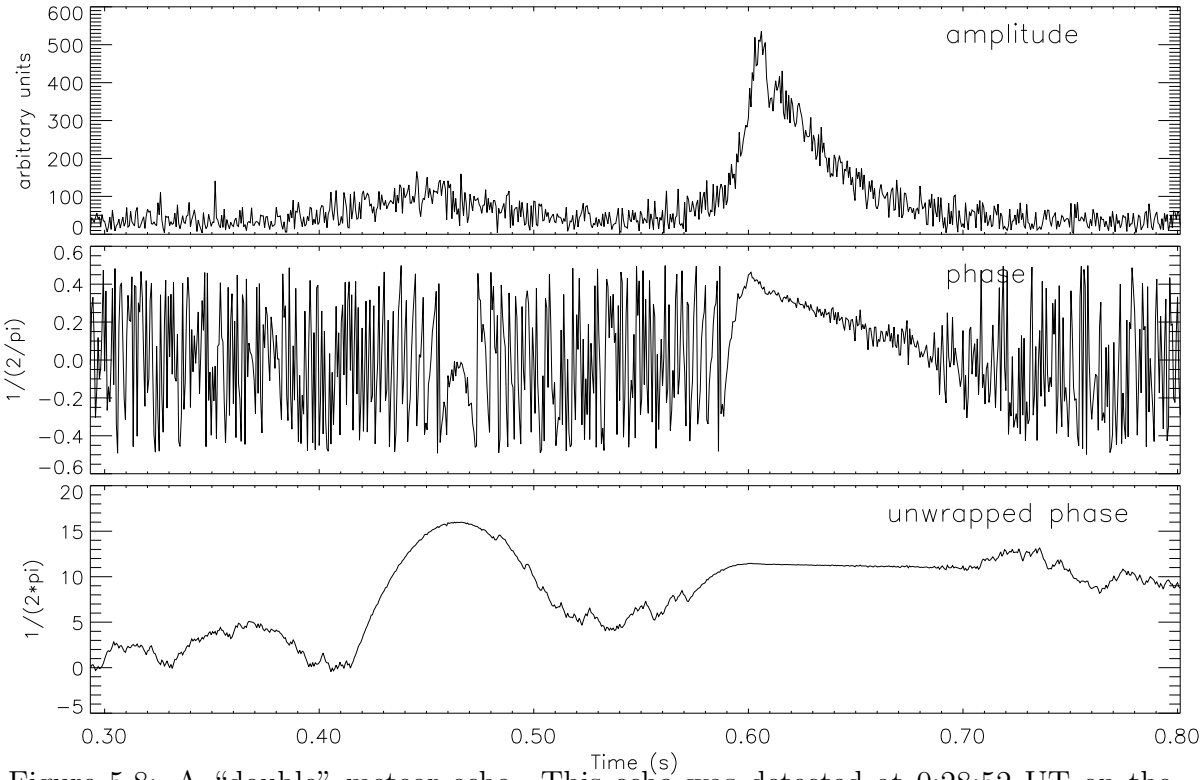

Figure 5.8: A "double" meteor echo. This echo was detected at 0:28:52 UT on the eighth of May 1999. Periodic noise reduction has been applied.

transverse echo, and the other quite different. The phase record shows the usual Fresnel diffraction pattern in the phase, but also shows a parabola, and there is even a suggestion of a second parabola at around 0.35 seconds. The major parabola looks like curve "D" in Figure 3.4, the phase curve of a transverse echo under extreme diffusion. The difficulty arising here is that the "two" echoes would have very different diffusion rates, and therefore must be ablating at different heights. While this could possibly be explained away if one has been detected in a sidelobe and the other in the main beam, the frequent occurrence of these type of echoes compared to the chance of getting two separate echoes in the same range bin in the same record makes the above hypothesis less plausible.

Another explanation presents itself when we note that the parabolic behaviour of the phase in the earlier part of the record resembles the parabolic portion of the pre t_0 phase of the "classical" echo later in the record. Modelling discussed in Chapter

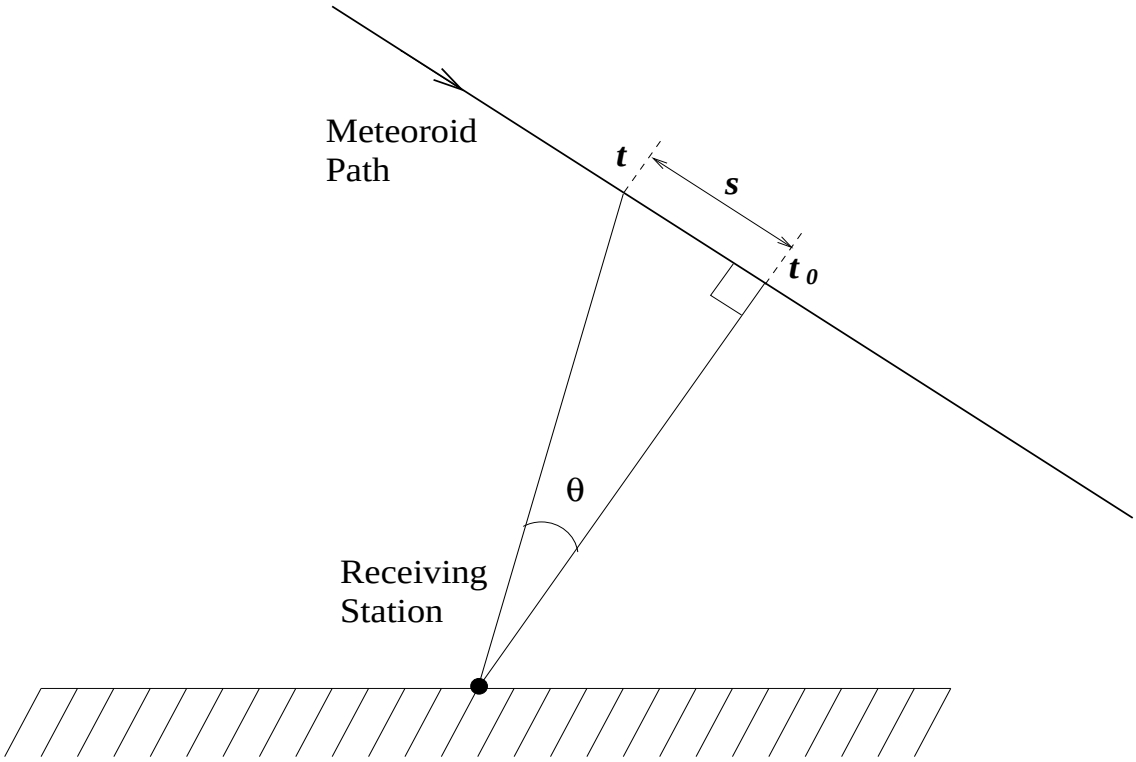

Figure 5.9: Diagram of the geometry of meteor head echo observation. The meteor is observed at a distance s, and a time t prior to the t_0 point.

6 shows that the parabolic phase behaviour is the result of inadequate sampling frequency, causing aliasing of the phase parabola when the change in the phase between each point becomes larger than one cycle. Normally this would produce a number of "half parabolae" joined to each other, but the phase unwrapping program unwraps every second "half parabola" backwards, causing a series of parabolae of the same shape. This will only occur where there is a signal from the trail while the meteoroid is still some distance from the t_0 point. The geometry of the situation is shown in Figure 5.9. We know that the meteor is already being detected at a time, t prior to the t_0 point. However no part of the trail has yet reached the central Fresnel zone (around the t_0-point), and thus the reflection is weak, probably mostly coming from the ionisation around the head of the meteor. This type of echo can be classified as an "aliased head echo".

If the hypothesis that the two apparent returns are from the same meteor is correct, then the speed measured from the two points on the trail should be the same (assuming

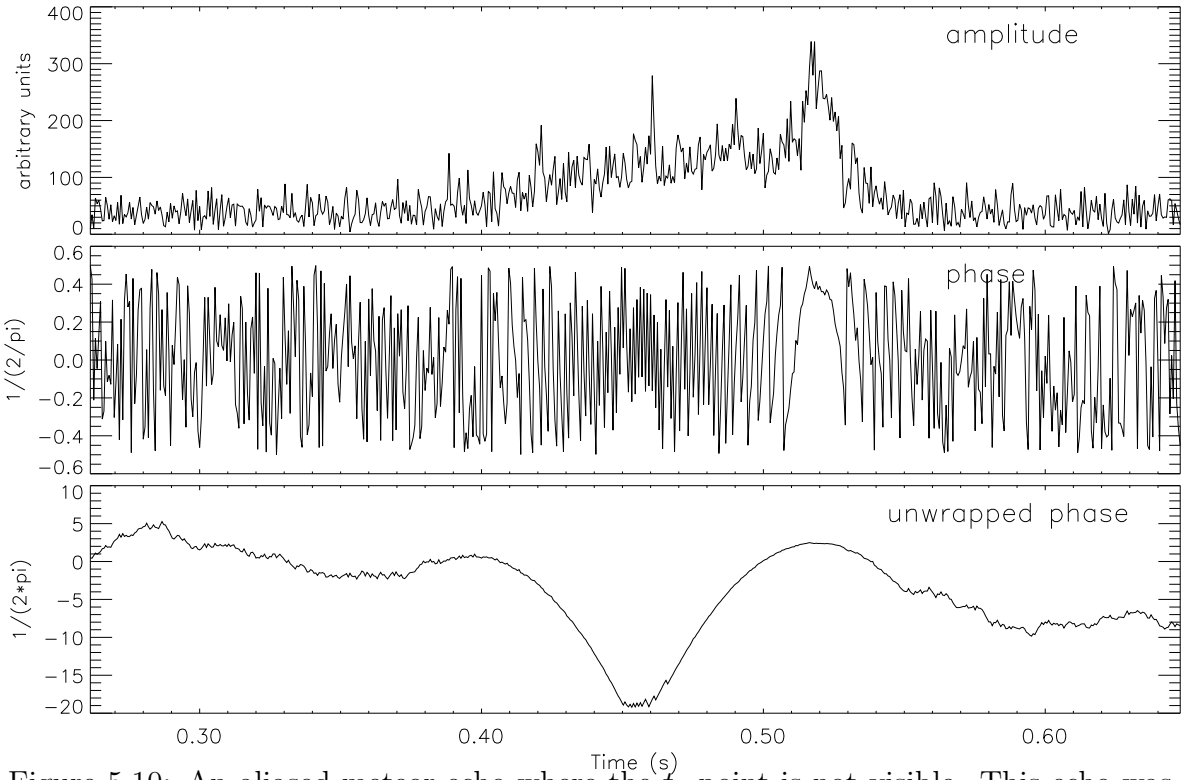

Figure 5.10: An aliased meteor echo where the t_0 point is not visible. This echo was detected at 1:23:43 UT on the eighth of May 1999. Periodic noise reduction has been applied.

no deceleration) and the two points must be occurring in the same range bin. This suggestion is readily tested as follows.

The technique used to obtain the two speeds was the pre-t_0 phase technique described in Chapter 6. The speed determined from the meteor head echo was 63.9 ± 0.3km s^{-1} and for the classical Fresnel trail echo was 61.3 ± 0.3km s^{-1}. The time interval between t and t_0 is 0.135 ± 0.005 seconds and the meteoroid would travel about 8 km in this time. The difference in the speed at the two points is assumed to be due to deceleration of the meteoroid, and gives a mean deceleration of $19 \pm 3 kms^{-2}$. A detailed discussion on the deceleration of meteoroids can be found in Chapter 6.

The range of the echo of 114.8 km gives an angular separation between the two speed measurements of about 4°. This means the difference in the range from the head echo and the trail echo is calculated to be about 280 m, so it is quite probable that the two echoes would occur in the same range bin, as a range bin is $2km$ wide. The

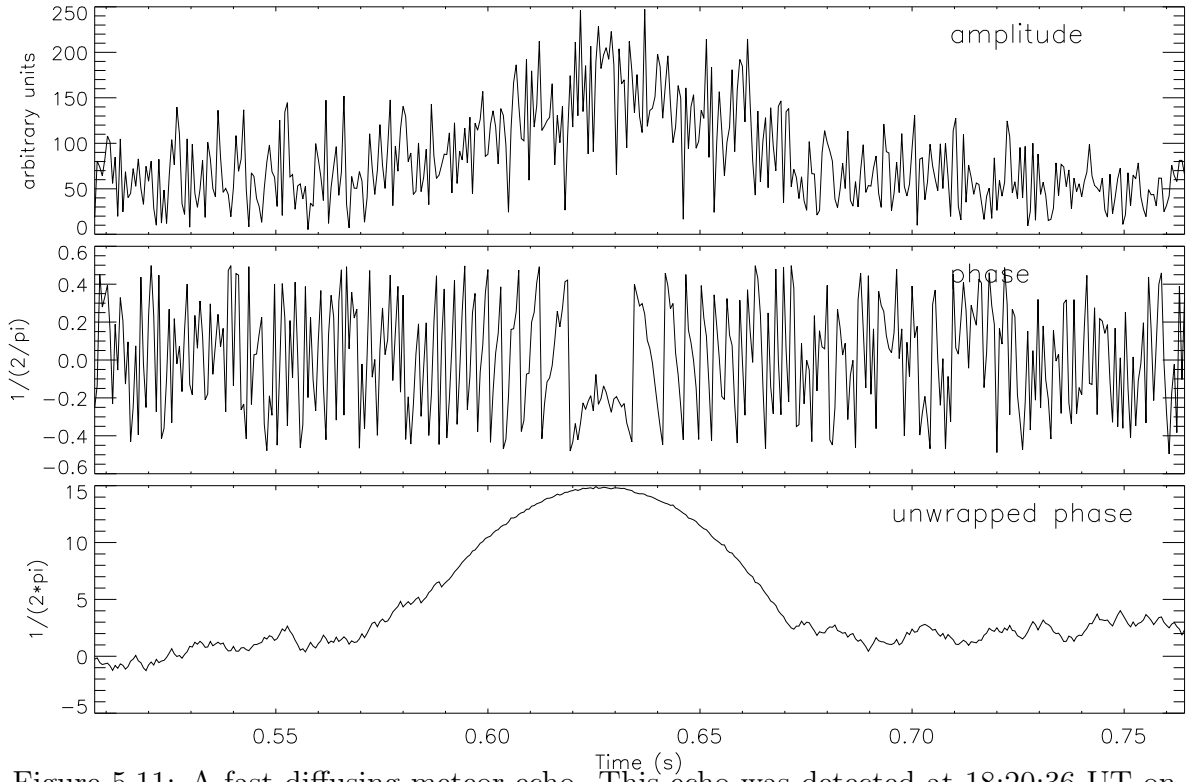

Figure 5.11: A fast diffusing meteor echo. This echo was detected at 18:20:36 UT on the eighth of May 1999. Periodic noise reduction has been applied.

angular separation of the two echoes is larger than the half power width of the beam, but could still lie between the zero points of the main lobe of the antenna pattern.

The next example (Figure 5.10) shows a meteor echo where the pre t_0 phase is again aliased, but no echo is apparent where we would expect the t_0 point. This is an echo similar to the previous example, but where the t_0 point occurs outside the radar beam, and thus no scattering occurs from the trail here. All that is visible is the aliased pre-t_0 phase. Another feature of interest in the echo shown in Figure 5.10 is the sudden increase in the amplitude at time 0.5 seconds. One possible explanation for this increase in amplitude is fragmentation of the meteoroid at this point in time, leading to a sudden increase in surface area, and thus ionisation production. The rest of the amplitude behaviour is consistent with that expected from a constant strength source crossing the antenna polar diagram.

Meteors which occur at great heights can diffuse very rapidly, depending on the orientation of the meteor trail to the geomagnetic field and the radiation field vector.

The effect of rapid diffusion is to limit the length of trail which is reflecting the signal to less than a Fresnel zone length. This will give a return similar to that shown by "D" in Figure 3.4. This parabolic shape looks similar to that in the previous examples, and it would seem that an echo where the "classical" t_0 point lies outside the beam could be confused with an echo from a meteor trail which is diffusing extremely rapidly with the t_0-point in the beam.

Figure 5.11 shows an example of this type of echo. The amplitude shows a symmetrical rise and fall, and is a cross-section of the antenna beam pattern, assuming that ionisation production is constant over the observed region. The phase follows a parabolic curve, which is consistent with the phase expected from an object which is travelling perpendicular to the radar and a trail experiencing extreme diffusion. The range of the echo is 128.8 km. For an off-zenith angle of 30°, the height would be 111.5km, high enough for rapid diffusion. However, the aliasing we have observed in previous examples is quite likely to be happening in this example. This implies that the t_0-point of this particular trail could lie outside the radar beam. Since the echo only occurs in one range bin and the amplitude profile shows a high degree of symmetry, it would seem that the t_0-point is at least not far from the beam, and the echo can be used to estimate the antenna beam width. The echo was detected at a range of $128.8km$ and the speed was measured to be 66.2 ± 0.26km s^{-1} (using the pre t_0 phase technique described in chapter 6). The time taken for the particle to cross the half power beam width is the time over which the amplitude is $1/\sqrt{2}$ times the peak amplitude (the half power points). This was measured as $0.080 \pm 0.005s$, giving a half power half width of $1.18° \pm 0.09°$ for the two-way antenna pattern assuming that the trail is perpendicular to the beam. Even if the trail makes an angle of 80° to the beam, this still gives a half power half width of $1.16° \pm 0.09°$ for the two-way antenna pattern, a difference smaller than the error. This agrees well with the theoretical antenna pattern half power beam widths from Chapter 2.

We conclude this catalogue of types of radio meteor echoes with a description of the appearance of a "down-the-beam" echo. When the path of the meteoroid departs

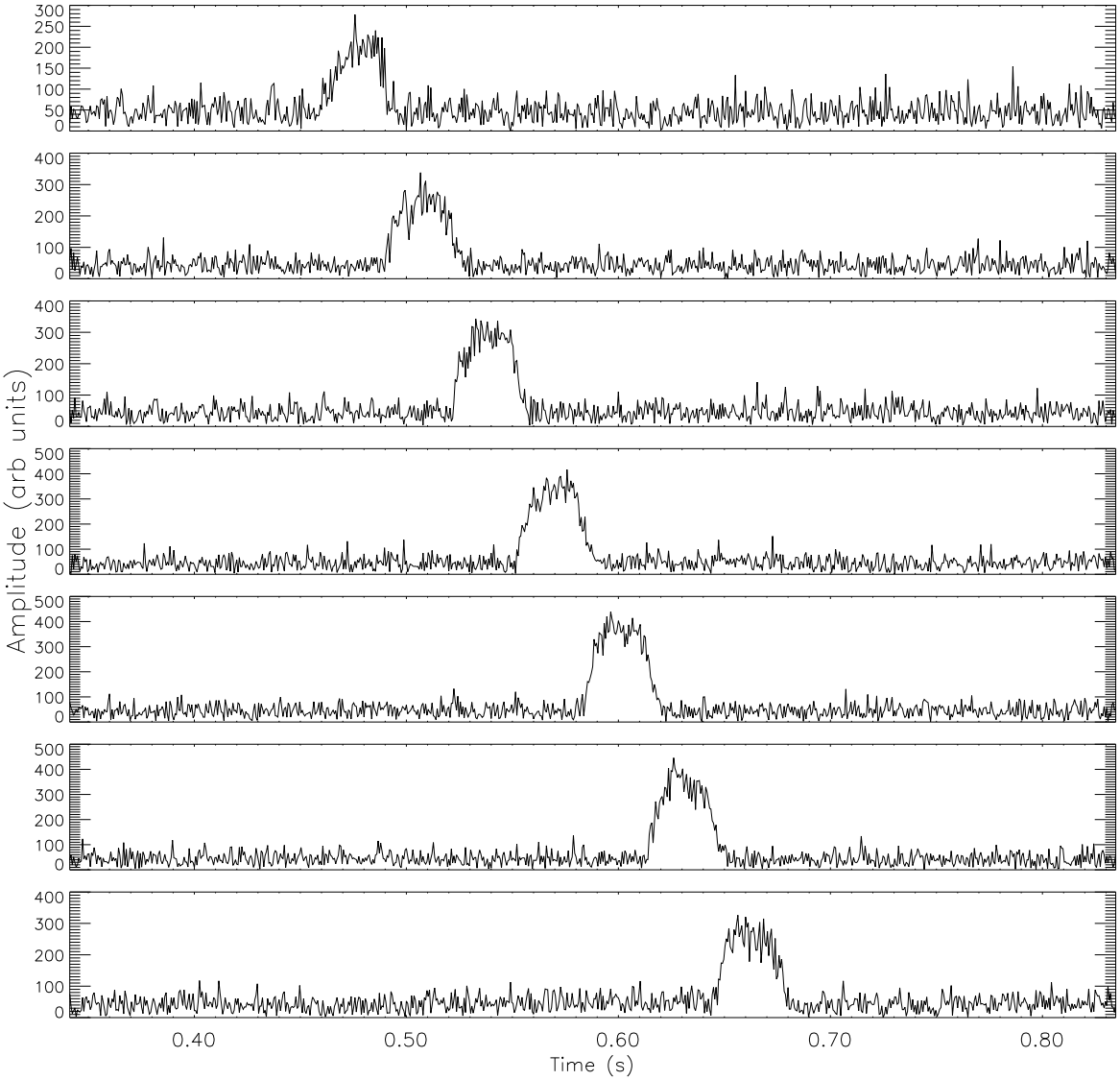

Figure 5.12: A down-the-beam meteor echo. This echo was detected at 21:47:17 UT on the fifth of May 1999. The panels show the amplitude of the echo in consecutive range bins from 110.8 to 122.8 km. Periodic noise reduction has been applied.

significantly from orthogonality with the radar beam, there is the possibility that the echo may show up in a number of range bins in succession. This is known as a "down-the-beam" meteor. An example of this is found in Figures 5.12 and 5.13, which show a meteor passing through seven range bins. Figure 5.12 shows the amplitude of the signal in each range bin, and Figure 5.13 shows the phase in each range bin. The amplitudes are a convolution of the range bin window with the cross section of the antenna pattern and the ionisation profile of the meteor. The phase records simply

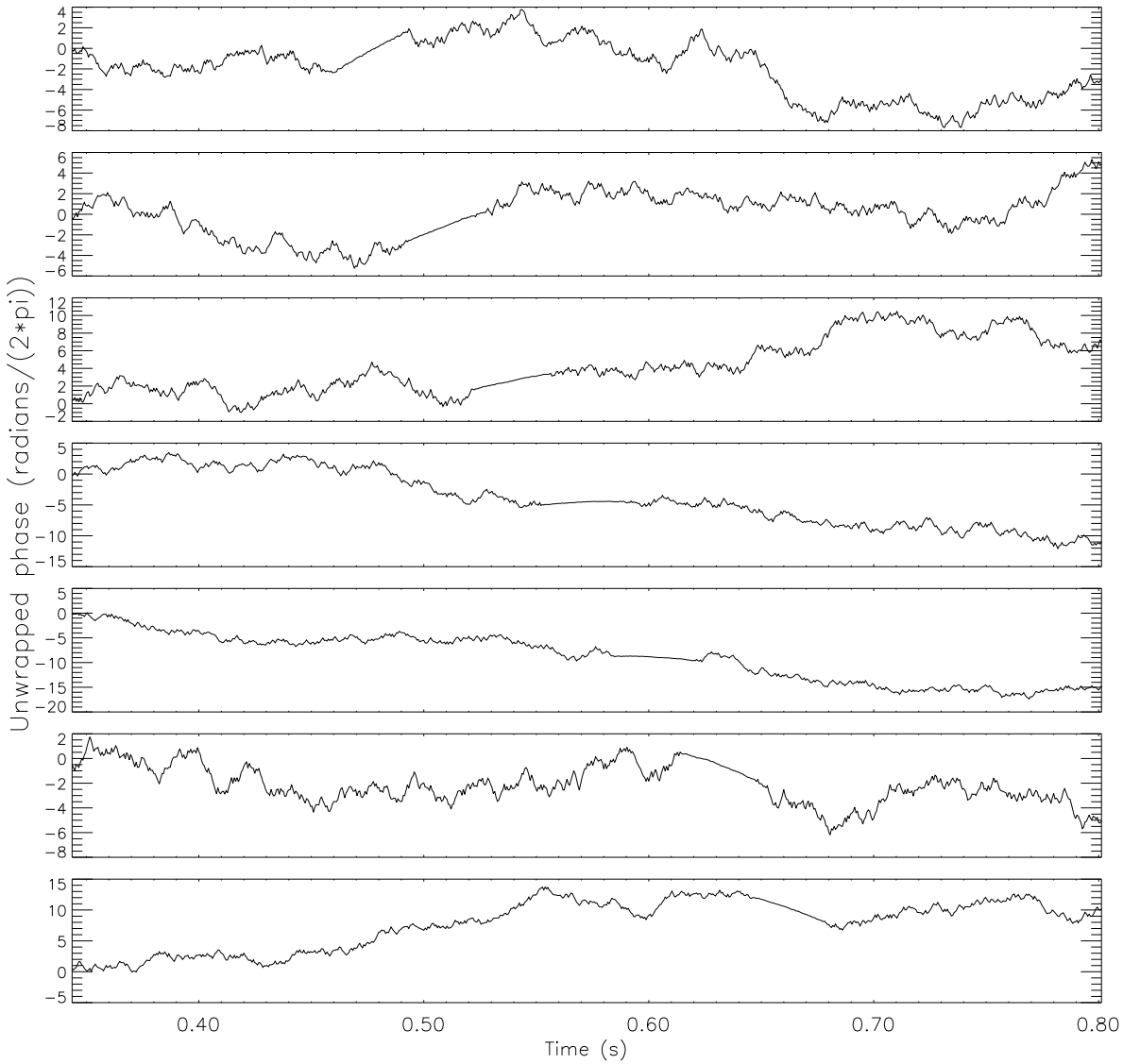

Figure 5.13: Phase of the down-the-beam meteor echo from Figure 5.12.

show sections of the parabolic curve, and can easily be added together to produce a phase curve for the whole echo, since the range bins have a small overlap. It should be noted that the pulse by pulse phase observations of down-the-beam meteors are severely aliased. Notwithstanding this aliasing, data such as in Figure 5.13 are the basis for the down-the-beam speed determination described in Chapter 6.

5.1.2 Echoes with other causes

The next two examples show the two main sources of false triggering in the detection algorithm. The first is that caused by aircraft flying through the beam or the sidelobes shown in Figure 5.14. While this is not technically a false trigger as the radar is actually detecting a real object, the source of this echo is not a meteor trail, and these events are undesirable. The Buckland Park field station is situated in a low flying zone, set aside for the training of pilots. This in itself is not as large a problem as it would seem, because the system is set to ignore echoes in several of the first range bins in order to eliminate false triggers due to atmospheric turbulence. More significant are echoes from commercial airliners travelling at a large horizontal distance from the radar. Although these aircraft are travelling at altitudes less than 15 km, because of their large size, metal construction, and the sensitivity of the radar, they produce strong reflections, even in the sidelobes, which means that they can be readily detected at angles other than in the main beam. Since the radar range bins are aliased (to give better height coverage at high pulse repetition frequencies), the echoes from these aircraft appear to the system at great ranges (90 - 110 km) when they are actually much closer (10 - 30 km). With the main beam tilted at an off zenith angle of 30° (as is commonly the case) they can appear in the main beam or in the further off zenith sidelobes. Depending on the beam direction, several echoes a day are caused by aircraft. Fortunately they are quite easy to identify and can be discarded.

The echo shown in Figure 5.14 is from an aircraft flying over the radar. It was detected at 18:13:05 UT on the sixth of May 1999 and continues for another seventeen seconds, passing from range bin 8 into range bin 9 after twelve seconds. There was also an echo detected at 18:13:01 UT in range bin 7 which has a very low amplitude signal, but appears to be from the same aircraft. Since the range is increasing, it is apparent that this aircraft is travelling away from the radar. The main features of the series of echoes are the slowly varying amplitude, which rises from zero to about 400 units, varies slowly about this value and then dies away again, and the rapidly

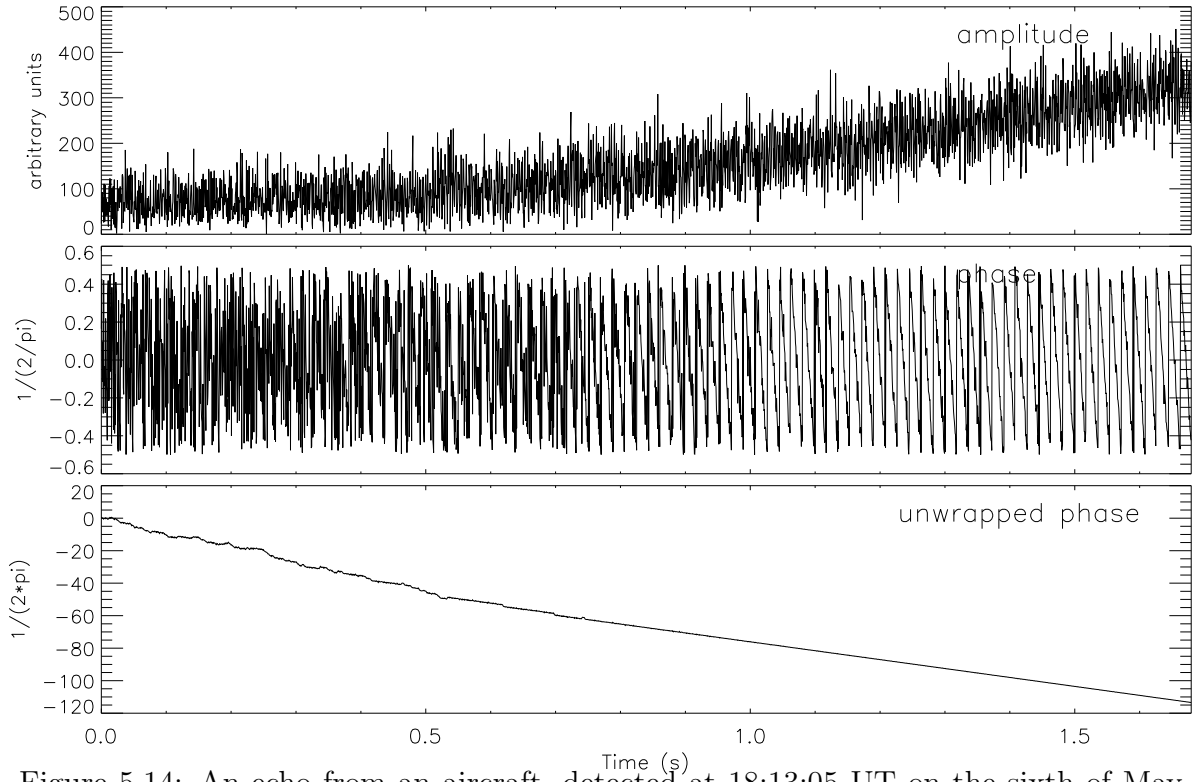

Figure 5.14: An echo from an aircraft, detected at 18:13:05 UT on the sixth of May 1999.

decreasing phase, with the rate of change of the phase slowly increasing with time.

Assuming that it is travelling at a constant height and with a constant speed, the speed and height, as well as it's zenith angle can be found from the radial speed (determined from the rate of change of the phase) and the range, in the same way as the down-the-beam meteor (see Section 6.6).

The second main type of false event is that caused by the periodic noise frequencies shifting close together and producing low frequency beating. These low frequency signals can fool the detection algorithm into thinking it is detecting meteors, although the later generation algorithms are less prone to this. An example of this type of event is shown in Figure 5.15. The oscillations in the amplitude are readily seen. The amplitude of the oscillations changes with time, the direction and the zenith angle of the radar beam.

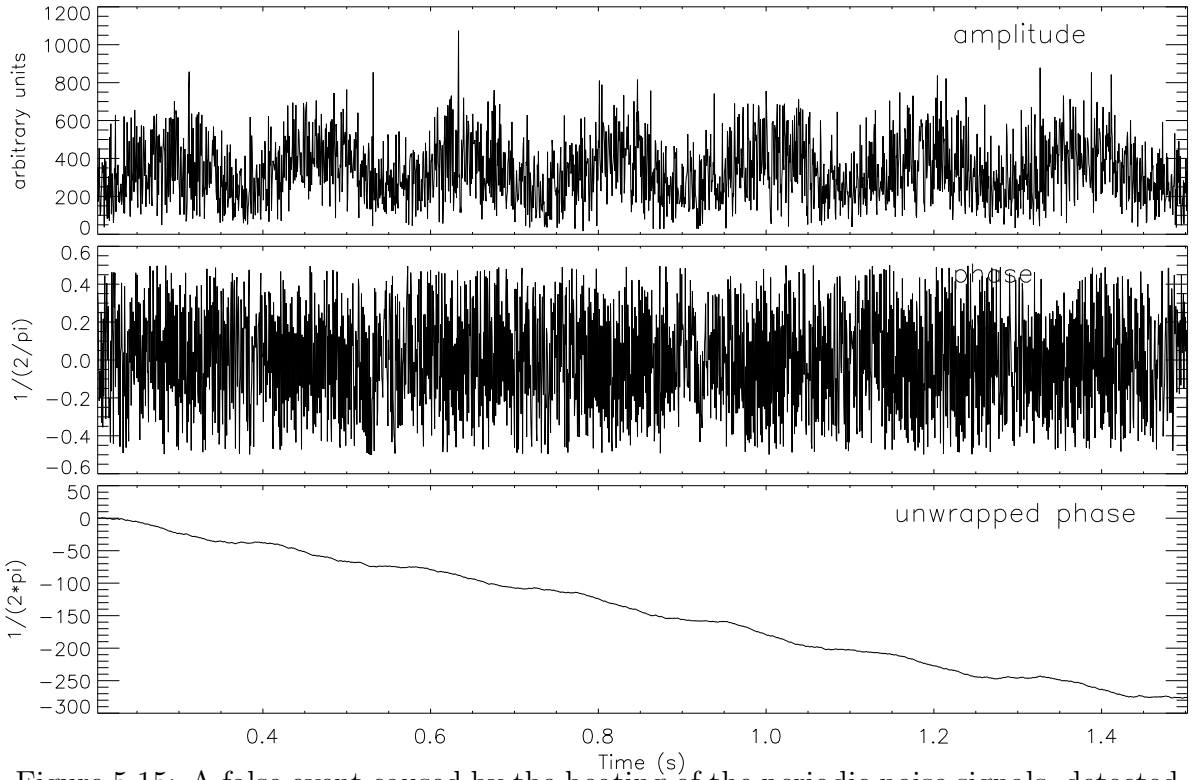

Figure 5.15: A false event caused by the beating of the periodic noise signals, detected at 0:06:42 UT on the fifteenth of November 2000

5.1.3 Rate of occurrence of different types of echoes

By far the most common type of echo encountered was the transverse type. From the 6369 recorded events which were analysed, 5483 (86.1 %) were of the transverse type. In 90.6 % of these transverse type echoes, the t_0 point was present in the record, and the radial wind drift could be measured. Of these echoes the speed could be measured to an accuracy better than one percent in 89.5 % of cases. Only 11.6 % of the echoes showing the t_0 point also showed two or more Fresnel oscillations. The remaining 9.4 % of transverse echoes were "near perpendicular" echoes, *ie* the t_0 point was not present but the pre-t_0 Fresnel diffraction pattern was visible (such as in Figure 5.11). The speed could be measured in all of these cases.

466 (7.3 %) of the total echoes were down-the-beam echoes (*ie* echoes were present in two or more range bins), and their rate decreased rapidly as the number of range bins crossed increased. A further 420 (6.6 %) of the recorded events were non-meteors, of these 80 % were due to aircraft, and 20 % were due to periodic noise. Thus the

actual false trigger rate was about 1 %.

5.2 Measurement of the ambipolar diffusion coefficient

As previously mentioned, the decay of the amplitude of an underdense meteor echo is related to the ambipolar diffusion of the trail, and by measuring the decay we can estimate the value of the diffusion coefficient. Based on the value of the diffusion coefficient, estimates of the height at which the diffusion is occurring can be made. This method has been used to check the height of the meteor trail which we obtain from the range of the echo and the zenith angle of the beam (Baggaley 1981), as this "range/angle" height is only accurate if the meteor is detected in the main beam of the radar and not a sidelobe (see the next section). As discussed in Section 3.4, the value of the diffusion coefficient is dependent on the local atmospheric density and the local temperature. To obtain a height from the value of the diffusion coefficient we use a standard atmosphere model to provide the density and temperature. This gives us a height accurate to about 5 km, which is close enough to check the range/angle height. Conversely if we assume that the range/angle height is accurate, then we can use the estimate of the diffusion coefficient to estimate the temperature at this height (Hocking et al. 1997, Hocking 1999). For heights above 90 km the effect of the geomagnetic field can decrease the diffusion coefficient considerably depending on the orientation of the radar beam with respect to the field. The issue is further complicated by the formation of instabilities in the ionisation which may increase the diffusion coefficient, although the significance of this effect on the relatively low electron density trail being considered is unclear (see Section 3.4).

In the meteor data analysis program the value of the diffusion coefficient is estimated in the following way: First the presence of a decay curve is determined by the analyst. The region of the decay curve is selected and the natural logarithm of the ratio of the amplitudes of the points on the curve to the amplitude of the first point

is divided by the time difference between the points. This gives a number of values for the decay coefficient b, which are then averaged. Exponential decay is described by the expression

$$A = A_0 e^{-bt}$$

where A is the amplitude of the signal at a time t and A_0 is the amplitude at $t = 0$. Recalling equation 3.39, and assuming that the amplitude of the returned signal is proportional to the reflection coefficient, we obtain,

$$A = cq\pi r_e \exp(-k^2(4Dt + r_0^2)^2) \tag{5.1}$$

where c is a constant of proportionality. Since $k = 2\pi/\lambda$, then the time dependent part of A is given by

$$A = A_0 \exp(-\left(\frac{2\pi}{\lambda}\right)^2 4Dt) \tag{5.2}$$

This leaves us with

$$D = \frac{b\lambda^2}{16\pi^2} \tag{5.3}$$

Once an estimate for D is obtained, an equivalent height is obtained by consulting two lookup tables. These tables contain the diffusion coefficients *versus* height from a standard atmosphere for June and December at the latitude of the Buckland Park VHF Radar, but do not include the effects of the geomagnetic field on diffusion or the effects of instabilities. They contain values similar to those in shown in Figure 3.6 as $D_{\|}$. For other months, these two are averaged on a *pro rata* basis to give a better estimate of the height.

Figure 5.16 shows distributions of range/angle heights for the different values of diffusion height. The top distribution is for echoes with no decay curve (generally head echoes). Each of the distributions has had an arbitrary constant value added for clarity. The range/angle height of the peak of each distribution corresponds well to the height as estimated from the diffusion coefficient, with a spread of about 5 km. Most distributions show a tail extending to greater heights, containing echoes taking longer than expected to decay, probably due to the magnetic effects described in Section

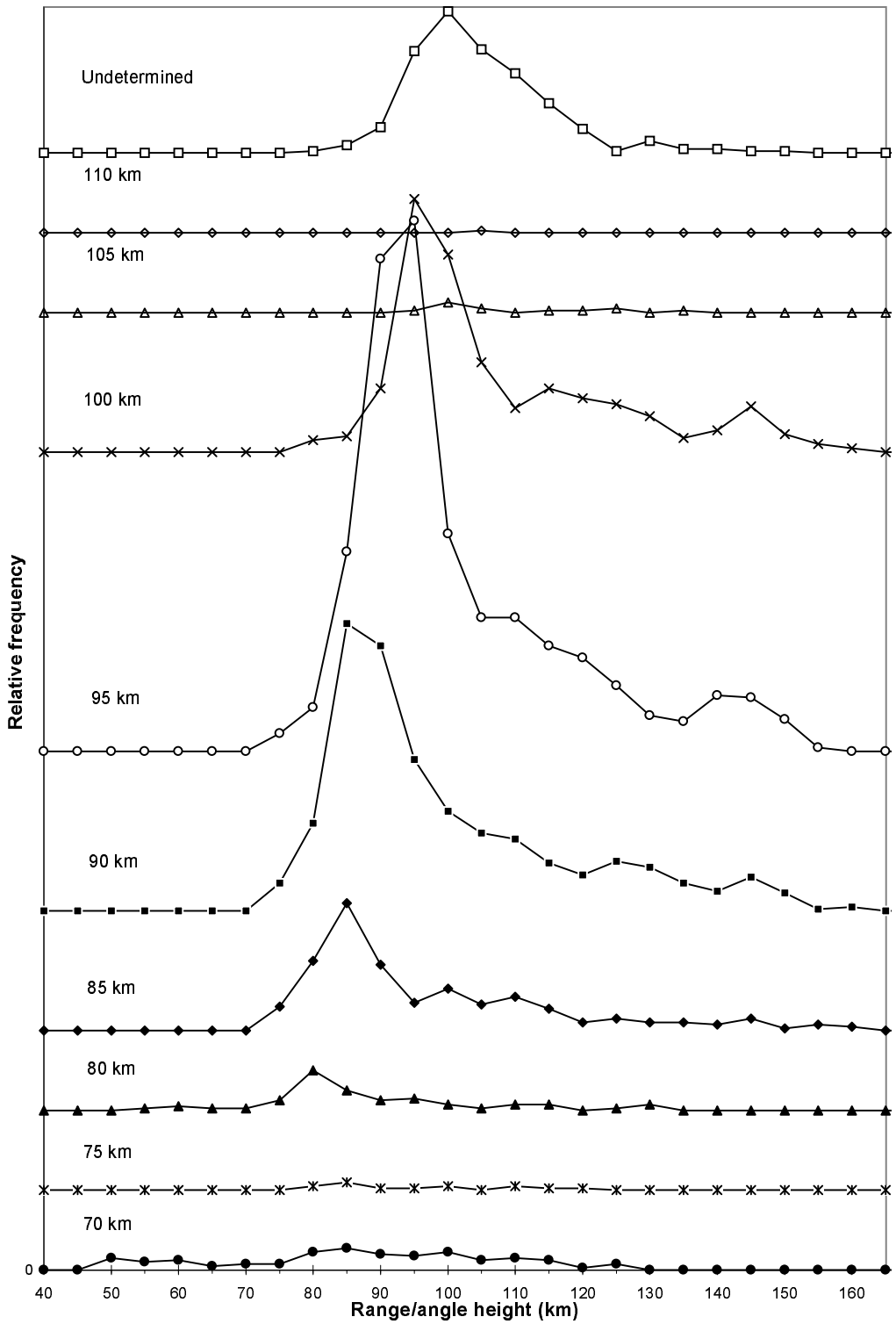

Figure 5.16: Distributions of heights calculated from range and zenith angle. Each of the distributions is for a different value of height as calculated from measured diffusion coefficient. The top distribution is for echoes where the decay curve was not present. The distributions have had an arbitrary constant value added for clarity. Bin widths are 5 km centred on the label values.

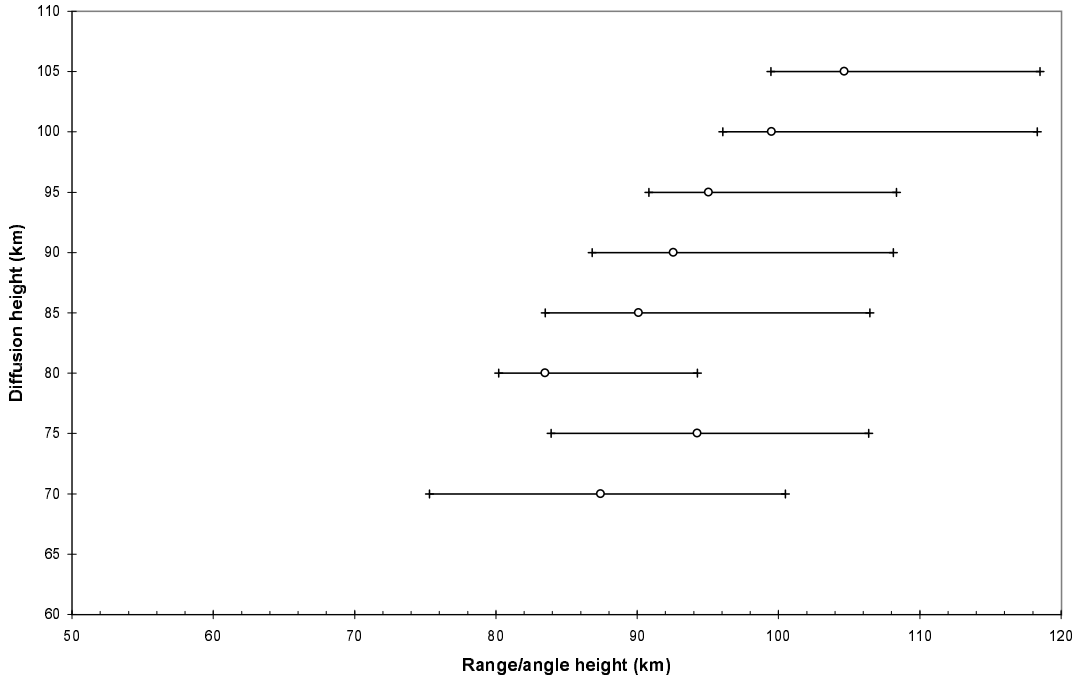

Figure 5.17: Median values of heights calculated from range and zenith angle (circles). Each of the median values of the distribution is for a different value of height as calculated from measured diffusion coefficient. The crosses represent the 25^{th} and 75^{th} percentiles.

3.4. It is probable that a number of these events are occurring in the sidelobes of the antenna pattern, but this would introduce an error in the range/angle height of no more than 11 %. However, it would introduce a change in the angle between the beam and the magnetic field, and this could have a significant effect on the duration of the echoes (see Figure 3.7). Looking at the distributions, there appear to be two distinct populations of echoes which have slower diffusion than expected. The distribution of height for the "undetermined" group of meteors peaks at 100 km. These echoes are aliased head echoes, generally have speeds in excess of 40km s^{-1}, and in this data are usually associated with the η-Aquarid meteor shower.

Figure 5.17 shows the median of the range/angle height distributions, as well as the 25^{th} and 75^{th} percentiles, plotted against the height calculated from the diffusion coefficient. For all heights above 75km there is good correlation between the median

value of the range/angle height and the diffusion height. The width of the distributions is about 5 km (as shown by the 25^{th} percentile) and the tail in the distributions up to greater heights is about 15 km long (shown by the 75^{th} percentile). For diffusion heights of 70 km and 75 km, the behaviour appears quite different, with wider distributions and higher values of the median than expected, but the small number of echoes means it is difficult to make conclusions about this region of the plot.

The large majority of echoes decay as expected, however there are a number of echoes which show much slower diffusion, probably due to the effects of the Earth's magnetic field. This effect is dependent on the angle of detection of the meteor with respect to the magnetic field. Diffusion coefficients can be an unreliable method of estimating the height of a meteor trail, unless the direction of arrival is known. The deduction of temperatures from the diffusion coefficient would also seem to be fraught with danger, considering the wide variations in echo decay rate seen here.

5.3 Meteor heights

In the previous section we have shown how the decay of the amplitude of an echo can give an unreliable estimate of the height of a meteor trail. We now turn to the method for which the system was designed, the range/angle method of determining the height. If the trail is assumed to have been detected in the main beam of the radar, then the height is the range of the echo multiplied by the cosine of the zenith angle of the beam. The range/angle method gives us the best estimate of the height of a meteor trail, with an error of 2-3 % (due to the 2 km width of the rangebins) when meteors are detected in the main beam.

The rate of meteors being detected in the sidelobes depends on the off zenith angle of the radar beam, but is generally less than 10 % of echoes. This is made up of about 6 % in the first sidelobe with a larger off-zenith angle, 1 % in the first sidelobe with a smaller off-zenith angle, and 3 % in the first sidelobes which are at the same off-zenith angle as the main beam (See Section 3.9). The additional height error from the latter

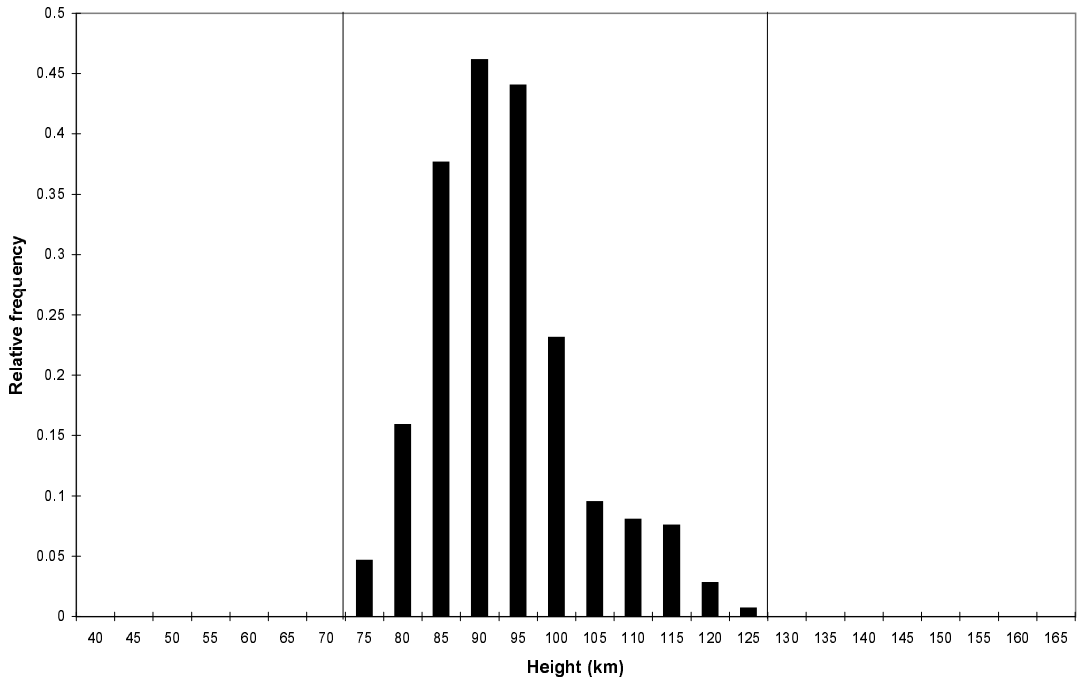

Figure 5.18: A histogram of meteor trail range/angle heights at a PRF of 2000Hz. Bin widths are 5 km centred on the label values. The vertical lines show the limits of detectable heights.

is about 1 %, the main error is due to the 6 % in the larger off-zenith angle sidelobe, increasing to a maximum of about 12 %. The proportion of meteors detected in the second and further sidelobes combined is less than 1 %.

Section 2.4 discusses the two different pulse repetition frequencies used for observation and the differing range and height coverage that they allow. A PRF of 2000 Hz and an off zenith angle of 30° allows height coverage of 68 to 129 km, whereas a PRF of 1650 allows coverage below 74 km and between 91 and 151 km. Figure 5.18 shows a histogram of range/angle heights at a PRF of 2000 Hz, with 2 km bins assuming all meteors were detected in the main beam. Note that the peak of the distribution is at 91 km, and there appears to be another small peak at about 109 km. The η-Aquarids meteor shower was present during the observations which make up this data, so it is reasonable to expect that there would be a secondary peak much higher, as the η-Aquarids are a high speed shower and should begin ablation significantly higher than

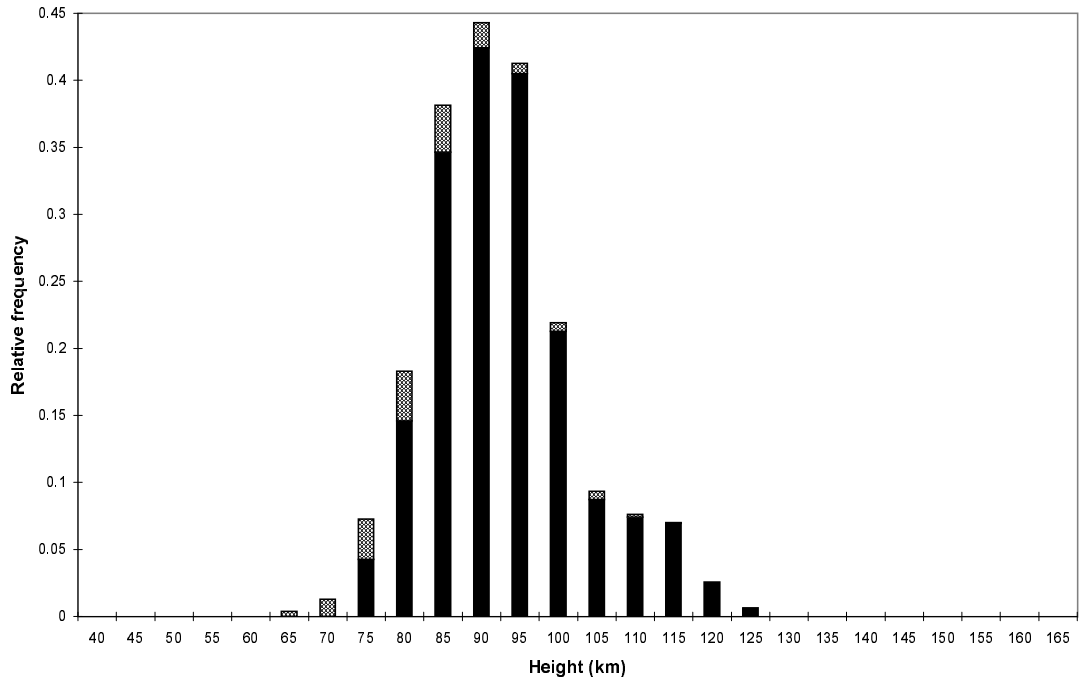

Figure 5.19: A histogram of meteor trail range/angle heights at a PRF of 2000Hz with correction for the effects of sidelobes. The shaded portions show the meteors which are in sidelobes. Bin widths are 5 km centred on the label values.

the average sporadic meteoroid.

If the effect of the sidelobes is corrected for, then the distribution is as shown in Figure 5.19. The shaded sections show the proportion of meteors which are detected in the sidelobes and their heights have been corrected accordingly. The effect of assuming all meteors are detected in the main beam is to slightly increase the calculated heights of a small proportion of the meteors. Since this effect is small, it is ignored for the rest of the height distributions presented.

Figure 5.20 shows another histogram of range/angle height, this time at a PRF of 1650 Hz. Most noticeable is the large gap in the distribution between 74 and 91 km, this is due to the aliasing distance and the range bins ignored to prevent atmospheric turbulence creating false triggers (see Section 2.4). The other glaring difference is the much greater spread of heights in this distribution. In Figure 5.18 the spread of the distribution is from 71 to 125 km, whereas the distribution in Figure 5.20 is from 60

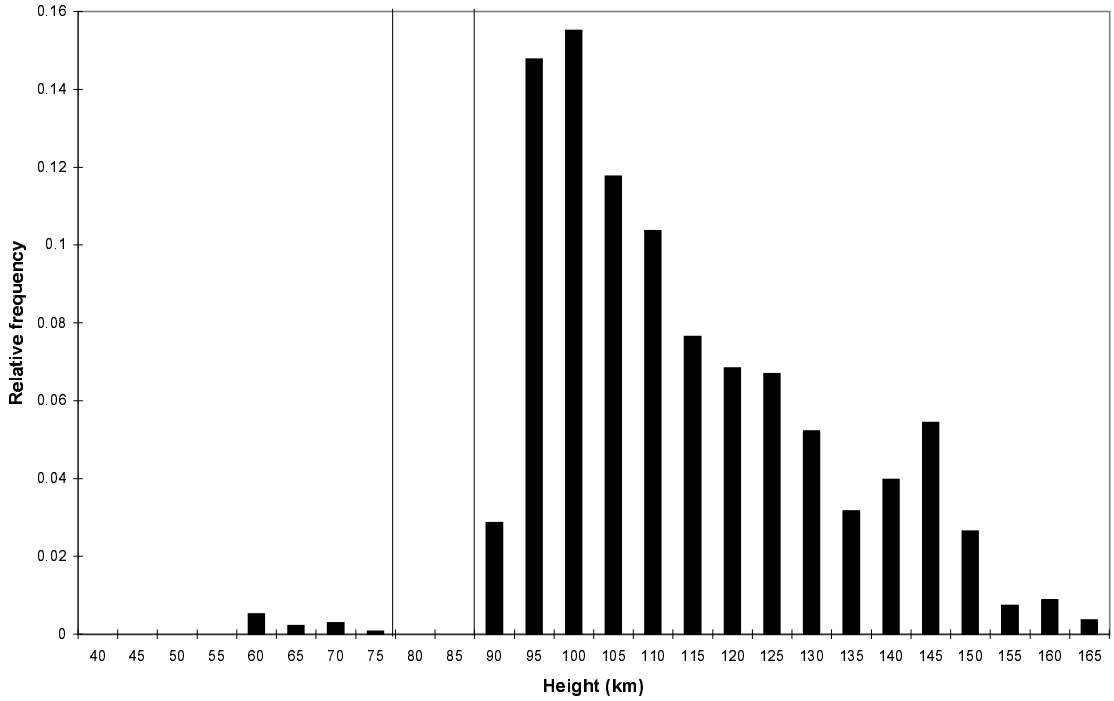

Figure 5.20: A histogram of meteor trail range/angle heights at a PRF of 1650Hz. Bin widths are 5 km centred on the label values. The vertical lines show the gap in detectable heights.

to 161 km. If we consider the possible distribution for a PRF of 2000 Hz we find that we would only see meteors from 68 to 129 km, which corresponds nearly exactly with what we see, although we would expect that an artificial limited distribution would show sharp edges. We observe that the meteors in the height region 60 to 74 km could have occurred in the region 138 to 152 km if they were echoes from the previous pulse (and *vice versa*). These "doubtful" echoes have been sorted between the two regions by the measured diffusion coefficient, which gives at least a general indication of the height (see previous section). If this extra spread were due to detection in the first sidelobe, then the spread would be at least 65 to 145 km, which is still much larger than that expected from traditional ablation theory.

There has been speculation that many small particles are made up of materials which are significantly different to those traditionally used for ablation theory, and

thus would ablate at different heights (see Section 5.6; (Lebedinets 1991)). Meteor echoes at heights up to 160 km have been detected in observations at other frequencies (Olsson-Steel & Elford 1987, Elford & Olsson-Steel 1988, Thomas et al. 1988, Steel & Elford 1991, Pellinen-Wannberg & Wannberg 1994). In Section 3.5.1 attenuation due to the initial radius of meteor trails was discussed, and calculations based on the work of Jones (1995) predicted that if meteoroids were ablating at heights above 105 km they should not be observed by the Buckland Park VHF radar as underdense echoes since the attenuation dependence on frequency produces an attenuation factor of 0 at 54.1 MHz above these heights (see Figure 3.8). A survey of the echoes with heights above 110 km shown in Figure 5.20 reveals that 34.2 % are overdense. Underdense echoes make up 62.9 % of the echoes and the remaining 3.0 % could not be classified, being due to drifting trails or beating between multiple trails. The large number of underdense trails which are being observed suggests that initial radius attenuation is not occurring as predicted, or that a strong central core of ionisation in the centre of the trail allows underdense echoes to be observed even at these great heights. It should be noted that many meteor observations at VHF frequencies are made with systems that have artificial height limitations, not expecting to detect meteor echoes at these great heights, and wide-beam systems may not be sensitive enough to detect echoes from the inner core of trails.

5.4 Radial wind drift

During and after formation of the meteor trail, it is influenced by the background wind. This shows up in the post-t_0 phase record as a phase change superimposed over the classically predicted phase behaviour. This is known as the "radial wind drift" and is the change in location of the trail due to the wind, measured along the direction of the orthogonal to the meteor trail. If it is assumed that the horizontal motion is much greater than the vertical motion, then with the use of different azimuthal beam directions, the mean background winds can be measured. (Stubbs 1973, Mathews

et al. 1981, Djuth & Elder 1993, Vincent et al. 1994, Cervera & Reid 1995). The Buckland Park VHF radar has been used in previous experiments for the determination of the mean background winds (Cervera & Reid 1995).

While no dedicated meteor wind observation experiments were performed as part of this project, the wind drift must be removed from the time series prior to meteoroid speed calculations. Thus radial meteor wind drifts are recorded for all meteor echoes processed to obtain meteoroid speeds. As the meteor shower observations usually have the radar pointed in one direction for some time, in general the direction and magnitude of the horizontal winds cannot be determined. There can also be an error introduced by the effect of diffusion in the geomagnetic field and any polarisation electric fields in the E-region. This causes the motion of the trail electrons to be dominated by the $E \times B$ drift velocity perpendicular to the geomagnetic field (Reid 1983, Klimov & Lyatskaya 1988, Oppenheim et al. 2000), although at the latitude of the Buckland Park VHF radar, there is likely to be a much larger effect from the $v \times B$ forces due to motion in the Earth's magnetic field above 90 km. When the radial wind drifts from the Buckland Park VHF radar are used to determine the background winds, then these factors need to be taken into consideration, especially considering the number of meteors detected at heights greater than 90 km.

5.5 Fragmentation

Radar observations of the formation of meteor trails are frequently different to predictions based on the ablation of a single body which maintains its integrity until ablation has ceased. Telescopic studies of meteors made in the 1950's suggested that many meteors were the result of the ablation of "dustballs" which broke into many pieces soon after entry into the atmosphere, while other meteoroids released fragments during ablation. Since then is has been accepted that fragmentation is a common feature of meteors, occurring before or during meteoroid ablation.

The ubiquitous nature of the fragmentation of meteoroids is supported by a number

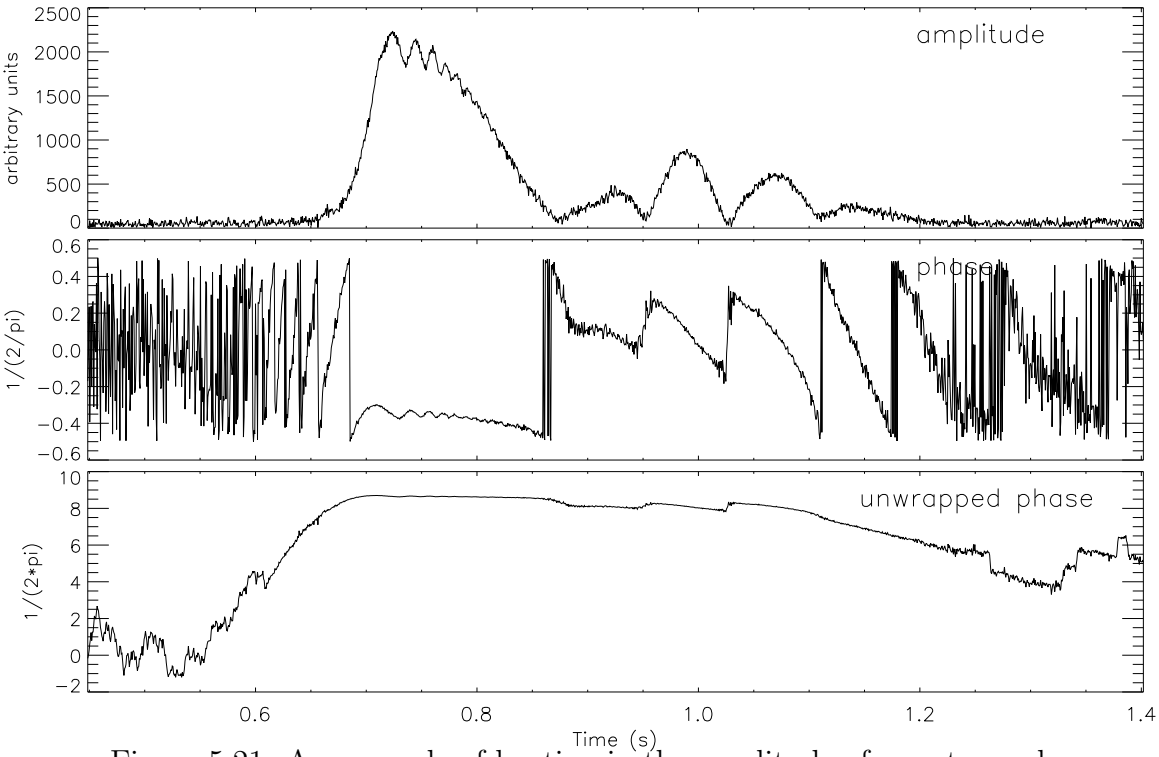

Figure 5.21: An example of beating in the amplitude of a meteor echo

of characteristics of radar meteor echoes. First is the lack of Fresnel oscillations after the t_0 point on many echoes. While these oscillations have been used in much radar research to obtain speeds of meteoroids, in fact they are not present in most radar reflections from meteor trails. This absence can be explained by the existence of more than one particle producing overlapping ionisation trails, thus washing out the oscillations. As mentioned in Section 5.1.1 Elford & Campbell (2001) have performed simulations of the returned VHF signal from trails caused by ten or more particles separated by varying distances along the meteoroid's path. These simulations show that the Fresnel oscillations are almost completely washed out by groups of meteoroids spread over as little as twenty metres. Of the transverse echoes showing the t_0 point analysed for this work, only 11.6 % showed two or more Fresnel oscillations. This strongly suggests that most of the meteor echoes detected by the Buckland Park VHF radar are caused by more than one ionisation trail, and that most of the detected meteoroids have fragmented before or during atmospheric flight.

There are a significant number of echoes in which there are sudden dramatic increases in the amplitude of the returned signal, implying that there has been a sudden catastrophic fragmentation which increases the surface area to mass ratio of the meteoroid and thus the rate of ablation and ionisation production. This in turn increases the amplitude of the returned signal. Other examples show apparent beating between two different ionisation sources. There are also echoes where there are two separate echoes with similar speeds detected in a short space of time, implying that they have separated in the pre-ablation phase.

Figure 5.21 shows an example of an echo which appears to be caused by two bodies which are travelling through the atmosphere with a small separation, possibly a meteoroid which has fragmented during flight. The echo begins in a conventional way, even showing some Fresnel oscillations as the amplitude decays, but the amplitude then begins to show beating, probably as the second body enters the radar beam and begins to produce radar returns. If we look at the change of phase associated with the radial wind drift, we note that the slope of the phase is significantly different at times 0.8 s and 1.2 s. This implies that the two trails are located in regions with different wind speeds or directions.

A second example, shown in Figure 5.22 shows a meteor trail being formed in the radar beam. As the trail is formed the Fresnel diffraction pattern is aliased in the unwrapped phase record to produce a series of parabolae (between 0.60 and 0.76 s), and the amplitude of the signal is increasing. At 0.72 seconds, something happens which causes the amplitude of the returned signal to increase by nearly four times, lasting for about 0.03 s and then the amplitude of the signal disappears into the noise. As the meteoroid approaches the t_0 point at about 0.82 s, the amplitude increases consistent with a typical transverse echo, and then decays as the trail diffuses. An increase in the ionisation produced in the meteor trail would explain the sudden increase in amplitude at 0.72 s, and this could be caused by the ablating body fragmenting, possibly a number of small pieces breaking off the main body before it had entered

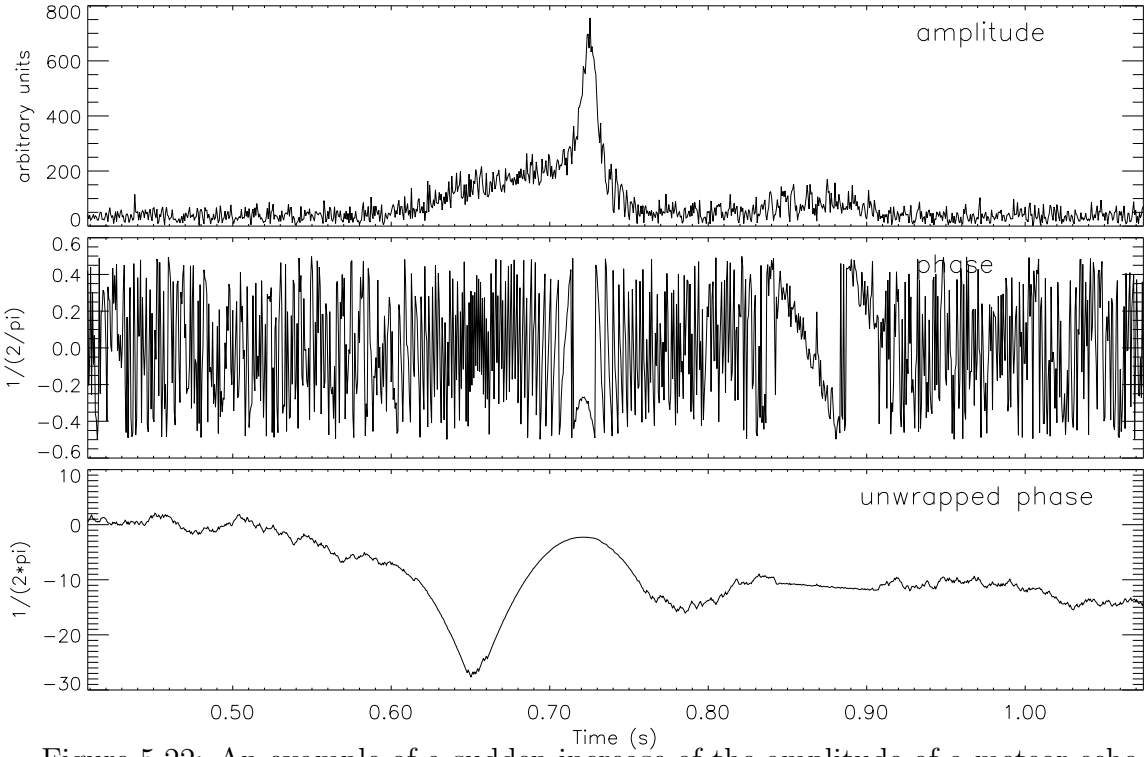

Figure 5.22: An example of a sudden increase of the amplitude of a meteor echo

the radar beam. These small pieces would continue to ablate, but with the mass-to-surface area ratio of the particles decreasing rapidly, a "flare" in the ionisation would be produced as the particles "burn out".

A technique which makes use of the properties of the Fresnel diffraction pattern can reveal the structure of a meteor trail (Elford 2001b). This techniques is discussed in detail in Section 6.2.9, but is essentially a transform between the time series of the returned signal and the distance along the trail from the frame of reference of the ablating body. While this gives a "snapshot" of the reflection coefficient along the trail, it is averaged over the whole time of the recorded signal. Since this time is short, the structure of the trail can be resolved quite accurately in most cases. Several examples have been found which clearly show multiple bodies producing the trails, often with different speeds (Campbell, private communication).

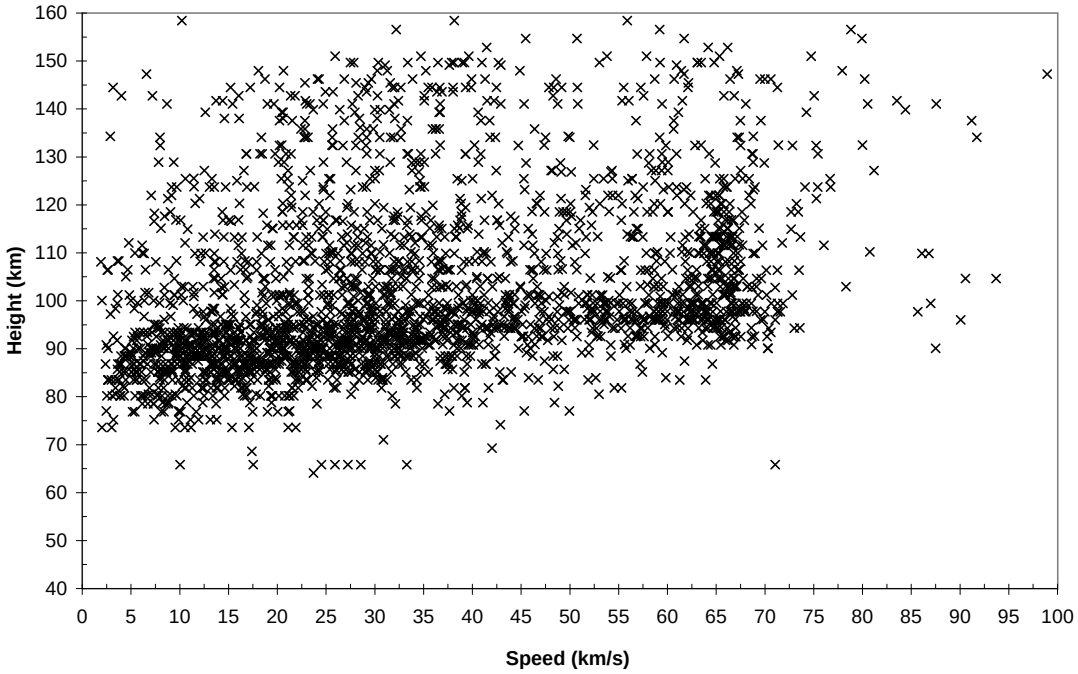

Figure 5.23: Speed-height scatter plot of meteors detected in April and May 1998 and 1999.

5.6 The physical properties of meteoroids

There has been much analysis of the meteoroids which survive to the surface of the Earth (*ie* meteorites) (Mason 1971), but there arises the question of whether the composition of these objects is representative of the total flux of meteoroids collected by the Earth. There are a few main classes of meteorites, namely; metallic, composed mostly of nickel and/or iron; stony, composed of oxides of silicon and other elements; semi-metallic, a combination of metallic and stony; and the carbonaceous chondrites, a dark, friable material made up mostly of heavy organic molecules, with an appearance similar to that of coal.

Independently, Jacchia (1958) and Ceplecha (1958) first observed the existence of separate meteoroid populations, most easily differentiated by the height of ablation when compared with the meteoroid speed (Ceplecha 1968, Ceplecha 1988), and was

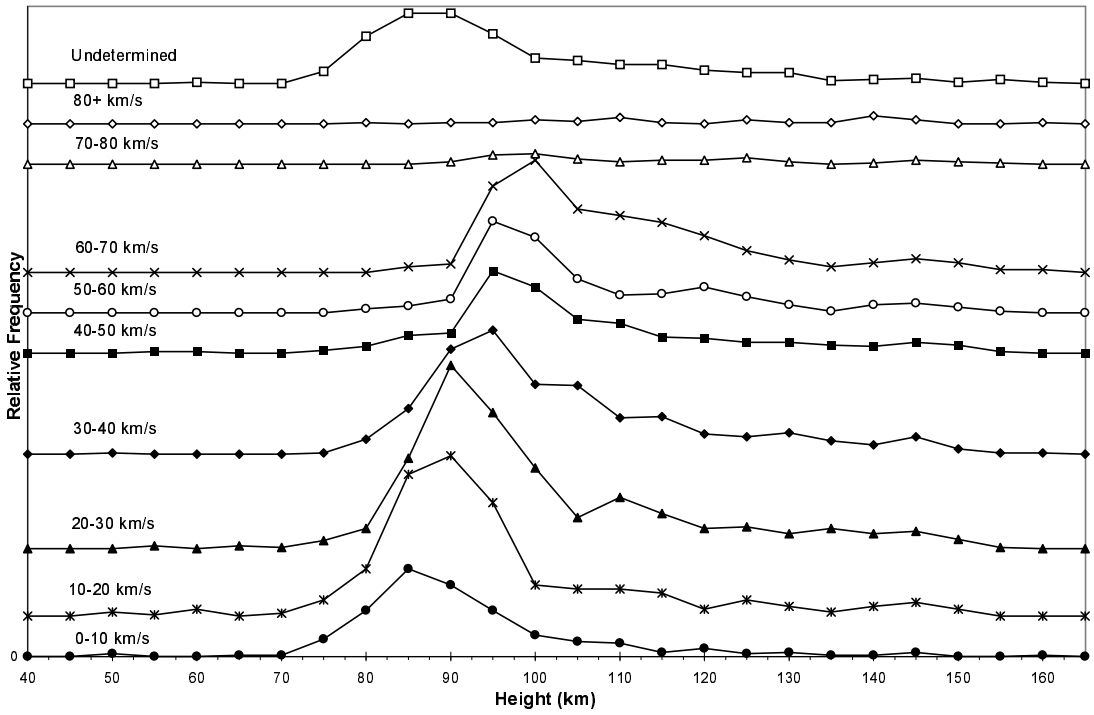

Figure 5.24: Height distribution of meteors detected in April and May 1998 and 1999 at different speeds. The heights are divided into bins of width 5 km centred on the label values. Each distribution has had an arbitrary constant value added for clarity.

extended to faint TV meteors (Hawkes et al. 1984, Jones et al. 1985, Sarma & Jones 1985) The density of the meteoroid body is the main factor attributed to the difference in ablation height. The populations which ablate highest are associated with cometary material, and we would expect the η-Aquarids meteor shower (associated with comet 1P/Halley) to show this property (see Chapter 7 for a detailed analysis of the η-Aquarids). Figure 5.23 shows a scatterplot of speed *versus* height for meteors detected during April and May 1998 and 1999, when the shower is active. The majority of meteor heights occur between 95 and 105 km, and show an increase in height with speed. However, there are a number of meteors ablating higher than expected, at all speeds. As expected. there is a "clump" of meteors with speeds around 66km s^{-1}, and a significant number of these are detected at heights greater than the heights of the sporadic background. There also appears to be a number of meteors with slightly

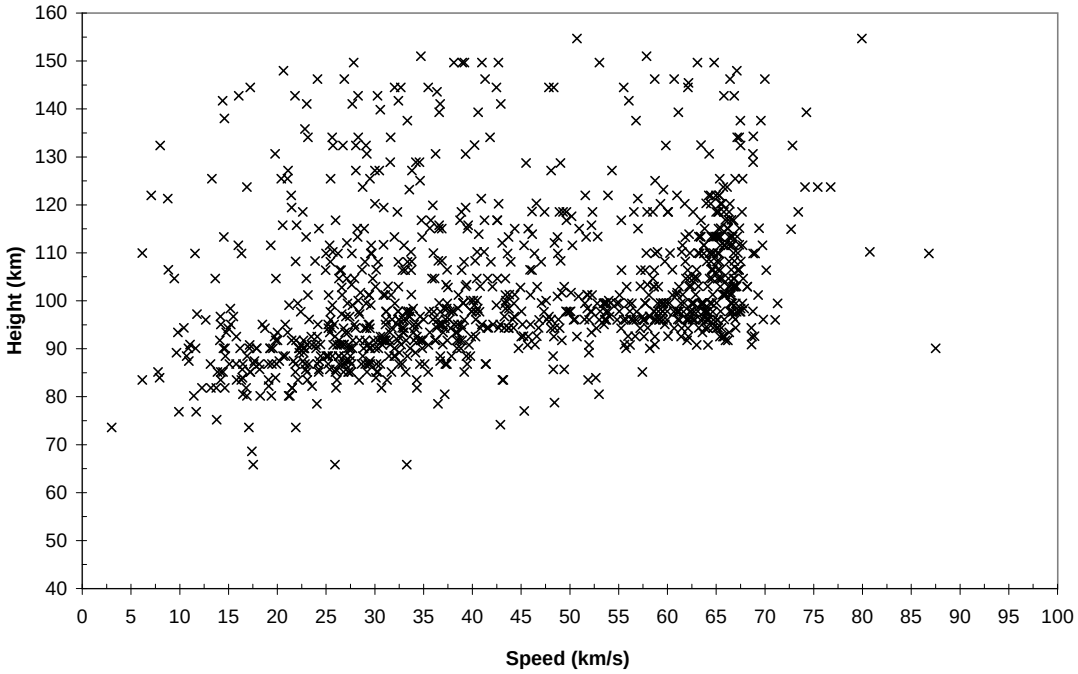

Figure 5.25: Speed-height scatter plot of Class A meteors detected in April and May 1998 and 1999.

lower speeds and heights than the clump associated with the η-Aquarids meteors, possibly due to deceleration of meteoroids from the shower. This is investigated later. There are a large number of meteors with speeds between 0 and 11 km s^{-1}. 11 km s^{-1} is the speed that an object would gain from falling due to the Earth's gravitational attraction, so it is a lower limit for meteoroid speeds. Ablation theory suggests that meteoroids travelling below about 10 km s^{-1} will not produce sufficient ionisation to be detected by the radar. A comparison with the Fresnel transform method shows the pre-t_0 phase method can underestimate the speeds of some low speed meteors (See Section 6.5). It is also likely that there is some contribution in this region from orbiting debris (which should have a speed of about 8-9 km s^{-1}, and that meteoroids which have decelerated to speeds in this region will be detected.

The data presented in Figure 5.23 is shown as height distributions for eight speed intervals in Figure 5.24. The heights are divided into bins of width 5 km centred on the

label values. Each distribution has had an arbitrary constant value added for clarity. The histograms clearly show that the most probable height increases with speed. In addition it is possible to separate the meteors detected into three groups. There is the main group, which has a height range from 70 to 105 km, and the second group range from 105 to 135 km. The heights of these groups increase with speed. The third group ranges from 135 to 155, and seems to have ablation heights independent of their speed. This is difficult to explain, and this "group" may in fact be composed of members of the second group which are "caught" between the hardware height limit at 161 km and an attenuation effect around 135 km. If this is the case, then the populations are extremely similar to those shown by Sarma & Jones (1985) in their plot of the beginning heights of TV meteors against speed, corresponding to two families of meteoroids with densities of 750 kg m^{-3} and 2000kg m^{-3} respectively.

If we look only at the Class A meteors (See Section 6.3.2 for a definition of "Class A"), we obtain the scatterplot shown in Figure 5.25. We can see that this scatterplot shows essentially the same features as Figure 5.23, although many of the meteors with speeds below 10 km s^{-1} are missing.

It is generally accepted that all meteor radars have a well defined height ceiling for underdense echoes due to diffusion and the finite initial radius of trails. However the results shown in Figure 5.23 indicate that a significant number of meteors have been detected well above the height ceiling of about 105 km for the Buckland Park VHF radar.

The occurrence of meteors at heights of 120 km for high speed meteors such as the Leonids is well documented . However, the occurrence of meteors between 105 and 145 km at speeds from 20 to 40 km/s as is indicated in Figure 5.23 would require meteoroids composed of low melting point organic or carbonaceous material (Lebedinets 1991, Elford & Taylor 1997, Steel 1998) (see Section 5.3). It has been suggested that such material comes from recent releases from comets (Lebedinets 1991, Steel 1998). Steel also suggests that there may be many more meteoroids impacting the atmosphere than we would assume from the numbers detected, and there may be a larger danger

to space vehicles than previously thought.

The other question to be addressed is how meteor trails in the height range 105-145 km have sufficient scattering cross-section at radio wavelengths to give echoes with a VHF radar. One explanation is that the radar echoes are from short lived overdense trails, but since the larger proportion of the observed meteors are underdense this can be discounted. Two other possibilities need examining: (1) Do some trails have an exceptionally dense core of ionisation, given the ideas presented by Jones (1995) (2) Can the Earth's magnetic field sufficiently inhibit diffusion to make radar detection more likely? The latter situation has been explored in Section 3.4 where it was shown that durations of radar echoes can be greatly enhanced when the radar beam is close to the orthogonal direction to the magnetic field. Unfortunately, the geometry of the Buckland Park radar is far removed from this condition. At the present time these high altitude echoes are an enigma, and clearly worthy of further study.

5.7 Summary

This chapter detailed observations made with the Buckland Park VHF radar. It covered a selection of types of echoes which were detected, different types of meteor echoes and echoes with other causes, both real (aircraft) and false (periodic noise); and discussion on the mechanisms which produce these echo characteristics. The distinction between transverse meteors, those which reflect specularly, and down-the-beam meteors was described and a subset of the transverse meteor, the aliased head echo was also discussed. A method for making measurements of the diffusion coefficient of meteor trails and deducing their height was discussed, and compared to the range/angle method for estimating the height of ablation of meteoroids. The height of detection of meteor trails was examined at different pulse repetition frequencies and compared with expected ablation heights. The effect of fragmentation on meteor echoes was discussed, along with examples of echoes showing fragmentation. Following this was a discussion on the composition of meteoroids, including the possibility of carbon based

(CHON) or tarry meteoroids which ablate at greater heights than expected for their speed, and the detection of such meteoroids.

Chapter 6

Meteoroid speeds

6.1 Introduction

Accurate measurement of the encounter speeds of meteoroids with the Earth is vital for determining the orbital parameters of these objects. Also of great value is the ability to obtain speed distributions of meteor showers and sporadic meteors, and to be able to detect hyperbolic (interstellar) meteoroids. There have been many methods, both optical and radio, used to obtain the geocentric speed of meteoroids, to varying degrees of precision, and all have their limitations and disadvantages. Optical techniques are very precise, but can only be used at night, and are limited to meteors brighter than about the fifth magnitude (McCrosky & Posen 1961). Television techniques, now using low-light-level TV systems, can detect meteors down to the ninth magnitude (Sarma & Jones 1985, Hawkes et al. 1993), but have small fields of view. These optical techniques can be compared to a modern meteor radar, such as AMOR, operated by Baggaley *et al* which has a limit as faint as +13.0 Magnitude (Baggaley et al. 1994). However, radio techniques have the disadvantage of strong selection effects. Firstly, the effect of initial radius and diffusion means that there is a theoretical frequency-dependent height limit, and since higher speed meteoroids tend to begin ablating at greater heights, they are selected against by this effect (however, see comments in Section 5.3). Secondly, higher speed meteoroids have greater ionisation efficiency, causing radio techniques to

be biased toward higher speed meteoroids.

The main purpose of this section is to describe and discuss the newly developed speed measuring techniques employed in this work. To set this in context we first summarise other radio speed measuring techniques. This is followed by the pre-t_0 phase technique, an adaptation of this technique to transverse head echoes, and also determining speeds from the down-the-beam echo.

6.2 Early and current radar speed measuring techniques

The development of radio methods for measuring meteor speeds has followed the general development of new radio and electronic techniques, such as solid state devices and digital recording and manipulation of data. The techniques are discussed in historical order.

6.2.1 The Range-Time method

The range-time method was developed by Hey & Stewart (1947) (see also Hey et al. (1947)) to measure the velocity distribution of the 1946 Giancobinid meteor shower, and was the first radio measurement of meteoroid speed ever made. The technique was later extended to the simultaneous use of three radars (McKinley & Millman 1949). This gave the meteoroid path in space and the ability to compute the orbit. In the range-time method the meteoroid is assumed to be following a straight path through the atmosphere with a constant speed and to generate intense ionisation around the meteoroid. The radar echo appears to come from a "hard target" at the position of the meteoroid and is usually termed as a "head echo" (see Chapter 5). By displaying the range-time records obtained on a cathode ray tube and recording on a moving

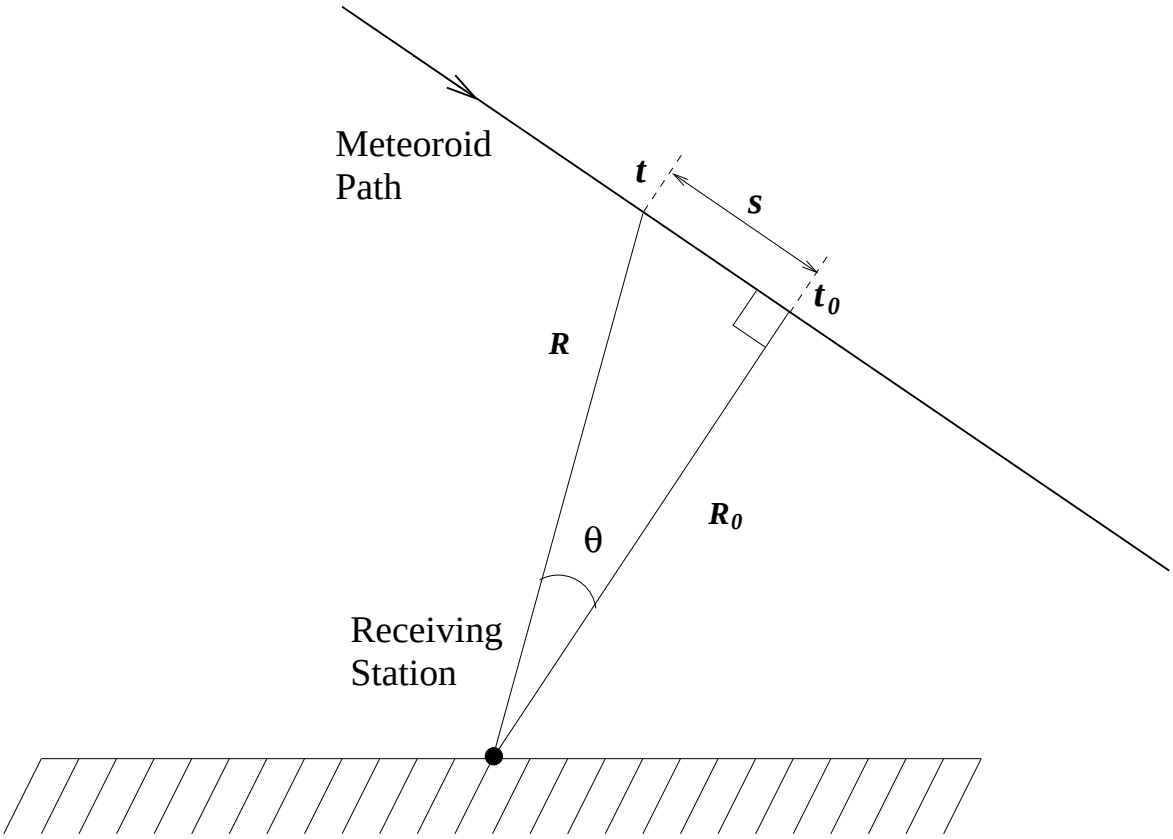

Figure 6.1: Geometry of a meteoroid's path through the atmosphere

film[1], the meteoroid path would show up as a segment of the hyperbola:

$$R^2 = R_0^2 + v^2(t - t_0)^2 = R_0^2 + s^2 \tag{6.1}$$

where s is the distance along the path relative to the point on the path which is closest to the radar (the t_0-point) and R_0 is the distance of that closest point to the station (that is, the range R at a time t_0). The geometry of the situation is shown in Figure 6.1. By fitting this hyperbola to the records the value of v can be found. The technique is applicable only to records (generally the brightest) where the meteor head echo is visible, and records showing the path over many kilometres are necessary to give accurate results. Any deviation from the hyperbolic shape in the record was assumed to by due to the effects of deceleration. This technique is also the basis for the recently developed down-the-beam method discussed later in this chapter.

[1]Hence the name of the "Range-time" technique, after the recording method.

6.2.2 The diffraction method

As a meteor trail is formed in the radar beam it will produce oscillations in the amplitude of the returned signal in accordance with the Fresnel integrals, as discussed in Chapter 3. Herlofson suggested that there should be such oscillations, from which the meteoroid speed could be determined (Herlofson 1948), and Lovell and Clegg showed that the post-t_0 oscillations are well described by the Fresnel theory of diffraction (Lovell & Clegg 1948). The technique was first put into practice at Jodrell Bank (Ellyett & Davies 1948, Davies & Ellyett 1949), and was used to measure speeds of meteors from the Geminids and Quadratids meteor showers; the results showed excellent agreement with photographic observations (Whipple 1947).

This technique has been the basis for the measurement of meteoroid speeds by many other researchers, but could only be used on echoes where several oscillations were clearly discernible in the post t_0 amplitude, and this situation is limited to only about 10 % of all meteor echoes detected (Davies & Gill 1960, Baggaley et al. 1994). The oscillations can be suppressed by a number of factors, including rapid radial diffusion, which means the oscillations are rapidly damped out by decay of the amplitude of the returned signal. However, the most important factor is probably fragmentation of meteoroids prior to, and during ablation which causes the oscillations to be smoothed out (Elford & Campbell 2001).

Figure 6.2 shows the theoretical amplitude Fresnel diffraction pattern for diffraction at a straight edge, plotting returned power (or intensity in the optical case) against the value of x, which for backscatter, is related to the distance s, by the following expression:

$$x = \frac{2s}{\sqrt{R_0 \lambda}} \tag{6.2}$$

Measurement of the value of the amplitude of successive oscillations is not necessary to obtain speeds, and since the ionisation production can be non-linear, using the amplitude would have led to inaccurate results (Ellyett & Davies 1948). Instead the ratios of the theoretical Fresnel Zone lengths for different maxima and minima can be

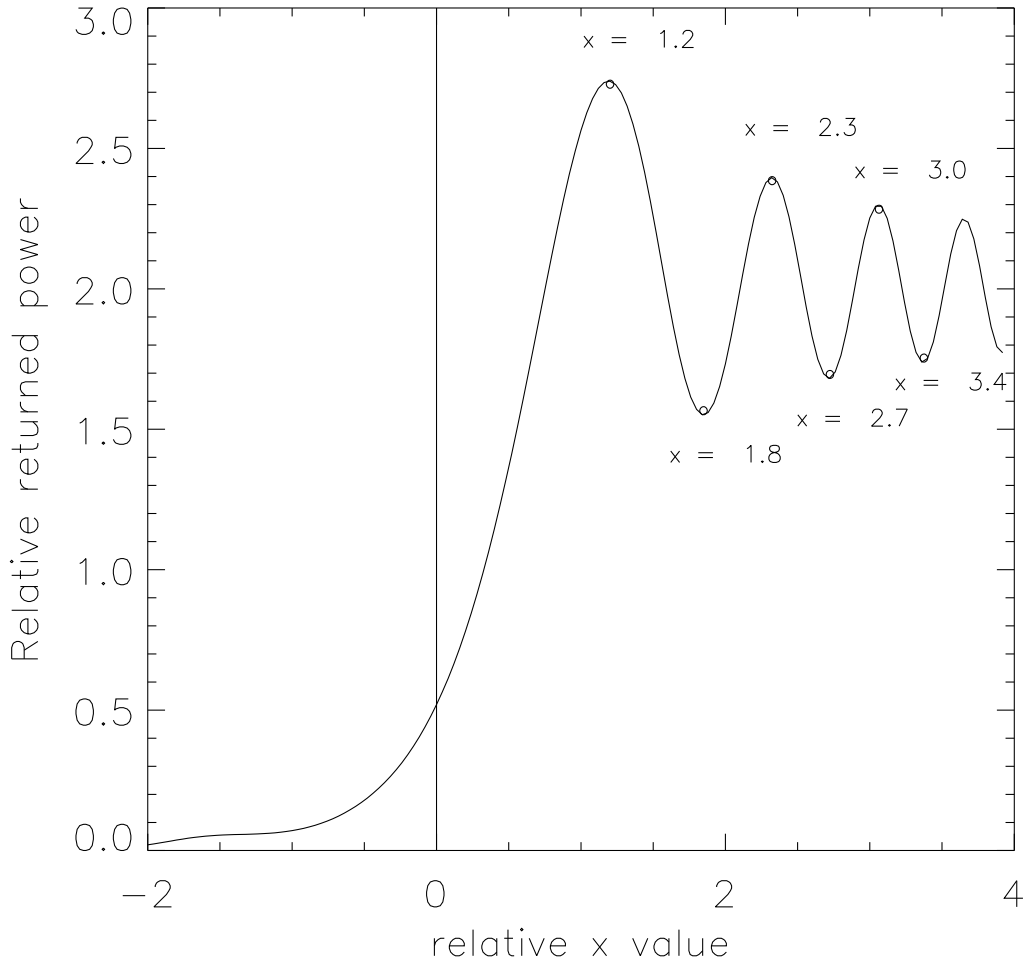

Figure 6.2: The amplitude Fresnel diffraction pattern for diffraction at a straight edge. The values of x are shown for the first three maxima and minima

calculated and compared to the observed diffraction patterns. The positions of the first three maxima and minima in the post t_0 oscillations are marked in Figure 6.2. From the time difference Δt between the n^{th} and m^{th} maxima (or the n^{th} and m^{th} minima) the speed of the meteoroid is given by McKinley (1961):

$$v = \sqrt{R_0 \lambda} \ \ \frac{x_n - x_m}{2\Delta t} \tag{6.3}$$

In a similar way other parts of the oscillations can be used to obtain a speed, and a more accurate method has been developed which uses a least squares fit to the oscillatory pattern to obtain speeds (Baggaley et al. 1994). In this latter case the fitting is started from the first minimum to avoid the time shift which occurs in the

first maximum (Šimek 1966). This method needs at least three oscillatory cycles to give sufficient accuracy in the speed measurement. Where many cycles are present, an estimate of the deceleration of the meteoroid can be obtained by measuring speeds from several sections of the oscillatory pattern.

An important development of the diffraction method was the introduction by McKinley of a phase reference signal, which in combination with the signal returned from the meteor trail, generated a resultant signal with amplitude oscillations prior to the t_0 point (McKinley 1951b, McKinley 1961). McKinley was able to determine meteoroid speeds for many echoes for which the post-t_0 oscillations were absent. As for the post-t_0 analysis, it was the positions of the minima and maxima of the oscillations that were used to obtain the speeds.

This method was used by Nilsson (1962) in his work at Adelaide to measure the orbits of shower and sporadic meteoroids. These observations were made before the introduction of digital techniques, and the data was recorded in analogue form, using a tape delay system to recover the early part of the meteor echo containing the vital pre-t_0 oscillation.

6.2.3 UHF Doppler techniques

A technique for measuring meteoroid speeds at UHF frequencies was developed to investigate both shower and sporadic meteors with the Millstone radar, which operated at 441 MHz (Pettengill & Pineo 1960, Pettengill 1962, Evans & Brockelman 1963, Evans & Brockelman 1964). The technique relied on the ability of the Millstone radar to measure the Doppler shift in the transmitted frequency of a single pulse. The Doppler shift was caused by the motion of the target body during the pulse, which lasted for 2 ms. The receiving system was equipped with a bank of 310 crystal filters, each with a bandwidth of 200Hz and centred on frequencies 160 Hz apart, giving a range of 24 kHz about the transmitted frequency. The Doppler shift was determined by noting the crystal filter which gave the strongest output signal.

If we recall the attenuation of underdense meteor echoes discussed in Section 3.5.1,

the attenuation factor α_r is dependent on the wavelength of the radio waves reflecting from the trail and the attenuation increases as the wavelength decreases. At the frequency used by the Millstone radar, the initial radius will be well in excess of the wavelength for most meteor trails, and only returns from overdense ionisation near the meteoroid will be observed. This means a meteor will only be detected as a small hard target travelling with the speed of the meteoroid (a head echo). The previously described range-time method could not be employed, as the long pulse (2 ms) gave a range error of $\sim \pm 30$ km, but the geometry shown in Figure 6.1 is the same. By differentiating equation 6.1 twice with respect to time we obtain:

$$R\ddot{R} + \dot{R}^2 = s\ddot{s} + \dot{s}^2 \tag{6.4}$$

since $\dot{s}$ is the meteor speed, equation 6.4 can be rewritten as

$$v = \sqrt{R\ddot{R} + \dot{R}^2 - s\ddot{s}} \tag{6.5}$$

Where $\dot{R}$ is related to the Doppler shift measured by the radar. The deceleration was assumed to be insignificant, simplifying the expression by setting $\ddot{s}$ to zero. The rate of change of radial speed, $\ddot{R}$ was determined by fitting a straight line to a plot of $\dot{R}$ against time. By observing meteoroids travelling at small angles to the beam of the radar, a simple expression for $\dot{R}$ can be obtained from the Doppler shift. By performing this analysis on echoes with long trails, it was possible to make several measurements of the speed along the meteor trail, assuming no deceleration in a short interval, and precise measurements of meteoroid deceleration could be made (Evans 1966).

6.2.4 The spaced receiver method

Kaiser was the first to suggest that meteor orbits could be obtained by the use of three or more closely spaced receiving stations (Gill & Davies 1956). The time differences between the stations were used to determine the direction of the meteoroid path, and the speed of a meteoroid was determined by the diffraction method. Thus the orbit could be calculated. We note that these multi-station systems were unable to

determine the elevation and azimuth of the meteors (Davies & Gill 1960). The Adelaide system was an exception, using a phase measuring system to determine the position of the reflection point (Nilsson 1962).

A technique to obtain meteoroid speeds using spaced receivers was developed for use with the Advanced Meteor Orbit Radar (AMOR) (Baggaley et al. 1994). AMOR has three receiving stations with baselines of 8 km, and the meteor speeds were determined by measuring the time differences between the occurrence of an echo at the stations. The AMOR radars use fan shaped beams, narrow in azimuth (3.2° half power full width) on reception, constraining the echo azimuth, and use 5λ phase pair antennas to obtain the echo elevation. The speed and the radiant coordinates can then be calculated from the time delays between the stations. A great advantage of this method is the high yield of speed measurements per echo compared to the diffraction method (about 60 % compared with less than 10 %), although the diffraction method is used wherever possible.

6.2.5 The amplitude rise-time technique

Another technique developed and used at AMOR is the amplitude rise time technique (Baggaley et al. 1997). This technique makes use of the rise of the amplitude of the returned signal, which is described by the Fresnel integrals. The amplitude increases rapidly after the t_0 point, with the greatest rate of change when the phasor is tangential to the spiral at $x = 0.572$ (see Figures 3.3, 6.2). The amplitude increases to a maximum at $x = 1.217$. By measuring the maximum slope of the leading edge of the amplitude and the peak amplitude the meteoroid speed can be found, and is given by

$$v = \frac{1.657\sqrt{R_0\lambda}}{2\tau A_{max}} \left(\frac{\Delta A}{\Delta t}\right)_{max} \tag{6.6}$$

where τ is the pulse sampling period and A is the recorded echo amplitude. This technique has the advantage of not relying on the often-missing Fresnel oscillations and is quite robust even when diffusion is rapid. Comparison with the diffraction method shows the uncertainty in this method to be < 10 % compared to ~ 1 % for

the diffraction method, but it's much wider application and ease of calculation means it is very useful for work where approximate speeds are extremely useful.

6.2.6 The Arecibo Multi-pulse Doppler method

Observations with the Arecibo Observatory 430 MHz radar system have detected meteors (Zhou et al. 1995) as have some other UHF radars (Pellinen-Wannberg & Wannberg 1994). Two related techniques have been used in an effort to obtain speeds and decelerations with the Arecibo radar (Mathews et al. 1997, Janches, Mathews, Meisel, Getman & Zhou 2000, Janches, Mathews, Meisel & Zhou 2000). As with the previously described UHF Doppler technique, the ~ 70 cm wavelength means that in nearly all observations, only the "head echo" is detected. In addition, the radar is generally pointed towards the zenith which tends to select against meteor trails which are orthogonal to the beam, since these would have radiants on the horizon, and the associated meteoroids would have to travel large distances at relatively constant heights, producing trails of relatively low line density.

The Arecibo radar beam has a full width of 10 arc minutes at -3 dB, and the system has range resolution of 150 m and time resolution of 1 ms. This resolution means that a technique similar to the range-time method can be employed very successfully (Mathews et al. 1997). Meteors which travel in the beam but at small angles to the beam axis (down-the-beam) reveal their presence by remaining in the beam over a large height interval. For this case, in equation 6.1, R_0 becomes close to zero, and we have $R \approx s$. Mathews *et al* assume the average meteoroid speed is equal to the change in range over the change in time. This assumption leads to an error in the speed determination depending on the actual angular difference between the reflected signal direction (in the beam) and the meteor path. The true speed is equal to the line-of-sight speed divided by the cosine of the angular difference. However, the examples given show only meteors with angular differences from the beam axis direction of less than 10° so that the error would be less then one percent. Any change in the value of the range-time ratio during the observed flight was considered to be caused by

deceleration of the meteoroid.

A refinement to this technique was the use of a measurement of the phase shift between pulses to give a better estimate of the change in range with time (Janches, Mathews, Meisel, Getman & Zhou 2000, Janches, Mathews, Meisel & Zhou 2000). This refinement is covered in some detail by Janches (2000). The phase technique was extended to all observed meteors, apparently with no regard to the large errors introduced by angular differences. One of the examples given shows an angular difference of more than 40°, giving an error of more than 25 %. This analysis was also extended to determine decelerations by assuming that the change in the instantaneous line-of-sight speed was entirely due to the deceleration of the meteoroid. While some of the change may be due to deceleration, a meteoroid travelling across the beam at a constant speed gives a change in the line-of-sight speed due to the change in the angular difference. This effect is discussed in more detail in Section 6.6, which describes a similar technique for determining speeds from head echoes, but takes into account the angular difference between the path of the reflected signal and the meteoroid path.

6.2.7 The Fourier method used with the SKiYMET radars

The SKiYMET radars are VHF meteor radars designed to observe the entire sky, the direction of arrival of the echo being determined by interferometric means (Jones et al. 1998, Hocking 2000). They have small antenna systems consisting of five vertically directed Yagi antennas for reception and one similar antenna used for transmission. The radar has a large collecting area which improves the detection rate, although with a corresponding reduction in the minimum line density detectable when compared to narrow beam radars. Thus the populations of meteoroid detected differ to those observed by the Buckland Park VHF radar. The SKiYMET radars detect only bright meteors, but over the whole sky, whereas the Buckland Park VHF radar detects smaller meteoroids as well, but only in a small part of the sky.

The analysis of the returned signals makes use of the Fresnel diffraction pattern produced as the meteor trail passes through the t_0 point. As the pattern is formed,

there are periodic oscillations in the inphase and quadrature components of the returned signal, corresponding to the rapid change in the phase of the returned signal. These oscillations are periodic in the square of time (t), and an estimate of the frequency as a function of t^2 can be obtained by a Fourier transform. By modelling the formation of the Fresnel diffraction pattern for meteors travelling at different speeds this frequency can be related to the speed of the meteoroid. This technique is used to determine speeds in real time, but this advantage also leads to limitations, in that any speed below 5km s^{-1} or above 40km s^{-1} is unresolved. The technique when applied to the data from the radar sited in London, Ontario obtained useful entrance speeds for only about 4.5 % of the meteors observed but it is postulated that efficiency as high as 10 % could be achieved with better siting of the radar.

6.2.8 The method used with the ALTAIR radar

The Advanced Research Projects Agency Long-Range Tracking and Instrumentation Radar (ALTAIR) in located in the Marshall Islands and is a powerful dual frequency (160 MHz and 422 MHz) radar with interferometric capability using a 46 m diameter mechanically steered dish (Close et al. 2000). It is principally used as part of the US Space Command satellite-tracking network, and has been used recently for meteor observations to help determine the risk to the satellite population from major meteor showers, such as the Leonids.

The radar produces 6 MW of peak power and has a beam width of 2.8° at 160 MHz and 1.1° at 422 MHz. The angular resolution in UHF is around 0.01° and interferometric techniques within the beam are used to determine the angular position (elevation, azimuth) of each pulse return relative to the bore site of the radar beam. At a 100 km range this translates to 20 m lateral position. It is unclear what is the precision of the absolute angle, but for measuring angular speed that is not important. The range resolution is about ±10 m. The speed and direction of the moving target (in the case of meteors, the ionisation around the head) is determined from the position data by simple geometry and kinematics. Accurate tracking of the meteoric head echo

produces extremely accurate line-of-sight and true speeds. The precision is sufficient to determine the deceleration of the meteoroid.

6.2.9 The Fresnel Transform Technique

As previously noted, the echoes received from a meteor trail as it forms perpendicularly to the radar beam can be considered to be a one dimensional Fresnel diffraction pattern produced by a moving source. This pattern contains information about the structure of the trail which can be revealed by the use of an appropriate Fresnel Transform. Elford (2001b) has developed such a transform which requires the correct speed of the meteoroid to produce a transform with good resolution. If the speed is not accurate to about 0.2 km s^{-1} then the sharp edge in the transform corresponding to the beginning of the trail is affected by oscillations. If the speed is unknown, then it can be obtained accurately by scanning through a number of possible speeds until the optimum shape at the start of the transformed trail is obtained. The major source of error in this method is the uncertainty in the range of the echo, typically about 1 % for the current configuration of the BP VHF radar, leading to an error of about 0.5 % in the speed. A comparison between this method and the pre-t_0 technique is conducted in Section 6.5.

6.3 The pre-t_0 technique for determining the speed of transverse meteors

As mentioned in Section 6.2.2, the phase information in the pre-t_0 portion of a radar meteor echo was exploited by McKinley and others to measure the speed of meteoroids. To make this phase information accessible, a phase reference signal was combined with the meteor echo to produce amplitude oscillations. The change of the instantaneous frequency of these oscillations as a function of time gave the speed of the meteoroid.

It was more than 30 years later that Elford showed that the pre-t_0 phase values

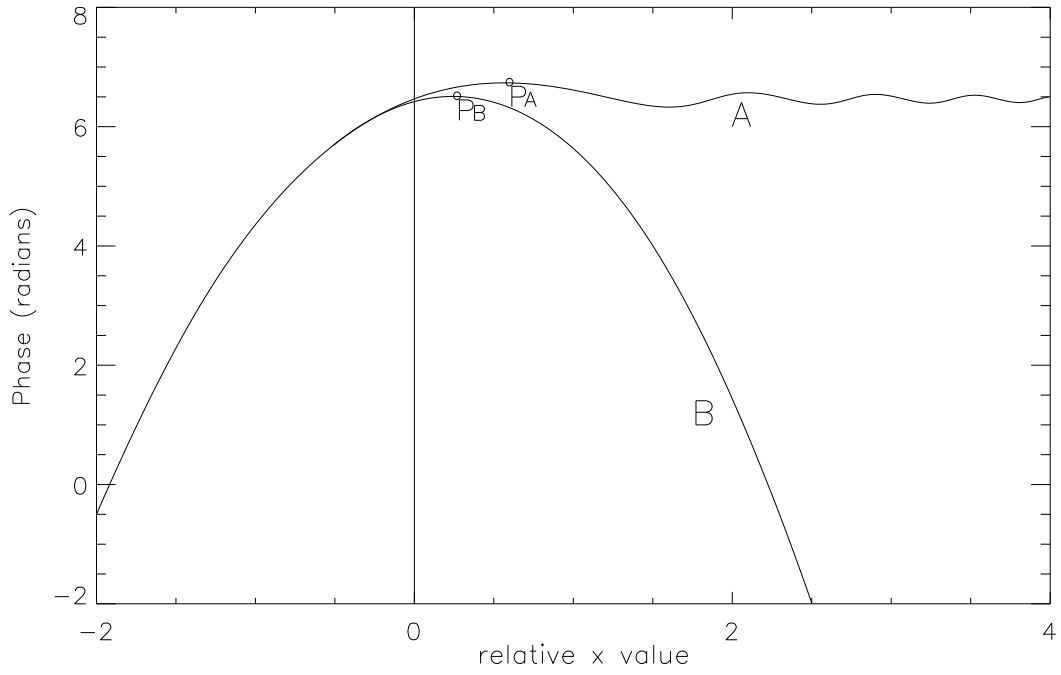

Figure 6.3: Phase of the Fresnel diffraction pattern of formation of a meteor trail for the case of no diffusion (A) and extreme diffusion (B) . The points P_A and P_B show the point of minimum phase on each curve.

were largely unaffected by the diffusion of meteor ionisation, leading to the proposal to use the actual phase values as a measure of the position of the meteoroid relative to the t_0 point on the meteoroid path to determine the speed of the meteoroid (Elford et al. 1995, Cervera 1996).

This technique can be used on echoes where the post t_0 oscillations have been washed out by fragmentation, diffusion or other effects, and as we have already seen, the phase information is available even when the amplitude of the echo is below the level of the background noise or when the amplitude is above the saturation levels of the receivers. In general the technique is considered to be very robust.

6.3.1 Theory of the pre-t_0 method for meteor speed determination

In Chapter 3, it was shown that as the meteor trail is formed, the scattered radio signals produce a moving diffraction pattern in the horizontal plane containing the receiving site. The output of the receivers as a function of time has an amplitude variation that is analogous to that produced by light at a straight edge. Figure 6.3 shows the phase of the returned signal for the case of no diffusion (A) and extreme diffusion (B) with respect to the dimensionless parameter x (See also Section 3.3.3).

6.3.1.1 Preliminary speed measurements

As previously stated in equation 6.2 $x = 2s(\lambda R_0)^{-1/2}$. The Fresnel integrals (equations 3.21 and 3.22) are:

$$\begin{aligned} C &= \int \cos\left(\frac{\pi x^2}{2}\right) dx, \quad \text{and} \\ S &= \int \sin\left(\frac{\pi x^2}{2}\right) dx \end{aligned}$$

The amplitude of the diffraction pattern is given by $\sqrt{S^2 + C^2}$ and the phase by $\arctan(S/C)$. The Cauchy approximations to the Fresnel integrals are valid for the regions $x > 1$ and $x < -1$, and are:

$$C = \begin{cases} \frac{1}{\pi x}\cos\left(\frac{\pi x^2}{2}\right) & \text{for } x < -1 \\ 1 + \frac{1}{\pi x}\cos\left(\frac{\pi x^2}{2}\right) & \text{for } x > 1 \end{cases} \tag{6.7}$$

and

$$S = \begin{cases} -\frac{1}{\pi x}\sin\left(\frac{\pi x^2}{2}\right) & \text{for } x < -1 \\ 1 - \frac{1}{\pi x}\sin\left(\frac{\pi x^2}{2}\right) & \text{for } x > 1 \end{cases} \tag{6.8}$$

Thus the phase behaviour for $x < -1$ is given by:

$$\phi_{x<-1} = \frac{\pi x^2}{2} = \frac{2\pi s^2}{R_0\lambda} = \frac{ks^2}{R_0} \tag{6.9}$$

Assuming that there is no deceleration ($s = vt$), we obtain:

$$\phi_{x<-1} = \frac{2\pi v^2}{R_0\lambda}t^2 \tag{6.10}$$

Thus the speed of the meteoroid can be obtained by fitting a quadratic to the phase data before $x = -1$. The accuracy of this method depends strongly on the number of points of pre-t_0 phase information available, and can attain an error as low as 1 % in the speed, although 10 - 20 % is more common. This method was used in the data processing software to obtain an estimate of the speed for the next method.

6.3.1.2 The phase model method

This was an improved method on that previously described, and was used to routinely calculate meteoroid speeds for transverse meteors where diffusion could be measured. It does not rely on the Cauchy approximations. Instead it uses a model of the expected phase behaviour as a function of x and includes the effects of diffusion, initial radius and direction of polarisation of the radio waves. This modelled phase can be compared to the phase of the returned signal to give the value of x as a function of time, and thus the speed of the meteoroid. This means that more of the phase record can be used to determine speeds, and results in improved accuracy over the parabolic method.

The model was developed by Elford (private communication), and a reprint of a paper detailing the model is reproduced in Appendix A. Elford made the following observations of the outcomes of his modelling:

- A trail with a "classical" ionisation profile produced results which were indistinguishable from those produced by a constant ionisation over the length of the trail. This is due to the section of trail immediately behind the meteoroid dominating the phase of the returned signal.

- A change in the height of ablation corresponds to a change in the ambipolar diffusion coefficient. As this was increased, there was little change in the phase for $x < -1$, and in the region $-1 < x < 0$ there were small changes for heights above 100 km. For $x > 0$ at great heights (large diffusion coefficient) the phase behaviour undergoes large changes, and in the limit the phase approached the parabolic shape seen in Figure 6.3. This is readily explained by the shortened

length of trail making the meteor appear almost as a point source.

- The point of minimum phase moves closer to the t_0 point as the diffusion coefficient increases, from $x = 0.57$ with no diffusion to $x = 0.24$ for extreme diffusion.

- In the region of the phase plot before the point of minimum phase (as shown in Figure 6.3) there was no significant difference between use of longitudinal or transverse polarisation. However this was not the case for the region after the point of minimum phase.

Thus the modelling indicated that the only significant change in Phase *versus* x prior to the point of minimum phase was due to a change in diffusion, and even here the relative change was very small. From this model of the phase of the returned signal, a series of lookup tables of phase against x for different heights (and therefore diffusion coefficients) and speeds were prepared. From the height of the echo and the speed estimated by the parabolic method the appropriate table is selected and used to convert the phase record from phase versus time to x versus time up to the point of minimum phase. A linear least squares fit is used to give the rate of change of x with time. Using the expression in Equation 6.2, $x = 2s(\lambda R_0)^{-1/2}$, differentiated with respect to time the rate of change of x can be transformed into rate of change of distance, that is, speed as follows:

$$v = \frac{ds}{dt} = \frac{1}{2}\frac{dx}{dt}\sqrt{\lambda R_0} \tag{6.11}$$

6.3.2 Preparing the phase data for speed determination

Before the pre t_0 phase data can be used to determine the speed of a meteoroid, the meteor echo record must be subjected to a number of pre-analysis routines, some of which have been described in the previous chapters. First the amplitude, phase and unwrapped phase of the echo record is displayed for manual assessment. If more than

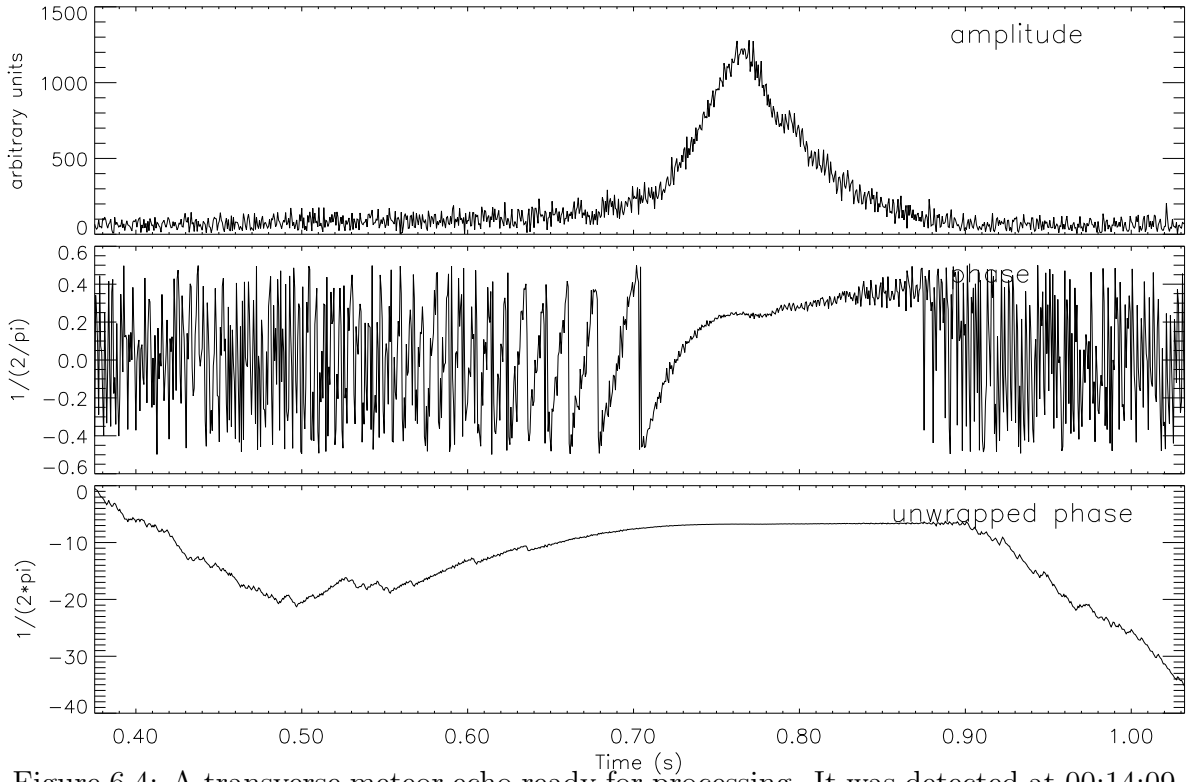

Figure 6.4: A transverse meteor echo ready for processing. It was detected at 00:14:09 UT on the 5th of May 1999

one range bin has triggered as containing an echo, the amplitude of up to ten range bins is displayed.

Figure 6.4 shows a meteor echo record as it would appear when first encountered by the operator, except that the time axis scale has been expanded for clarity. A record would generally show 1.7 to 1.9 seconds of data (depending on the observation settings), but since the sections not shown contained only random noise, they were omitted in order to show more detail in the record. The amplitude series shows a gradual increase in the returned signal, visible from the 0.5 second time mark, but probably beginning before that time; then rising rapidly from about 0.70 seconds to a maximum at about 0.76 seconds and then decaying exponentially. There is a hint of a couple of post t_0 Fresnel oscillations at 0.79 and 0.81 seconds. Based on the theoretical amplitude diffraction pattern the t_0 point, where the meteoroid is at its closest approach to the radar station and the trail is oriented orthogonally to the line-of-sight from the radar, would occur at about 0.74 seconds. Soon after this, the meteoroid is at

the central Fresnel Zone and the echo amplitude reaches its maximum amplitude. The echo amplitude then quickly decays as the trail diffuses due to ambipolar diffusion.

The phase series shows what appears to be random variations in phase except for a coherent area from 0.7 to 0.9 seconds, but closer inspection reveals that the area from about 0.5 seconds on is coherent, but is broken up by the discontinuities caused by the calculation of the arctangent, which can only take values from π to $-\pi$ radians (Note that the phase and unwrapped phase series are shown in units of cycles, not radians; one cycle equals 2π radians). The phase unwrapping, discussed in Section 4.1 removes these discontinuities by adding or subtracting multiples of one cycle to the data. Visible in the wrapped phase series are the Fresnel oscillations at 0.79 and 0.81 seconds, and the slow phase change from 0.78 to 0.92 seconds caused by the radial wind drift (see Section 5.4). In the unwrapped phase record it can be seen that the phase is coherent back to 0.5 seconds, but the unwrapping algorithm has failed in a number of places, at 0.64, 0.61, 0.57 and a region from 0.55 to 0.53 seconds. Of note however is the large number of cycles of phase visible back from the t_0 point (at least ten). This change is so much larger that the change due to wind drift that the latter section looks almost flat.

A close inspection of Figure 6.4 reveals the presence of a low level periodic signal, identified as the consequence of a design fault in the system. As described in Section 4.2, this signal can be reduced by a Fourier transform technique, and the result of this process is shown in Figure 6.5. The signal-to-noise ratios of the amplitude and phase series have improved significantly, allowing another post t_0 Fresnel oscillation to be seen at 0.83 seconds; in the unwrapped phase, all but one of the discontinuities has been removed, showing coherent phase well before 0.5 seconds. Note that when removing the periodic noise the entire record is used, not the shorter one as shown, since the larger the data length supplied to the Fourier transform, the better the frequency resolution. After the periodic noise reduction the operator would usually change the scale of the display to enable better selection of the regions of the record required for the speed analysis.

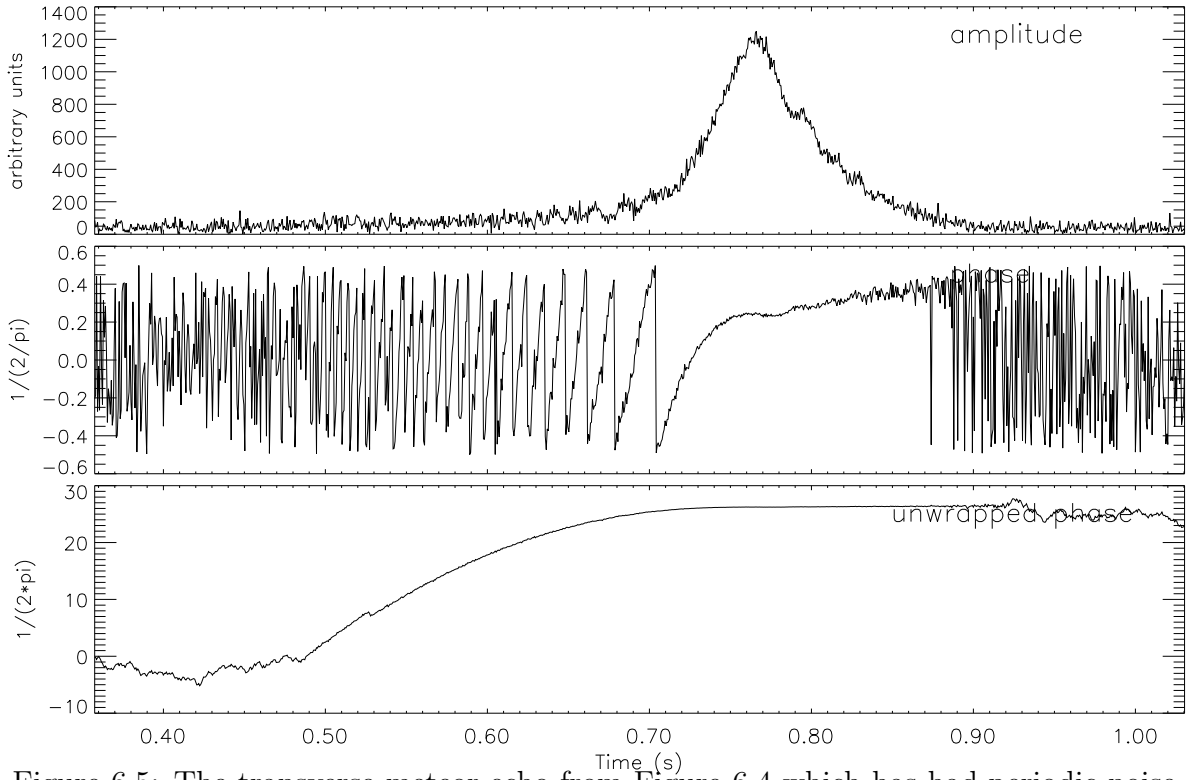

Figure 6.5: The transverse meteor echo from Figure 6.4 which has had periodic noise reduction applied.

Since there is still one discontinuity in the unwrapped phase record it is of interest to examine the effect of applying a three-point boxcar average to the inphase and quadrature data. This process, which is described in Section 4.3, would not usually be applied except to try to remove a discontinuity such as in this example. The result of the coherent smoothing is shown in Figure 6.6 with over twenty-five cycles of coherent phase change[2]. Of note also is the further increase in signal-to-noise ratio in both the amplitude and the phase records.

Now that the phase record has been "cleaned" of periodic noise, and unwrapped, the speed measuring algorithm can be applied. The first step is to estimate the diffusion coefficient. The amplitude record as shown in Figure 6.7 is displayed and the operator selects the beginning and end of the decay section in the amplitude record.

[2]A boxcar with more than three points or two points usually causes more discontinuities by rounding off their edges but a three-point boxcar rarely produces more discontinuities, and can often remove them. In this case the smoothing succeeds in removing the discontinuity, although it introduces one around 0.5 seconds.

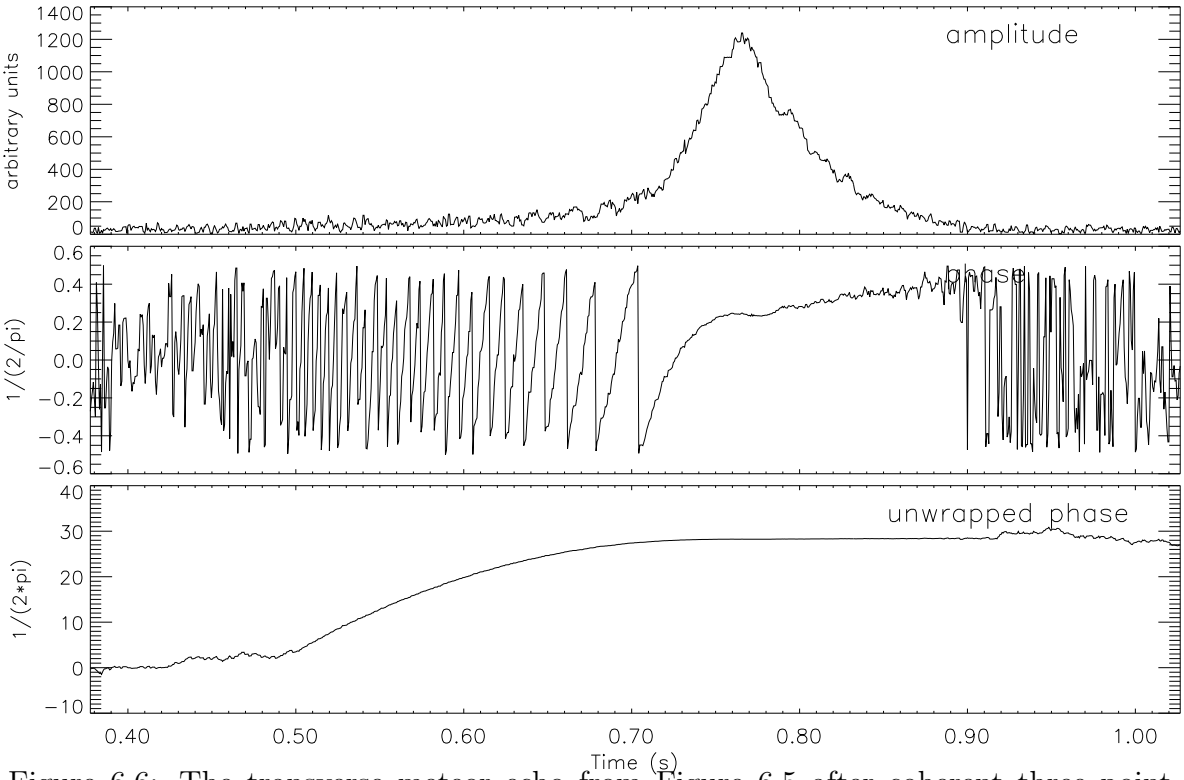

Figure 6.6: The transverse meteor echo from Figure 6.5 after coherent three point boxcar smoothing has been applied.

If no decay is present then this stage is skipped. The diffusion coefficient is estimated as explained in Section 5.2. In this example the diffusion coefficient was estimated to be 3.95 m^2s^{-1}. This corresponds to a height of around 95 km (with an error of about 5 km), if the effect of the geomagnetic field on diffusion is ignored. The range of the echo was 106.8 km, and at an off zenith beam tilt of 30° this gives us a height of 92.5 km assuming the meteor was detected in the central lobe of the antenna, which appears to be the case. The diffusion height of the echo is used later to decide which phase model is used when calculating the speed of the meteoroid. In creating the phase models, height was used to determine the value of the diffusion coefficient used in calculations (the effect of the geomagnetic field was ignored here also). This means that the estimate of the height from the diffusion coefficient may have an error due to the effects of the geomagnetic field, but these errors are not carried into the speed calculations, as we simply need the diffusion coefficient to select the model.

In general, each phase record has a Doppler shift due to the action of the local

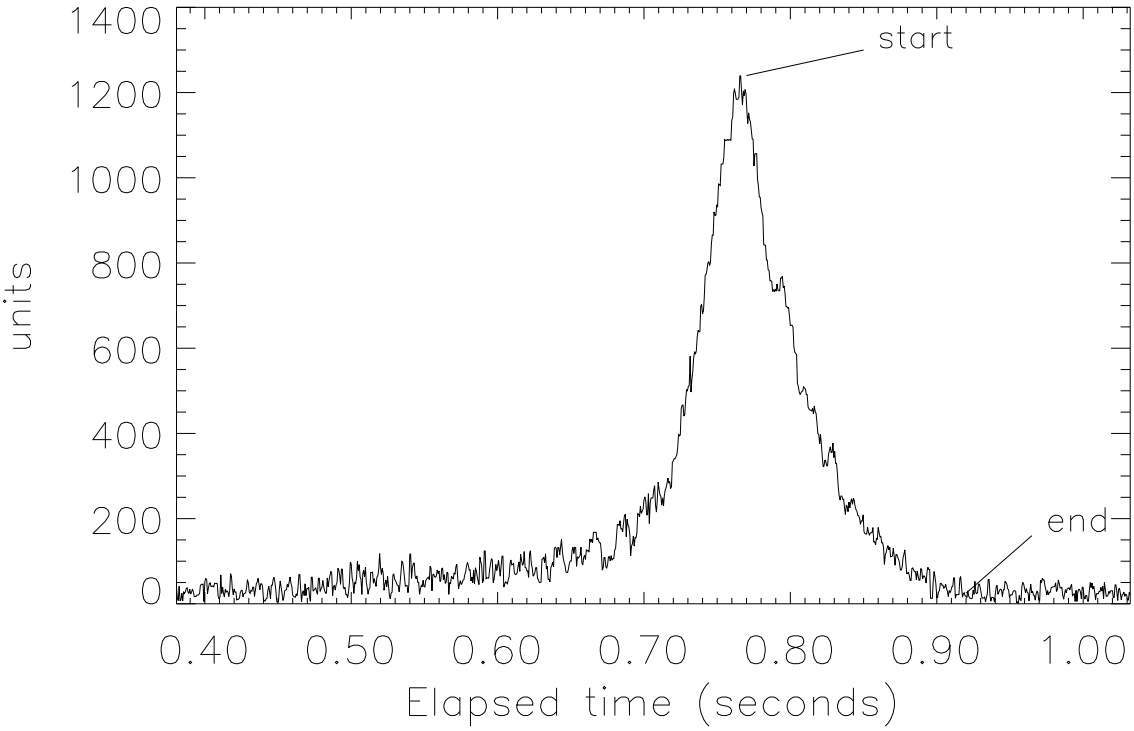

Figure 6.7: Estimating the diffusion coefficient from the amplitude decay. The points shown are the start and end point as selected by the operator.

wind on the forming trail, and the effect of the radial wind drift must be removed from the phase record. The Doppler shift, Δf is given by:

$$\Delta f = \frac{d\phi}{dt} \tag{6.12}$$

where ϕ is phase and t is time. The Doppler shift can be measured from the echo by fitting a straight line to the linear portion of the phase after the time of maximum amplitude, and this is shown in Figure 6.8 (the fitted line has been extended for clarity). Note that the phase is now shown in radians and not in cycles as previously. For this echo the measured radial wind speed was 3.7 ms^{-1} and this speed is recorded as part of the output of the code.

If the returned complex signal from a meteor trail which has experienced a constant Doppler shift over a time, t is E', then the signal with the Doppler shift detrended is:

$$E = E' e^{i\xi} \tag{6.13}$$

where $\xi = t\Delta f$ is the change in phase over time due to the Doppler shift. If p' and q'

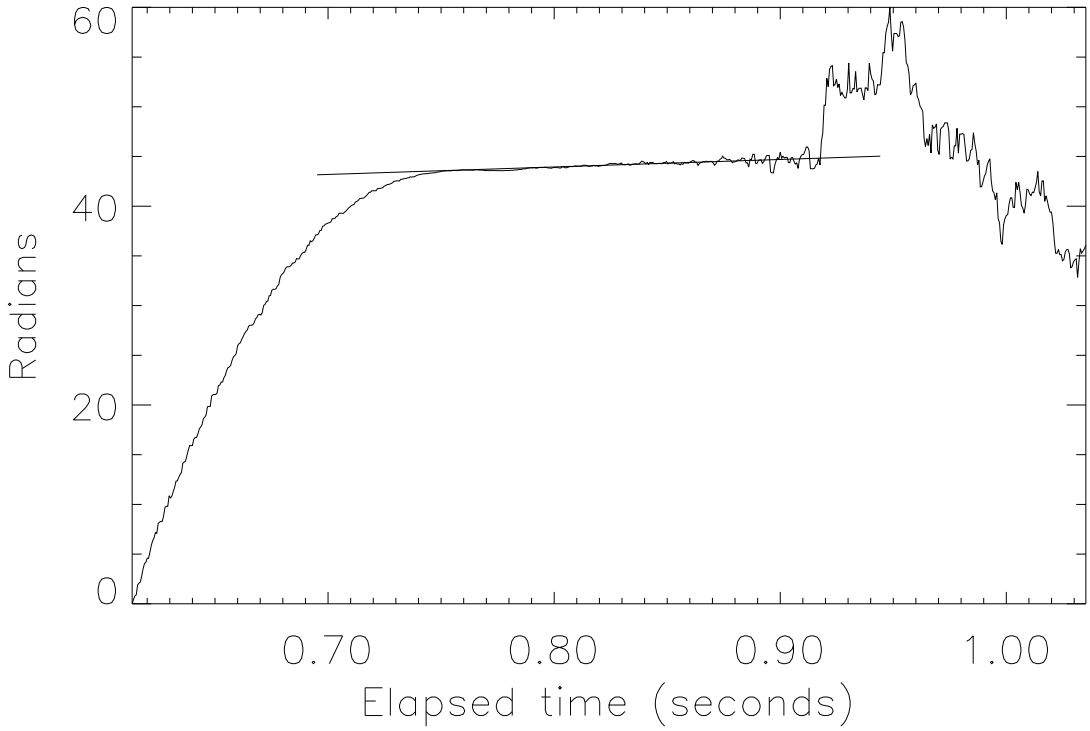

Figure 6.8: Detrending the radial wind drift. Shown is part of the unwrapped phase series from Figure 6.6 with a straight line fitted to the wind drift.

are the inphase (real) and quadrature (imaginary) components of E' and p and q are the inphase (real) and quadrature (imaginary) components of E then we can write:

$$\begin{pmatrix} p \\ q \end{pmatrix} = \begin{pmatrix} \cos\xi & \sin\xi \\ -\sin\xi & \cos\xi \end{pmatrix} \begin{pmatrix} p' \\ q' \end{pmatrix} \tag{6.14}$$

This equation is applied to the phase data and the result is shown in Figure 6.9 which also shows the start point and the region of the minimum phase point which are selected by the operator to begin the speed measurement. All but the last twenty points of the selected phase are least squares fitted with a quadratic to give a first guess at the speed using the Cauchy approximations to the Fresnel integrals (see Equation 6.10). The reason that the last twenty points (those nearest the phase minimum) are omitted, is that the Cauchy approximations are not valid for $-1 < x > 1$, and the phase minimum occurs close to $x = 0.5$, so omitting the points reduces the error in the first estimate of the speed.

This speed estimate, along with the diffusion height determined earlier, is used to

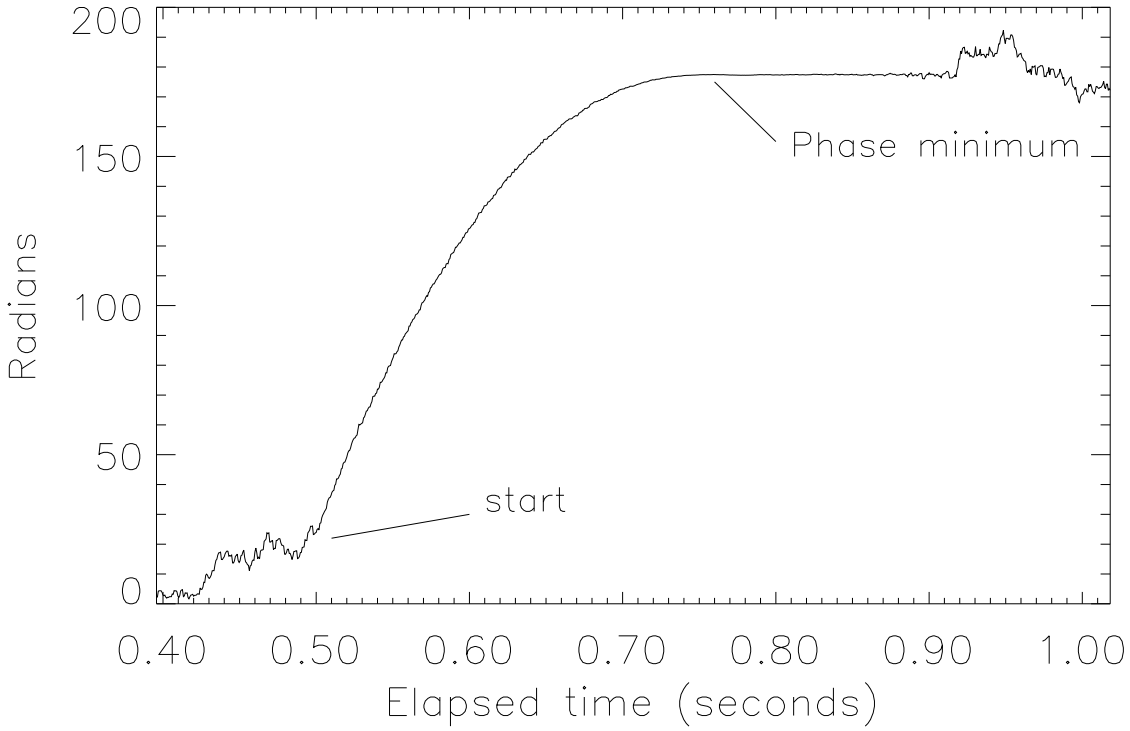

Figure 6.9: Unwrapped phase series from Figure 6.6 with the radial wind drift detrended. The points shown are the start and phase minimum as selected by the operator.

select the appropriate sets of phase obtained from the model. The full set of phase data as selected by the operator is transformed into x values by making the arbitrary value of the phase minimum on the record equal to the model data minimum value. Working back along the adjusted phase data, each point of this data is transformed to the appropriate x value of the selected look-up table of (x, Φ). Once the phase *versus* time data has been transformed into x *versus* time, a linear least squares regression is used to produce the slope of the line. An expression to convert the slope to a speed can be obtained by differentiating Equation 6.2:

$$v = \frac{ds}{dt} = \frac{dx}{dt}\frac{\sqrt{R_0\lambda}}{2} \tag{6.15}$$

where the range of the echo is used as the value of R_0.

As the choice of the position of the phase minimum on the record could be affected by noise, it is assumed that the "true minimum" could possibly occur at a slightly earlier or later time. Thus the process is repeated for each of the twenty points on

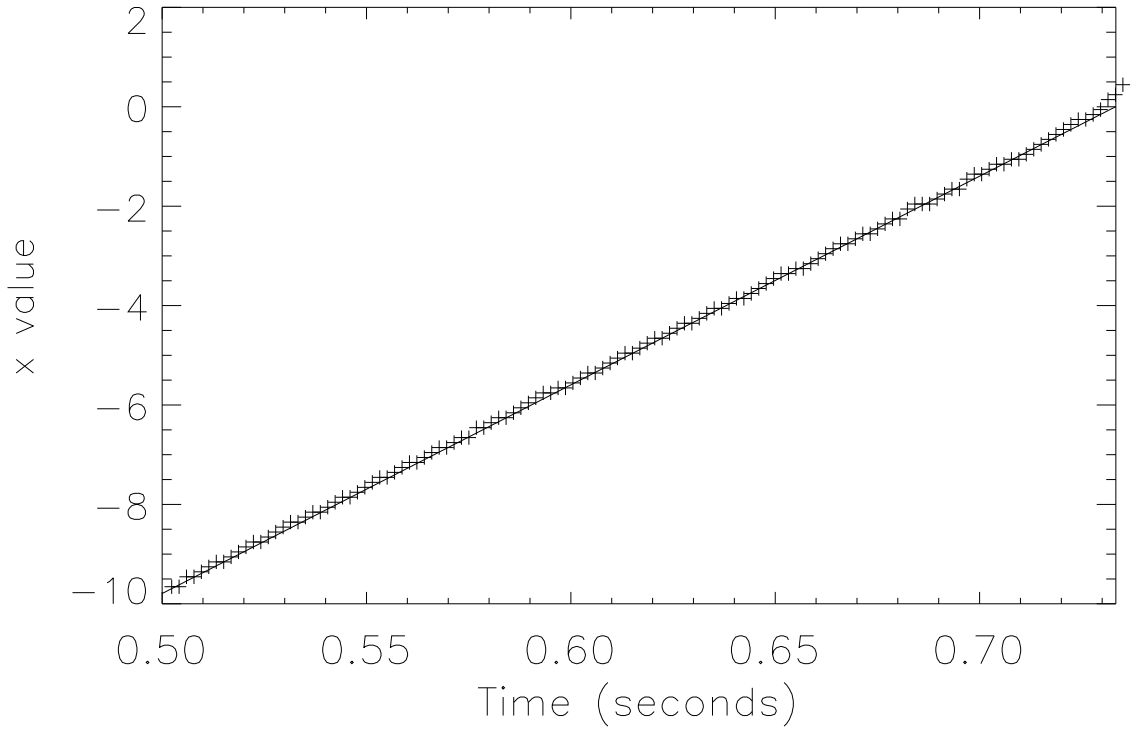

Figure 6.10: Dimensionless variable x versus time for the data selected in Figure 6.9. The '+'s represent the recorded data and the line is the linear least squares fit to the data

each side of the phase minimum point selected by the operator. For each of the forty-one values for the slope calculated, the variance, σ^2 is also calculated, using the expression:

$$\sigma^2 = \frac{1}{n-2}\sum_{i=0}^{n}(f_i - s_i)^2 \tag{6.16}$$

where n is the number of points, the values of s_i are the values of x to be fitted and the values of f_i are those generated by the linear regression as a fit to the s_i. The phase minimum position from the forty-one which produced the minimum value of σ was chosen as the best fit, and the corresponding slope was used to calculate the speed of the meteoroid. The variance was also used to give the standard error in the slope, s_{slope} as follows:

$$s_{slope} = \frac{\sigma}{\sqrt{\sum(s_i - \bar{s})^2}} \tag{6.17}$$

where $\bar{s}$ is the mean value of the x values of the data. When combined with the error in the range (estimated to be half the range bin width of 2 km) this gives an estimate of

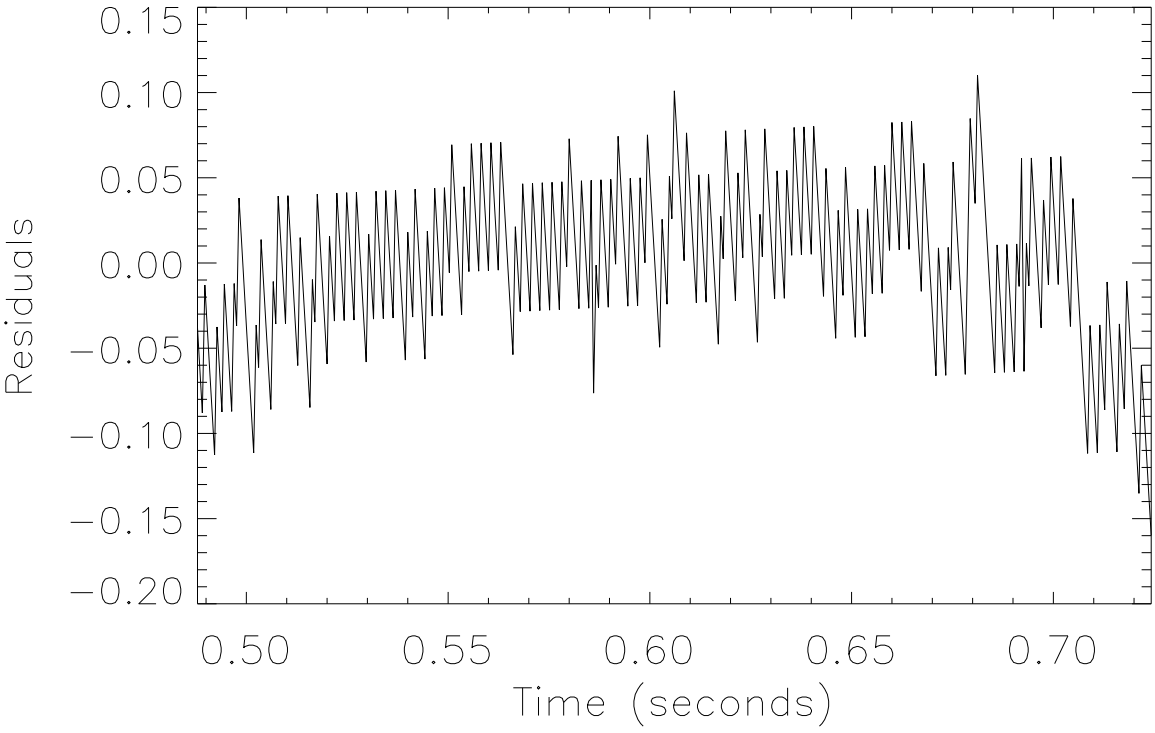

Figure 6.11: Residuals of the linear least squares fit to the data selected in Figure 6.9. The residuals are the differences between the data and the fitted line

the error in the speed. Figure 6.10 shows a plot of x versus time for the data selected in Figure 6.9. The "+" signs represent every third value of the data (for clarity) and the line is the linear least squares fit to the data. The phase minimum point with the smallest value of σ has been used to transform the data from phase into x. It is plainly visible how well behaved the x data is, especially considering that at 0.5 seconds the amplitude of the echo is barely visible above the noise.

Figure 6.11 shows the residuals of the linear least squares fit shown in Figure 6.10. The residuals are the differences between the data and the fitted values of x plotted against time. The rate of change of x was estimated as 41.21 units per second with $\sigma = 0.0406$, and this corresponds to a speed of 15.85 ± 0.07km s^{-1} The reason that the residuals seem to have such a wide range is that the values of phase are only calculated for every 0.1 units of x. In this case the change in x between points is smaller than this, and therefore the converted x values are quantised. This results in a series of values which ascend like a flight of stairs. When a line is fitted to this the error is

small, but it produces a residual plot which jumps up and down rapidly with each "stair". Note that the residuals are smaller than 0.05 x for nearly all of the data, and the data ranges over 10 units of x. Most of the error in the speed determination is actually due to the uncertainty in the range.

If we compare the initial estimate of the speed (using the parabolic method) with the final result (the model method) we often find they are different. This is because much of the phase information is ignored when using the parabolic method, and this can produce large errors when used on echoes where little phase information is available. If we separate those echoes where the two methods produce speeds which differ by less than 5 %, then we can be extra confident of the accuracy of the speed. This subset of meteors are defined as "Class A" meteors, with the remainder being "Class B". Of all meteors where the speed could be determined, Class A meteors made up 38.8 %. The properties of this subset of meteors are essentially the same as the whole set, with no major differences in speed or height distribution.

6.3.3 Deceleration of meteoroids?

From the residual plot of Figure 6.11 it would seem that a quadratic fit to the data may be appropriate since there is a curvature in the plot. Fitting a second order polynomial to the data would then produce a deceleration for the meteoroid. In practice this is not possible for most echoes as the effect of the deceleration is smaller than the error in the measurements. Looking at the axis scale of the residual plot (Figure 6.11) compared to the axis scale of the x versus time plot (Figure 6.10) it can be seen that the curvature produces a difference in the x values which is two orders of magnitude smaller than the range of x. Consider Figure 6.10, which spans 0.23 seconds. In this time, assuming no deceleration, the distance the meteoroid would travel is 3646 m. If we assume the speed at the beginning of the record to be the calculated speed of 15.85km s^{-1} and a moderate deceleration of 5km s^{-2} which is constant over the duration of the record,

the application of the kinematic equation:

$$s = v_0 t + \frac{1}{2} a t^2 \tag{6.18}$$

where v_0 is the initial speed and a is the acceleration over a time, t, gives a total distance, s of 3513 m. This is a reduction of about 132 m, or about a 4 % change compared to the no deceleration distance. If we were to use another kinematic equation:

$$v_t^2 = v_0^2 + 2as \tag{6.19}$$

where v_t is the final speed after time t, then we obtain a speed of 14.70km s^{-1}, a difference of about 1.2km s^{-1}. This effect should be visible if present, and this leads us to conclude that the deceleration of this particular meteoroid during the observation is smaller than 5 km s^{-1}. Fitting a quadratic to the data in Figure 6.10 yields an initial speed of 15.55km s^{-1} and a deceleration of 0.84km s^{-2}, leading to a difference in s due to the deceleration of 22 m (or 0.5 %, about the same as the error in the measurement of the speed) and a difference in the speed of about 0.3 km s^{-1}.

The deceleration of a meteoroid can be estimated from ablation theory (Equation 3.3), and it depends on the size, shape, density and speed of the meteoroid, as well as the air density (*ie* its height). For the point of maximum ionisation, a meteoroid with an initial speed of 20km s^{-1} which produces a maximum electron line density (which relates to the size, shape, density and speed) of 10^{12}electrons m^{-1} the deceleration is about 5km s^{-2}. Deceleration increases throughout the interaction with the atmosphere as it is proportional to the local atmospheric density. Larger objects (which will produce more ionisation) will be decelerated by a smaller amount, since they have a smaller surface area to mass ratio.

Decelerations have been determined from measuring the speed on echoes with aliased pre-t_0 phase such as in Figure 5.8, producing speeds at two different times in the record, allowing an average deceleration to be determined, but this type of echo is rare.

6.4 Adaptation of the pre-t_0 technique to aliased transverse head echoes

If we recall the examples of meteor echoes in Chapter 5, in particular Figures 5.11, 5.10 and 5.8 we see there are cases where there is a return from the meteor trail which occurs only in one range bin, but the phase record shows a parabolic shape, and often there is no sign of the characteristic shape of the phase around the t_0-point. For a beam width of 3° the beam is about 5.5 km wide at a range of 100 km. With the range bin width of 2 km, the largest possible angle a meteor trail can make to the beam and still produce a return in only one range bin is 71°. If we define a transverse echo as one which only occurs in one rangebin, then these special cases with no t_0-point can be labelled "transverse head echoes", as the returns away from the t_0-point are mostly from the area immediately around the meteoroid body (or "head"). The parabolic behaviour is caused by aliasing in the phase record (discussed later in this section), so we then label these echoes as "aliased transverse head echoes".

If the t_0-point is not visible in the record, then the previously mentioned phase model method cannot be used to find the speed, but since the phase record is far from the t_0-point, we may be able to adapt the Cauchy Approximations to find the speed.

The phase record of these echoes contains a parabola or part of a parabola which looks like the parabolic behaviour of the phase under extreme diffusion shown in Figure 6.3. While it is possible that the phase record of the echo is due to the echo passing through the t_0 point with extreme diffusion, the amount of diffusion required to give the shape in Figure 6.3 is so extreme that it is unlikely that the atmosphere is dense enough to cause any appreciable ablation, and the height would certainly be above the ceiling for radars operating in VHF frequency region[3]. We must conclude that this type of echo is caused by aliasing of the phase record. This happens when the phase is changing so quickly that the difference in the phase value between two consecutive pulses is greater than one cycle. Combined with the effect of the unwrapping, this

[3]See Chapter 7 for more discussion on this ceiling effect

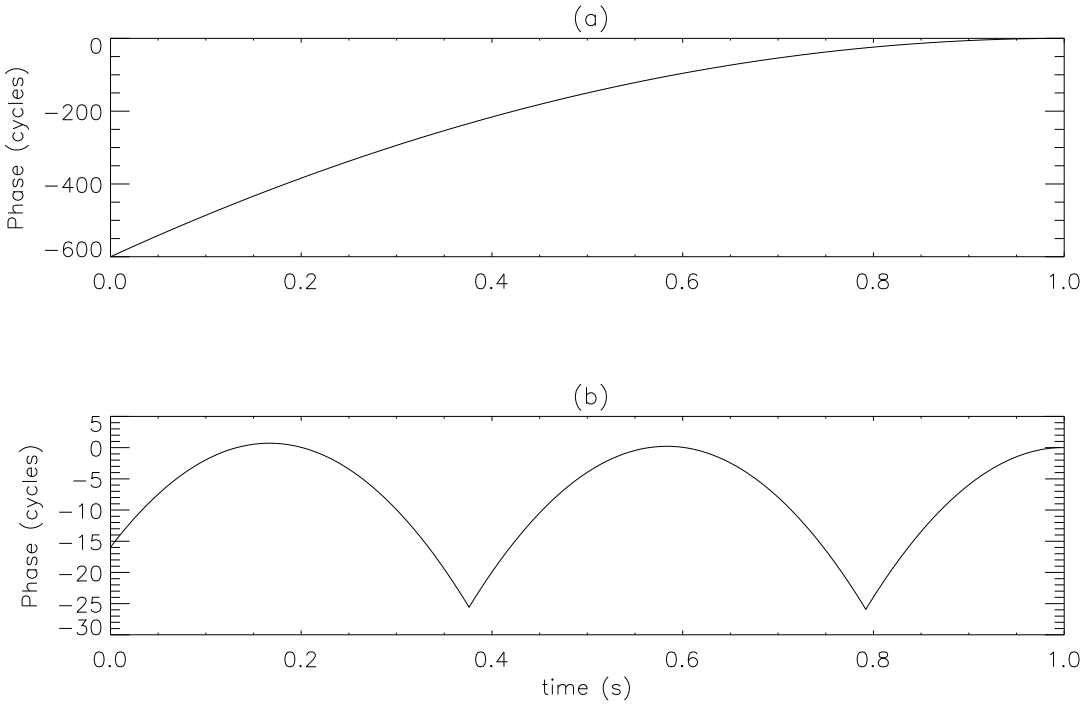

Figure 6.12: The effect of aliasing due to rapid phase change. Panel (a) shows one second of phase parabola sampled at 2000 Hz. Panel (b) shows the same phase sampled at 250 Hz. Both phase series have been unwrapped.

gives rise to a number of parabolae, joined end to end, with the last one peaking near the t_0 point. Figure 6.12 shows this effect. Panel (a) shows a phase parabola sampled at 2000 Hz, and panel (b) shows the same data sampled at 250 Hz. Both panels have been unwrapped from right to left. The aliasing due to the sampling frequency is obvious in the second panel where the phase has been unwrapped into two parabolae centred on 0.175 and 0.575 seconds. The rightmost parabola, peaking at 1.0 seconds, is identical to the rightmost portion of panel(a), note the difference in the scale of the two panels. The parabola at 0.175 seconds is missing two cycles between each point and the second, at 0.575, is missing one. These parabolae appear to closely match the rightmost (original) parabola, and it can be demonstrated that if the original parabola is a quadratic then these aliased parabolae will be described by the same quadratic, simply displaced in time. Fitting least squares quadratics to aliased phase generated from the Fresnel integrals showed an error in the squared term of 1.4 % when the

quadratic is fitted to half of the aliased parabola (from 0.375 to 0.575 seconds in Figure 6.12 (b))when compared to a fit of the whole of the unaliased phase. A similar fit to the whole of the parabola (from 0.375 to 0.79 seconds) gave an error of 0.15 %, the errors due to the reduced number of points, and supporting the hypothesis that the phase obeys a quadratic relation (Equation 6.10). This property means that the speed of the meteoroid can be obtained from one of these aliased parabolae as if it were the original parabola, but with no errors due to the effects of diffusion or closeness to the t_0 point. A simple quadratic is fitted to the aliased phase, which obeys the expression in Equation 6.10, assuming that acceleration is zero, and the speed is easily determined. If the deceleration is not zero then Equation 6.10 becomes:

$$\phi_{x<-1} = \frac{2\pi}{R_0\lambda}(v_0 t + \frac{1}{2}at^2)^2 \tag{6.20}$$

where v_0 is the speed of the meteoroid at the start of the record, t is the time from the start of the record and a is the deceleration. It would be necessary to have either large decelerations or long records for the deceleration to be visible in the phase record, but any measurements of the speed made by using aliased parabola would show the speed at the time of the formation of the parabola not the t_0 point, so for cases where both an aliased parabola and the t_0-point can be used to obtain speeds, decelerations can be estimated from the two measurements.

This section of the program is activated if the previous section to determine the ambipolar diffusion coefficient has been bypassed by the operator (since there is no decay curve to fit). The errors are determined in a similar way to that previously described for the model fitting technique.

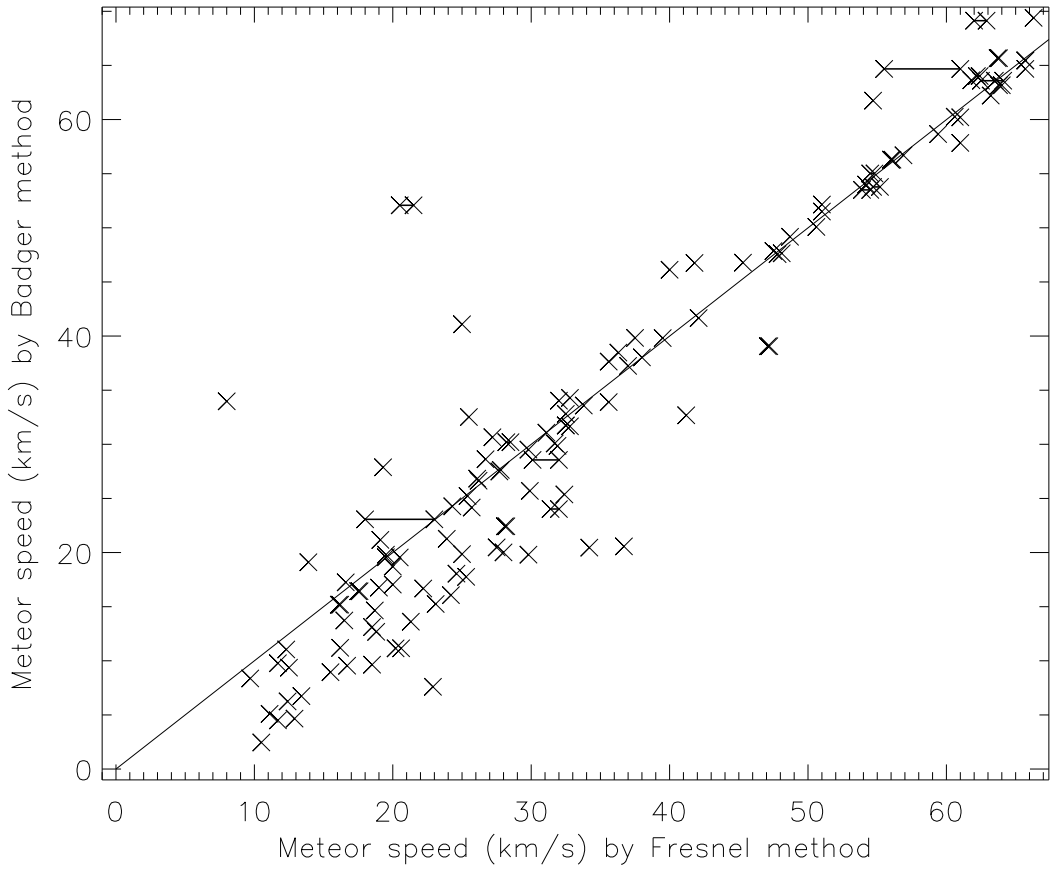

Figure 6.13: Comparison of the speed of 141 meteor echoes detected on 01 May 1998. The solid line has slope = 1. The "x"s which are joined by horizontal lines are echoes where two different speeds have been measured by the Fresnel transform method.

6.5 A comparison of the pre-t_0 phase method and the Fresnel transform method for measuring speed

A comparison between the Fresnel transform method for determining the speed of meteoroids and the pre-t_0 phase method, including the adapted method applicable for aliased head echoes was conducted using a number of meteor echoes recorded on 01 May 1998 by Campbell (Private communication). Figure 6.13 shows a plot of the speeds resulting from the Fresnel transform method against the speed as determined by the combined pre-t_0 methods (Badger method). The "x"s which are connected by

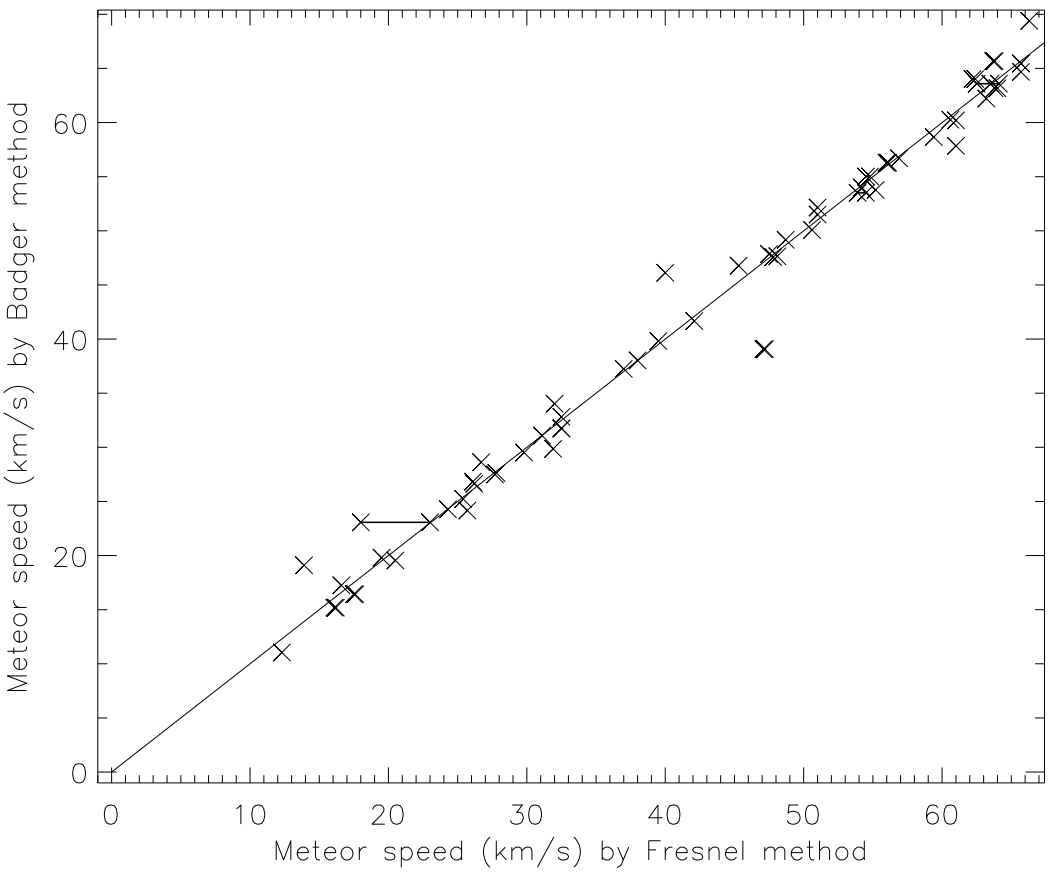

Figure 6.14: The speeds of meteors from Figure 6.13 excluding Class B meteors.

a horizontal line are cases where more than one speed was determined for that echo. This is generally due to fragmentation of the meteoroid body, and the subsequent formation of two (or more) ionised trails. Depending on the distance between the trails, and how they move with respect to each other, this can cause errors in the pre-t_0 method, which assumes that the phase of the received signal is reflected from only one meteor trail.

The methods generally show good agreement, especially for speeds greater than 30km s^{-1}. Below 30km s^{-1}, many speeds are underestimated by the pre-t_0 phase method, typically by about 5 km s^{-1}. This is due to two factors affecting slower meteoroids. Firstly, the ionisation production of meteors reduces rapidly with the speed. This reduces the amplitude of the returned signal, and thus the signal-to-noise ratio of the record. It also means that the returned signal prior to the t_0 point is

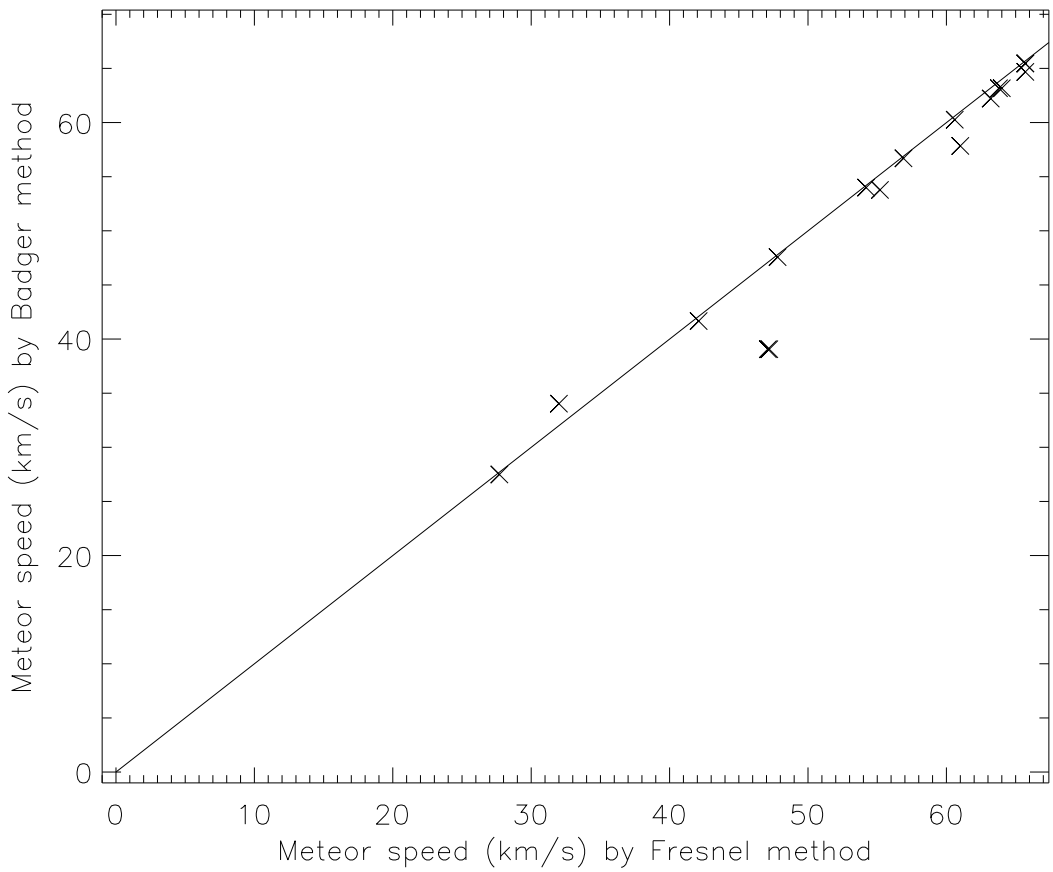

Figure 6.15: Comparison of the aliased head echo (Badger method) and Fresnel transform methods.

weaker and reduces the number of data points in the pre-t_0 phase which are used to estimate the speed. Secondly, the slower the motion of the meteor, the slower the change in the phase of the returned signal. Thus for the same number of data points in the pre-t_0 phase, the phase change is smaller, and this makes it difficult to determine the position of the phase minimum. The combination of these factors results in the underestimation of the speed of echoes where the amplitude is small.

In Section 6.3.2 meteors with measured speeds were divided into Class A and Class B subsets, based on the difference between the parabolic estimate of the speed and that obtained from the model. Figure 6.14 shows the meteors from Figure 6.13 with the exception of the Class B meteors. The agreement is greatly improved at low speeds.

Figures 6.13 and 6.14 included a number of echoes where the model method could

not be applied, as the t_0 point was not present in the record. The speed for these meteors was obtained by using the method described in Section 6.4 for aliased head echoes. Figure 6.15 shows a comparison between this method and the Fresnel transform method. Again a good agreement is seen, and also apparent is the characteristic of this type of echo, in that it is produced only by high speed meteoroids.

6.6 Down-the-beam speed measuring

When we find echoes in which the meteor echoes show up in a number of range bins sequentially, it is apparent that the meteor trail cannot be orthogonal to the beam, but that the meteoroid is coming "down the beam". Of course events where the meteoroid is travelling exactly in the beam and parallel to the axis of the radar are rare, but meteoroids travelling at large angles (up to 71°) to the beam can still produce returns in several range bins. These echoes act as if they are reflected from a "hard target" which is at the position of the meteoroid body, and should be described by the geometry of the situation.

These sorts of echoes have been considered previously, and there is some discussion on the range-time method, the UHF Doppler method, and the Arecibo method earlier in this chapter. There has also been some analysis of this type of echo detected with the Buckland Park VHF radar (Taylor et al. 1996), which is the basis of this method.

Considering the situation illustrated in Figure 6.1 we can write :

$$\theta = \arctan\left(\frac{s}{R_0}\right) \tag{6.21}$$

and differentiate to give:

$$\frac{d\theta}{dt} = \frac{\frac{v}{R_0}}{1 + \left(\frac{s}{R_0}\right)^2} = \frac{v}{R_0}\cos^2\theta \tag{6.22}$$

It is apparent from this expression that not only does θ change with time, but the rate of change of θ changes with time, for constant (non-zero) values of v.

For fixed values of v and R_0 we can model the rate of change of R which is the phase of the returned signal. Figure 6.16 shows in panel (a) the phase of the returned

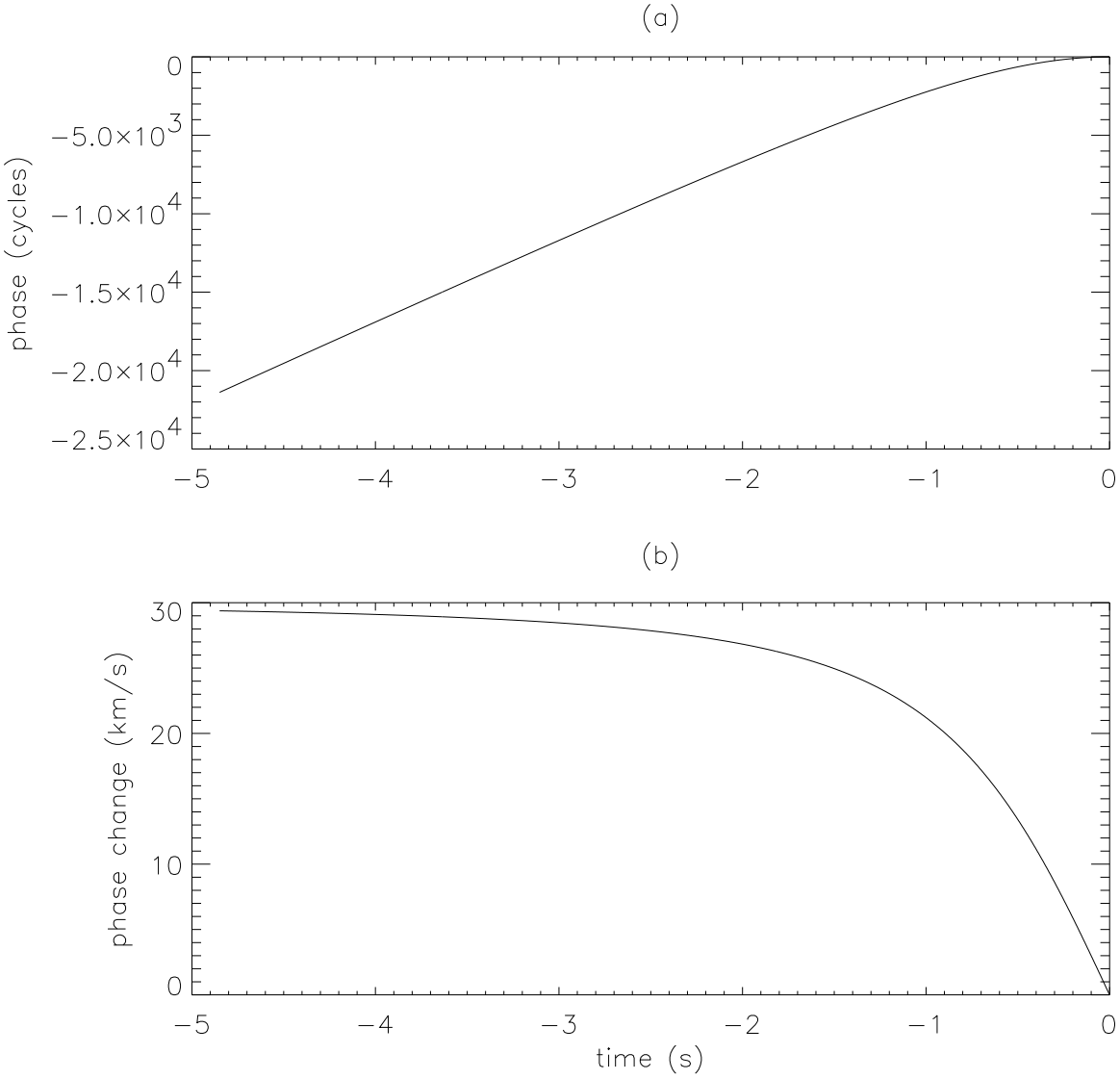

Figure 6.16: Modelled phase of the signal returned from a meteoroid travelling at 30km s^{-1} (Panel (a)). Panel (b) shows the rate of change of the phase in km s^{-1}. The x axis shows time prior to the t_0 point in seconds

signal for a meteoroid travelling at 30km s^{-1} plotted against time prior to the t_0 point. Note that near the t_0 point the phase has a parabolic shape. Panel (b) shows the rate of change of phase of against time for the same meteoroid. Notice that as we get further away from the t_0 point the line-of-sight speed (*ie* the rate of phase change) approaches the true speed of the meteoroid. This part of the Figure closely resembles the diagrams produced by Janches (2000) which showed the rate of change of phase changing with time. Janches claimed that the change was due to deceleration of the

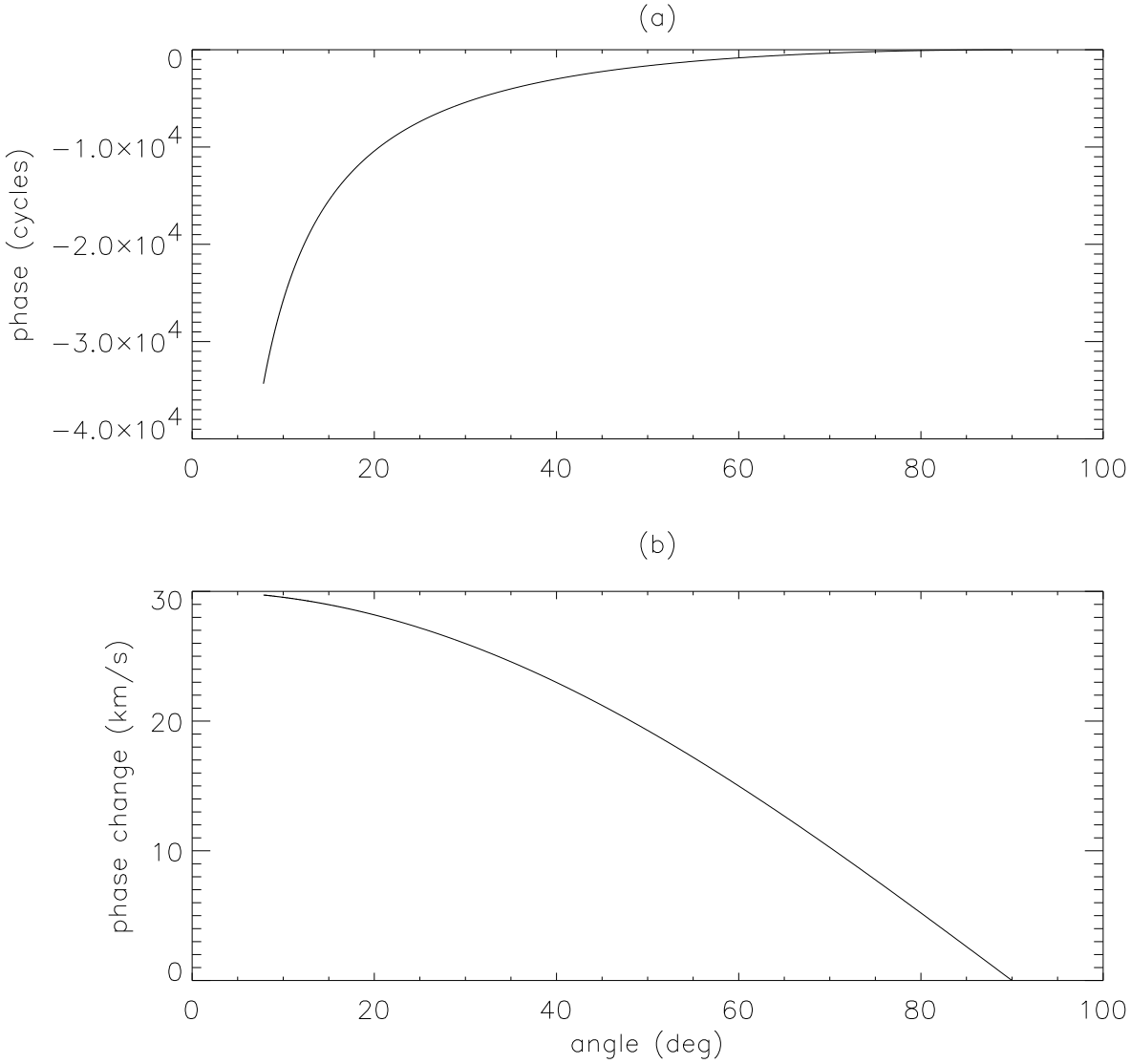

Figure 6.17: Modelled phase of the signal returned from a meteoroid travelling at 30km s^{-1} (Panel (a)). Panel (b) shows the rate of change of the phase in km s^{-1}. The x axis shows the angle the trail makes to a line from the radar to that point on the meteoroid path, in degrees.

meteoroid, but in this model, with a constant speed of 30km s^{-1} it is plain that the change in angle produces this apparent deceleration. While it is quite probable that meteoroids are decelerating, the effect of this on the line-of-sight speed is generally much smaller than the effect of the change of the angle. In addition to this error, it appears that Janches *et al* gave little regard to the difference between the line-of-sight speed and the true speed of the meteoroid.

During the travel of the meteoroid across the sky the angle the trail makes to

the line-of-sight from the meteoroid to the radar changes considerably, and so it is useful to plot the phase and the rate of change of phase against this angle. Note that $\theta = 90 - \phi$ where ϕ is the angle the trail makes to a line-of-sight from the meteoroid to the radar. Figure 6.17 shows the same modelling as in Figure 6.16, except that the length of time has been extended to just over 7 seconds and angle ϕ is the x axis in degrees. The phase behaves just as you would expect, extending towards infinity as the meteoroid begins travelling directly away from the radar (at 0°), and the line-of-sight speed approaches 30km s^{-1} at the same point. The line-of-sight speed simply obeys the relation:

$$v_\theta = v \sin\theta = v \cos\phi \tag{6.23}$$

where v_θ is the line-of-sight speed at an angle θ or ϕ. In the region near the t_0 point the phase returns will be dictated by the Fresnel diffraction pattern, and at some point the phase will change over to a geometrical relation. In this case we are only looking at echoes which occur in multiple range bins, and so we are only concerned with values of ϕ less than 72°. The change in the angle is not constant over time, and is much faster near the t_0 point, so Figures 6.16 and 6.17 appear to have different shapes, even though the phase and rate of change of phase data is the same. The shape of the plots of phase and line-of-sight speed are similar for different true speeds of the meteoroid, the major change being only the asymptote of the line-of-sight speed plot. Changing R_0 simply changes the rate of change of the angle with time, having no effect otherwise.

6.6.1 Speeds from down-the-beam meteors

The question now arises about whether it is possible to use the observed phase of a down the beam echo to estimate the speed of that echo. Taylor et al. (1996) performed this analysis. However, the angle of the trail to the line-of-sight from the radar to the beam was estimated from the first few points of data in the trail assuming no deceleration, and no change in the angle throughout the record, leading to substantial errors in the estimate. A better method to estimate the angle is required, and then a

complete analysis of the behaviour of the phase to produce the speed.

We have the range, R, and the phase over time, and therefore the rate of change of the phase. We can estimate the angle based on the number of range bins in which we see the meteor. Table 6.1 shows the maximum angle a meteor can make to the beam based on the number of 2 km range bins in which it appears, when the furthest range bin is at 110 km.

Range bins	2	3	4	5	6	7	8	9	10	11	12	15	20	25	30
Max Angle	71	55	43	35	29	24	21	18	16	15	13	10	7.2	5.4	4.2

Table 6.1: Maximum angle to the beam for meteors appearing in multiple range bins with the furthest range bin at 110 km. The angle is given in degrees.

We can see that the uncertainty in the angle, which is the difference between the maximum for the number of range bins traversed and the maximum for bin number plus one, decreases as the number of range bins traversed by the meteor increases. The angle will change while the meteor is in the beam too, by the angular width of the beam. The angle given in Table 6.1 is the angle at the centre of the beam. The uncertainty in the angle is smaller as the range to the meteor increases, but this effect is small.

We also must consider the problem of aliasing in the phase when the phase change is greater than one cycle between pulses. This is the same as that described in the previous section, except worse, since the phase is changing faster when the angle is smaller. This problem can be solved by looking at the amplitude data, where each range bin shows an echo in sequence. By measuring the time gap between the appearance of the meteor in each range bin we can estimate the line-of-sight speed and thus the number of missing cycles between each pulse. In the case where there is more than one parabola in the phase record, ie the number of missed cycles changes over the record, this can be remedied by adding or subtracting one cycle between each point for sections of the record.

As shown previously, the line-of-sight speed depends on the angle of the trail to the

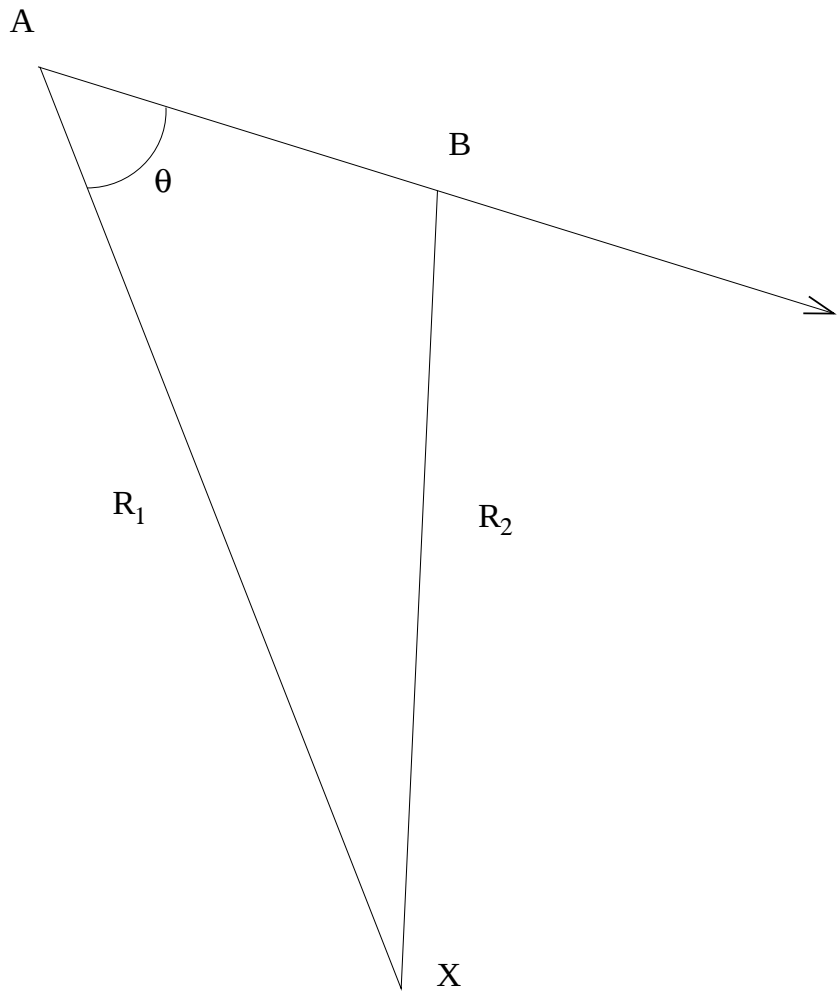

Figure 6.18: Geometry for a down the beam meteor over a short time.

line-of-sight, so if we can accurately find this angle then the true speed can be found. Consider the situation shown in Figure 6.18. At some time a meteoroid is at a point A, travelling at a speed V and slowing down with an acceleration of a. We ignore the effects of gravity, so the deceleration is due to collision with air molecules. The distance from point A to the radar station at point X is R_1. The line AX makes an angle of θ to the direction of travel of the meteoroid and the instantaneous change in R_1 is given by the line-of-sight speed, $V_1 = V \cos\theta$. After a short time t, the meteoroid has moved a distance s to a point B. The distance from point B to X is R_2 and the line-of-sight speed is now $V_2 = \frac{dR_2}{dt}$. The angle that BX makes to the direction of travel

of the meteoroid is not equal to θ. The relationship of R_2 to R_1 is given by:

$$R_2^2 = R_1^2 - 2R_1 s\cos\theta + s^2 \tag{6.24}$$

where s is a function of time. If $a = 0$ then $s = Vt$. This leads to

$$R_2^2 = R_1^2 - 2R_1 V\cos\theta t + V^2t^2 = R_1^2 - 2R_1V_1t + V_1^2\sec^2\ \theta\ \ t^2 \tag{6.25}$$

Differentiating with respect to t gives:

$$\frac{dR_2^2}{dt} = 2R_2V_2 = -2R_1V_1 + 2V_1^2\sec^2\ \theta\ \ t \tag{6.26}$$

and leads to:

$$V_2 = \frac{d\phi}{dt}\frac{\lambda}{4\pi} = -\frac{R_1V_1 + V_1^2\sec^2\ \theta\ \ t}{R_2} \tag{6.27}$$

where ϕ is the accumulated phase of the returned signal in radians, each cycle corresponding to a change in R_2 of $\frac{\lambda}{2}$. Substituting Equation 6.24 for R_2 we obtain:

$$\frac{d\phi}{dt}\frac{\lambda}{4\pi} = -\frac{R_1V_1 + V_1^2\sec^2\ \theta\ \ t}{\sqrt{R_1^2 - 2R_1V_1t + V_1^2\sec^2\ \theta\ \ t^2}} \tag{6.28}$$

where t is the only variable. For the situation where $a \neq 0$, similar expressions can be obtained.

Equation 6.28 was used as the basis of an analytical process to determine θ from the recorded values of ϕ in down-the-beam echoes, and thus the speed V, but even small accelerations had a large effect on the value of $\frac{d\phi}{dt}$ and produced meaningless results. Once the further variable of the acceleration was introduced it became impossible to analytically solve for θ. A model was developed which used the range bin method from earlier in this section to estimate θ, and from that to estimate the total change in the angle over the length of the record. This was applied to the line-of sight speed to estimate the acceleration at several points along the record. These estimates were used to generate models of $\frac{d\phi}{dt}$ for varying speeds, accelerations and angles, the closest of which was chosen by a χ^2 test. More detailed models were then produced which further narrowed down the estimates, producing a speed and deceleration for the echo. The error in these estimates was determined by the results of the χ^2 test.

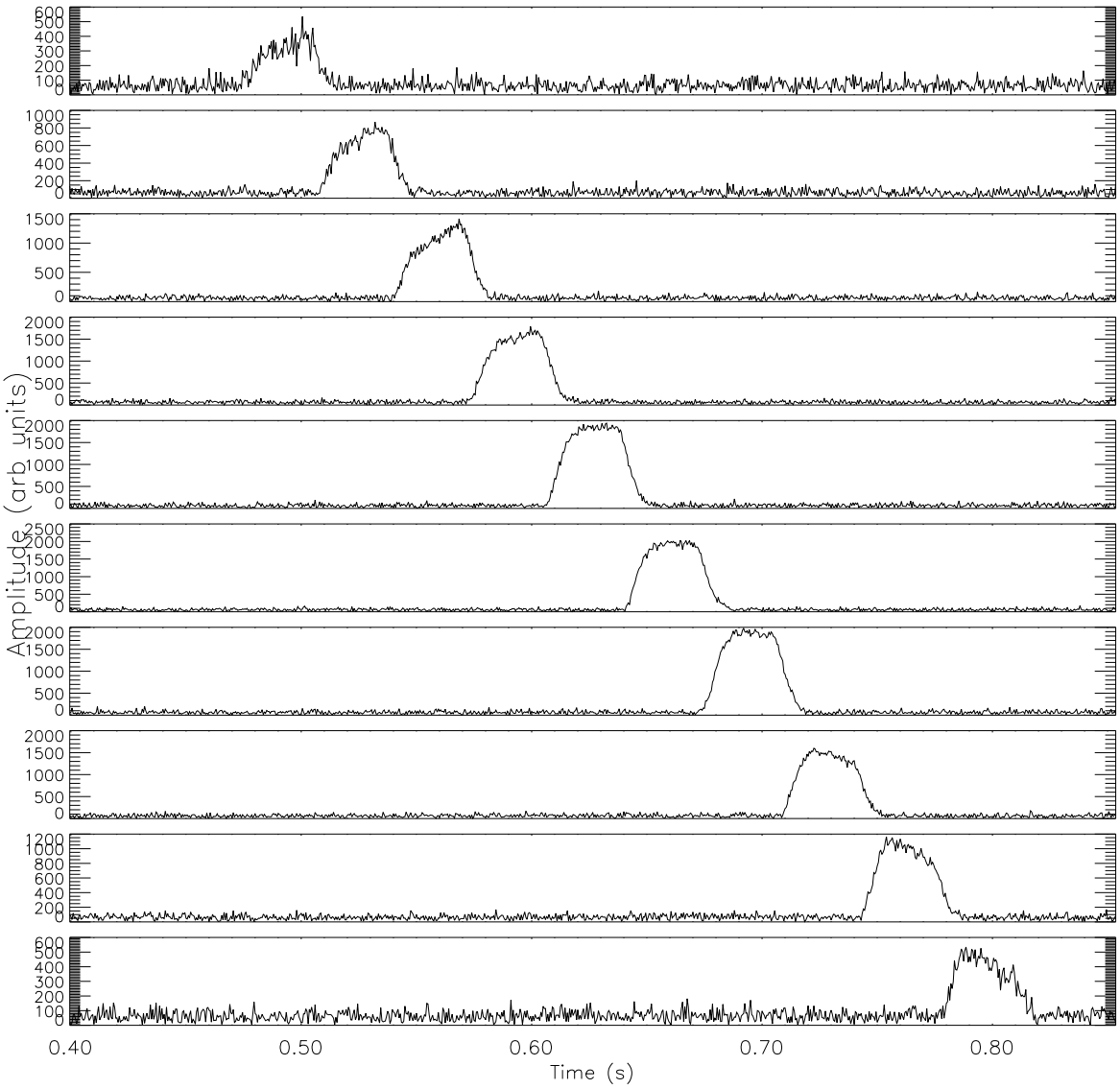

Figure 6.19: A down-the-beam meteor echo. This echo was detected at 21:25 UT on the 18^{th} of October 1998. The panels show the amplitude of the echo in consecutive range bins from 107 to 125 km. Not shown are echoes in one range bin lower and one higher than those depicted. Periodic noise reduction has been applied.

To obtain $\frac{d\phi}{dt}$ for use in the model it was necessary to process the raw data quite extensively. Figures 6.19 and 6.20 show an example of a down the beam echo, showing the amplitude of the returned signal in several range bins and the unwrapped phase respectively both with periodic noise reduction applied. The area of coherent phase in each range bin is selected by the operator and the rate of change of the phase between each pulse is calculated, producing a time series of $\frac{d\phi}{dt}$.

The line-of-sight speed for one cycle of phase per pulse at a PRF of 1650 is

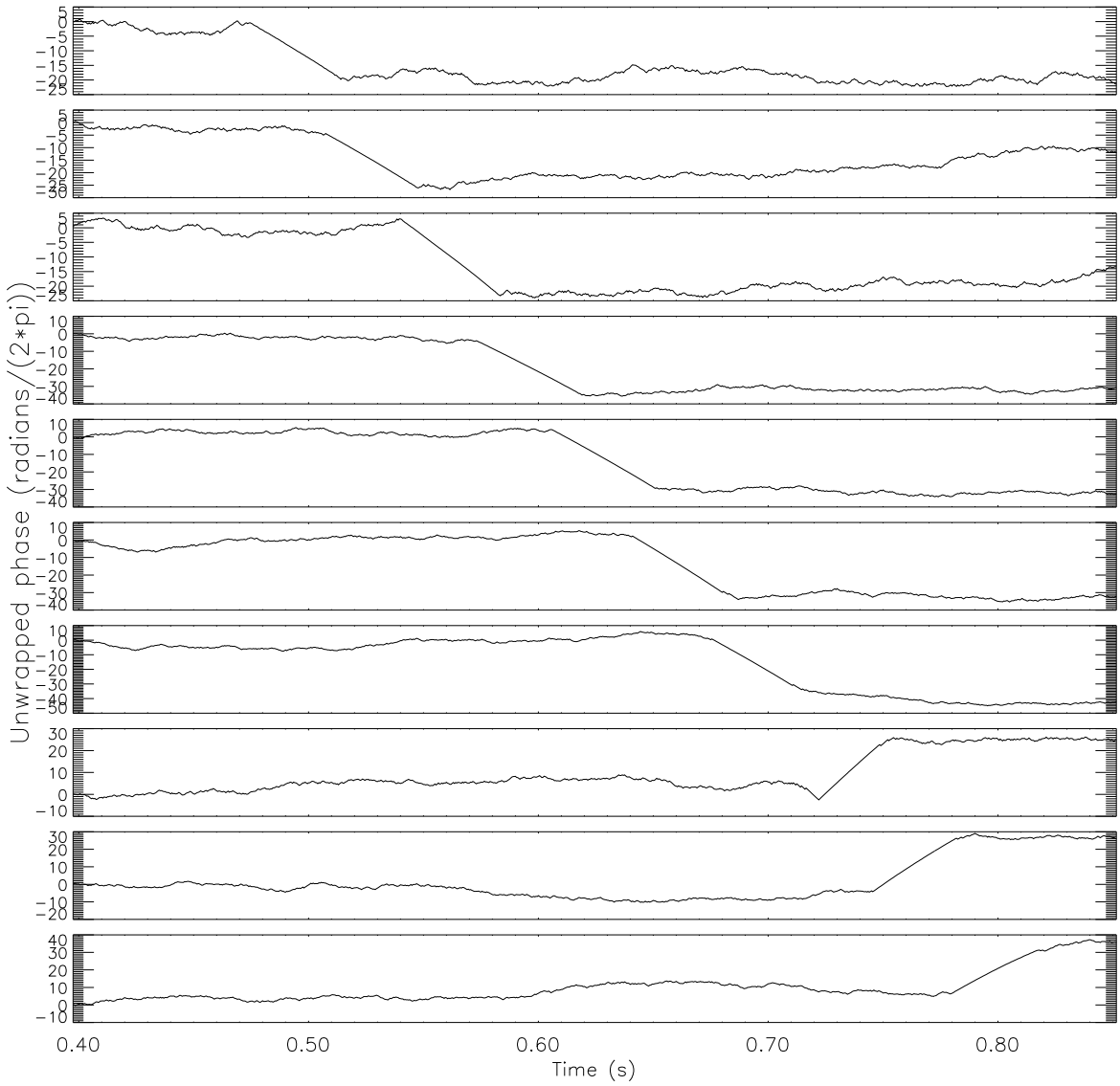

Figure 6.20: A down-the-beam meteor echo. This echo was detected at 21:25 UT on the 18^{th} of October 1998. The panels show the phase of the signal in consecutive range bins from 107 to 125 km. Not shown are echoes in one range bin lower and one higher than those depicted. Periodic noise reduction has been applied.

4.4km s^{-1}. The average meteor speed is about 30km s^{-1}, and the highly ionising meteoroids which cause down-the-beam echoes are likely to be much faster (around $50 - 70$km s^{-1}). These high speeds mean the introduction of aliasing in the phase as the meteoroid moves more than one cycle of phase closer to the radar between pulses. For a transverse echo, the effect of the angle reduces this aliasing to only one or two cycles of phase, but as the angle between the trail and the line-of-sight to the radar decreases, the number of cycles of phase in between each pulse increases. In this

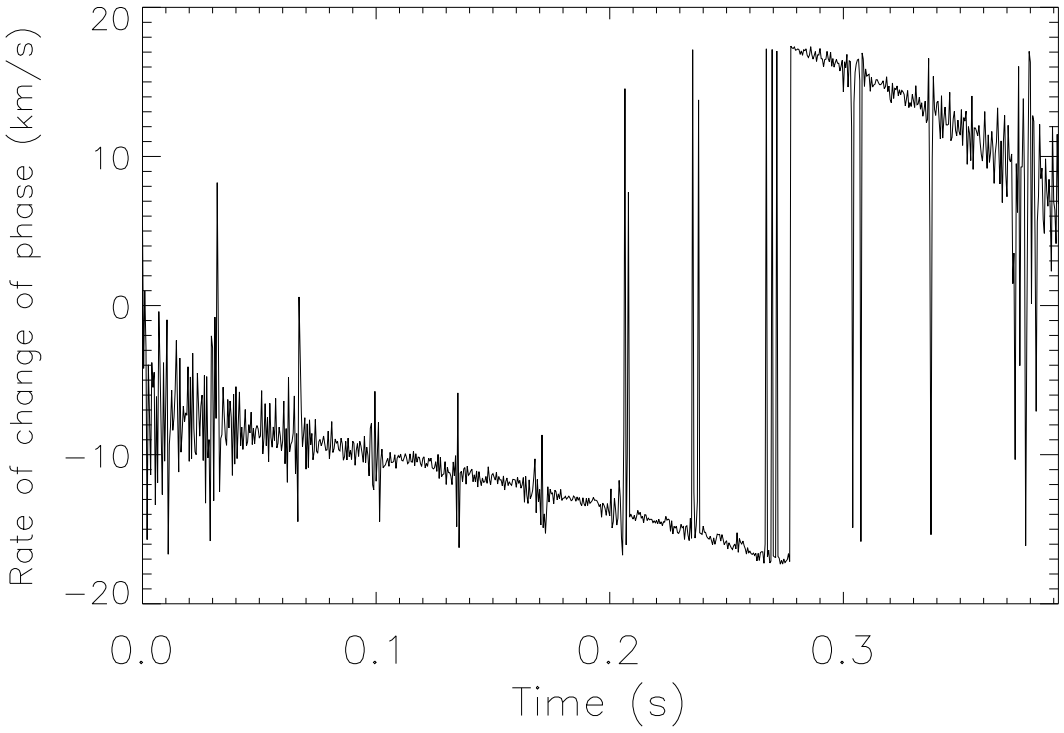

Figure 6.21: Rate of change of phase of the down-the-beam echo shown in Figures 6.19 and 6.20. Note the discontinuity in the phase at 0.28 seconds.

example, there were 16 cycles between each pulse.

To determine the number of cycles missing, the line-of-sight speed is estimated by the use of the amplitude information. A segment of one range bin containing the returned signal from the meteor is selected and convolved with all the other range bins to give a time of arrival in each range bin. Since the range bins are 2 km wide, this gives a number of estimates of the line-of-sight speed. The number of cycles missing is determined from the difference between $\frac{d\phi}{dt}$ and this estimated line-of-sight speed. Occasionally the number of missing cycles of phase will change throughout the record, producing a discontinuity in $\frac{d\phi}{dt}$. This can be removed by the operator by selecting the position of the discontinuity, whereby the extra phase cycle is added to the data to the left of the discontinuity. Figure 6.21 shows the rate of change of the phase shown in Figure 6.20. Note the discontinuity at 0.28 seconds. There are also a number of regions in the Figure 6.21 which show appreciable noise. These correspond to the changeover points of the rangebins, and are caused by edge effects. As the signal nears

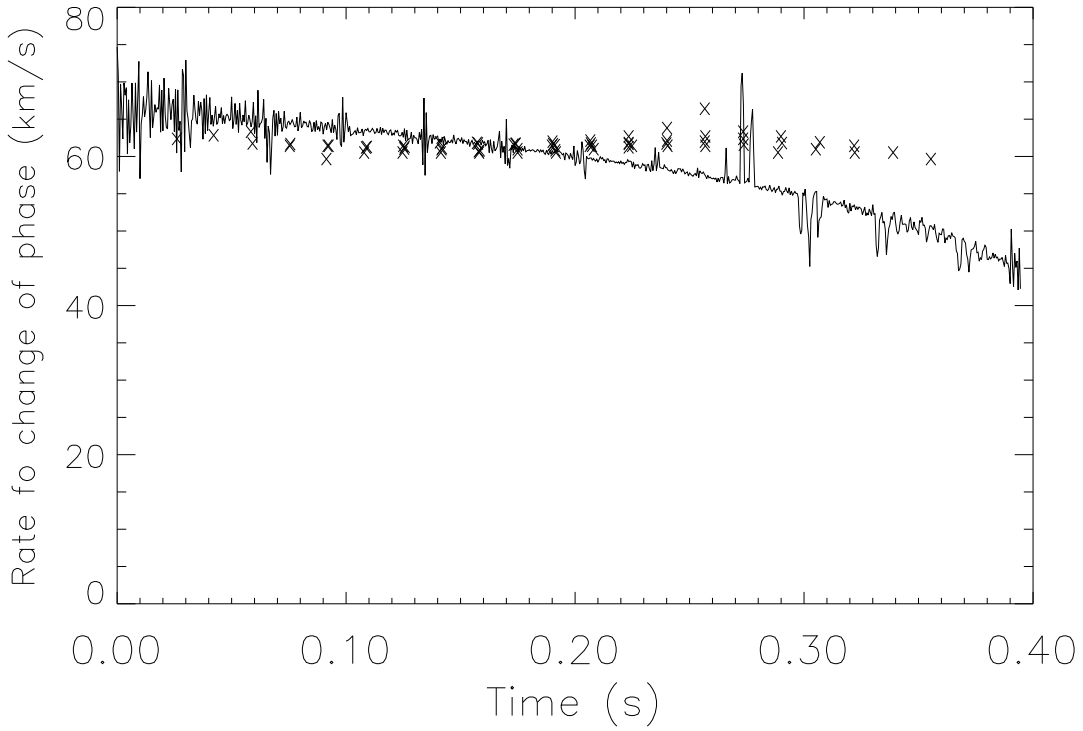

Figure 6.22: line-of-sight speed of the down-the-beam meteor shown in Figures 6.19 and 6.20, obtained by adding a number of cycles of phase between each point in the record and removing the discontinuity. The "x"s show the values of the line-of-sight speed obtained from the amplitude data.

the edge of the rangebin, the signal-to-noise ratio increases, and the phase record becomes "noisy". Although the phase record appears normal, when the rate of change is calculated, the effect is magnified. Fortunately these "noisy" regions can be easily ignored in the subsequent analysis.

Figure 6.22 shows the rate of change of phase once the discontinuity has been removed and the 16 missing cycles added between each point. Also shown are the estimates of the line-of-sight speed obtained from the amplitude data (denoted by the "x"s), which were used to determine the number of cycles which should be added. Once the line-of-sight speed has been obtained, the model can be used to determine the true speed and the angle of arrival. In this case the speed of the meteoroid was determined to be 68.7 ± 0.2km s^{-1} with the meteor path making an angle to the beam direction of $15.5° \pm 0.5°$. The mean deceleration during the record was 49.9km s^{-2}.

6.7 Summary

This chapter has been concerned with obtaining the speed of a meteoroid from analysis of the radar returns from the meteor it produces. Firstly previously used techniques were described, including the Range-Time method, the diffraction method, a UHF Doppler method, the spaced receiver method used with the Advanced Meteor Orbit Radar (AMOR), the amplitude rise-time method, the Arecibo Multi-pulse Doppler Method, the Fourier Method used with the SKiYMET radars, the position-time method used with the ALTAIR radar and the Fresnel transform method.

Next the pre-t_0 method was introduced and the principles behind it explained. The required preparation of the data was outlined, and the semi-automated method of determining the speed described. This was followed by a discussion on measuring the deceleration of meteoroids and then an adaptation of the technique for transverse head echoes.

The problem of the down-the-beam echo was discussed, and also how obtaining the speed and deceleration of a meteoroid in the atmosphere was possible through modelling of the motion of the meteoroid and fitting the models to the recorded data.

Chapter 7

Meteoroid streams and Meteor Showers.

7.1 Introduction

This chapter is concerned with the observation of groups of meteors, known as meteor showers. The origin of these showers is discussed, and is followed by a review of the history of meteor shower discovery, their association with comets, and techniques used to observe meteor showers with radars. Next is a discussion on the statistics of events randomly spaced in time, and of meteor rates. Following this is a discussion on the structure of meteoroid streams, and how this relates to the meteor showers they produce. We then move on to observations of meteor showers with the BP VHF radar, in particular the η-Aquarid meteor shower, which was observed over several years and has been thoroughly analysed. We also look at some other prominent showers, and there is a short discussion of the sporadic background.

7.2 Meteor Showers

A large number of meteoroids in similar orbits is designated a stream, and a meteor shower is observed when the Earth passes through a meteoroid stream and there is an

increase in the rate of occurrence of meteors. This will generally occur annually as the Earth passes through the same portion of space (that portion containing the stream of particles), but changes in the orbit or composition of the stream can alter shower activity in any particular year.

The meteoroids in a stream enter the atmosphere on parallel paths and the meteors they produce appear to be originating from a common point called the "radiant". A meteor shower is generally named after the constellation in which the radiant occurs, or the name of a nearby star. The apparent position of the radiant depends on the combination of the orbit of the Earth and the orbit of the meteoroids and from day to day the radiant of a given shower will change slowly with respect to the star background. Due to the spread of orbits contained within a stream, most meteor showers demonstrate a spread or diffuseness of the individual radiants.

7.2.1 Discovery of meteor showers and association with cometary activity

Meteor showers were known to the ancients (Imoto & Hasegawa 1958, Hasegawa 1993), and the first meteor observations would have been of high activity annual showers. Steel (1995) has suggested that Stonehenge on the Salisbury Plain in England was built for the purpose of observing the Taurid complex of meteor showers, which he postulates was extremely active around 3000 BC. The Leonids meteor shower was observed by large numbers of people in 1833, and aroused great interest in the scientific community, leading to investigations of historical observations of meteor showers and observation programs to discover new showers. In 1834 Olmstead and Twining suggested that the Leonids meteor shower was caused by a cloud of particles which was intersected by the Earth each November. In 1838 Herrick showed that the Perseid meteor shower was periodic. Kirkwood, in 1861, was the first to suggest that meteor showers may be caused by the debris from comets. Schiaparelli announced in 1866 that the meteoroids which produce the Perseid meteor shower move in the same orbit as comet 1862 III

(Swift-Tuttle). This was followed by accounts of similar relationships, between the Leonids and comet 1866 I (Temple-Tuttle), the Andromedids and comet Biela, and the Lyrids and comet 1861 I (Thatcher). The behaviour of comet Biela played a large role in the association of comets and meteors. This comet was discovered by an Austrian Army officer by the name of Wilhelm von Biela in 1826, and it was found to have a period of about six and a half years. It was recovered on its next return in 1832, but in 1839, conditions were not favourable for observation. In 1845 the comet was recovered, and it became apparent that the comet appeared elongated, and later the elongation separated into two distinct nebulosities. At the next return (1852) the two comets were very faint and had become further separated. Neither comet has been seen since that time, but at the time of the predicted subsequent returns in 1872, 1885, 1892, and 1899, a strong meteor shower was observed - it seemed that the cometary break-up produced a dense meteoroid stream. There is some evidence to suggest that the break-up of the comet was caused by collision with the Leonids meteoroid stream in either 1832 or 1846 (Bosler & Roure 1937, Babadzhanov et al. 1991).

The first, and simplest observations of meteor shower concentrate on the activity of the shower, and involve the determination of the time of maximum activity, the duration of the activity, a profile of the activity curve, and the magnitude distribution of the trails, and by inference the mass distribution of the particles. According to the activity, the showers are designated “major” or “minor” showers, although there are rare instances of “temporary” showers, which do not have regular annual activity. There are also instances where showers exhibit occasional “outbursts”, sudden enhancements of their activity, and many annual showers show variations in their activity from day to day or year to year, which are indicative of the structure of the stream.

It seems clear while most meteor showers are produced by comets, some are of asteroidal origin (Whipple & Hughes 1955, Sekanina 1973*a*, Sekanina 1973*b*, Drummond 1982, Olsson-Steel 1988). Williams (1993) has described mechanisms for the production of meteoroids from both comets and asteroids, as well as the evolution of meteoroid streams once they are formed. Once particles are released from their parent bodies,

they will immediately be acted upon by radiation pressure and the Poynting-Robertson effect, and they are subject to gravitational perturbations due to the planets. These perturbations are very important in the evolution of the stream as a whole, and the orbital evolution can be studied theoretically by numerical integration of the equations of motion of a number of individual test particles. The use of such numerical integration is now widespread.

As a comet approaches the sun, the volatile materials near the surface sublime into space, pushing with them particles which have a much higher boiling point. This effect causes the particles to be accelerated away from the comet. These particles, when acted upon by radiation pressure and the Poynting-Robertson effect, spread out behind the comet and away from the sun, forming a curved trail of particles known as the "dust tail". Solar UV photons striking the gases and particles ionise molecules and atoms, which are swept away from the comet in the antisolar direction by the action of the solar wind, forming the "ion tail".

Acceleration along the path of the comet spreads the particles along the comet's orbit, and after a few passages about the sun will have formed a stream of particles with very similar orbits. Acceleration due to ejection in other directions makes the column wider, and this together with the Poynting/Robertson effect, solar radiation pressure, orbital precession and planetary perturbations cause particles in the stream to move a great distance from the comet's present orbit. For "older" showers sufficient time has elapsed to spread the particles throughout the cometary orbit, while 'young' showers like the Leonids (associated with Comet P/Temple-Tuttle) have strong spatial concentrations of particles near the comet and thus show marked increases in meteor rates when the Earth crosses the stream soon after the comet has visited our part of the solar system.

It is quite possible to have more than one shower produced by the same comet because the stream's orbit passes through the Earth's twice, once on the way into the solar system and on the way out again, producing a night time shower (on the way in) and a daytime shower (on the way out). An example are the η- Aquarid and the

Orionid streams which have the same parent body, namely comet Halley. Further, comet Halley precesses between two extreme angles (a motion called libration), and this causes the separation of the two streams mentioned. One can easily surmise that these greatly separated streams would themselves be made up of a large number of small streams, each created on a subsequent return of the comet. Simulations of the orbits of particles ejected from the comet P/Temple-Tuttle by Asher (1999) show that this is indeed likely to be the case, and his predictions of the time of enhanced activity of the Leonids Meteor shower in 1999, 2000 and 2001 based on the relative positions of these streamlets and the Earth proved to be very accurate.

7.2.2 A survey of radar techniques for observation of meteor showers

The introduction of photographic techniques in the early 1900's allowed accurate determination of meteor shower radiants (the apparent source of meteors in the sky) but had limited use in the search for new showers because of the relatively small field of view. The search was dramatically aided by the sudden increase in the use of meteor radars after the Second World War. Radio techniques can be used to observe meteors under all conditions, in day-time and moonlight, and through rain and cloud cover. Many different techniques have evolved since the 1940's to study meteor showers. Clegg (1948) used a single station fan-beam pulsed radar, and determined activity and radiant position with a Range-Time envelope technique. In general, a statistical method is required to detect meteor showers with single station radars. Morton & Jones (1982) developed a technique, able to "image" the showers using observed positions of the radar reflection points. Multi-station systems enable the determination of the radiants (and orbits) of individual meteors but are much more expensive and complex than single station radars.

7.2.2.1 The Range-Time envelope technique

Clegg's technique (Clegg 1948) required that the polar diagram of the antenna was accurately known and assumed that all echoes detected obeyed the condition of specular reflection. He also assumed that the echoes occurred within a limited range of heights. Given a certain minimum sensitivity, Clegg could calculate the variation in time associated with the minimum and maximum ranges for a given radiant. This produced an area in a Range-Time plot containing all meteors associated with the radiant. Observations over several days were made with a change in the azimuth of the radar beam each day to enable determination of the declination of the radiant. Clegg was able to determine the radiants of the showers to within 1° under the best conditions, but only for showers which lasted for several days.

Aspinall et al. (1951) modified Clegg's method by using two independent antennas directed at different azimuthal bearings. This allowed the determination of shower radiants from the data obtained in one day. Keay (1957) used a narrow range band centred on the most probable range to perform an effective reduction in the vertical beam width, making use of the limited height range of meteor echoes. This refinement was known as the partial rate curve technique but was only useful when echo rate were greater than about 50 per hour.

The Range-time envelope method has been until recently the only method useful for single station monostatic meteor radars, but it has difficulty in detecting weak showers above the background sporadic meteors.

7.2.2.2 The shower imaging technique

Morton & Jones (1982) developed a technique for determining meteor shower radiants based on earlier ideas (Weiss 1955, Jones 1977, Jones & Morton 1977). Meteors are observed with a set of at least three closely spaced antennas, and the phase information from each is combined to find the position of the meteor echo. Applying the condition of specular reflection to the echo constrains the meteor trail to a plane. Morton and

Jones applied this method to a continuous wave bistatic radar, and this allowed high resolution contour maps of the shower radiants to be produced, thus "imaging" the radiants. It was found that this method produced elongation of features in the maps, identified by Morton and Jones as "astigmatism" caused by the narrow beam of the radar. Poole & Roux (1989) showed that this effect could be reduced by the use of an all-sky radar, but was still present, depending on the radiant declination.

7.2.2.3 Multistation Radar Systems

In Chapter 6 the methods of speed determination by multistation orbit measuring systems such as the Advanced Meteor Orbit Radar (AMOR) have been described. In combination with the determined speed, the multiple observation of each meteor trail defines its path and therefore its orbit. The common association of the orbits of the detected meteoroids gives the radiant position of any showers which are present.

7.2.2.4 Radar response function method

This is a development of the method of Aspinall et al. (1951), where the two antennas are replaced by a single narrow beam which can be directed to different positions in the sky. The method is based on the theory of the radar response function (Elford 1964) and was first used to identify the June Librids in 1992 (Cervera et al. 1993, Elford et al. 1994) The technique is described in detail by Cervera (1996) so only a brief outline is given here. The development of the response function has been described in Chapter 3, and it is based on the combination of the antenna pattern of the radar, and the conditions for specular reflection. Figure 7.1 shows a contour plot of the response function for the Buckland Park VHF radar for a beam tilted eastward (azimuth 86°) at 60° elevation. The response has been calculated for a meteoroid speed of 30km s^{-1} and normalised to its peak value. The contours shown are at levels of 20%(outermost contour), 40%, 60%, 80% and 95%(innermost contour). While the response function is dependent on the speed of the meteoroid, the effect is only on the relative responses of the sidelobes and the absolute response of the main beam. The

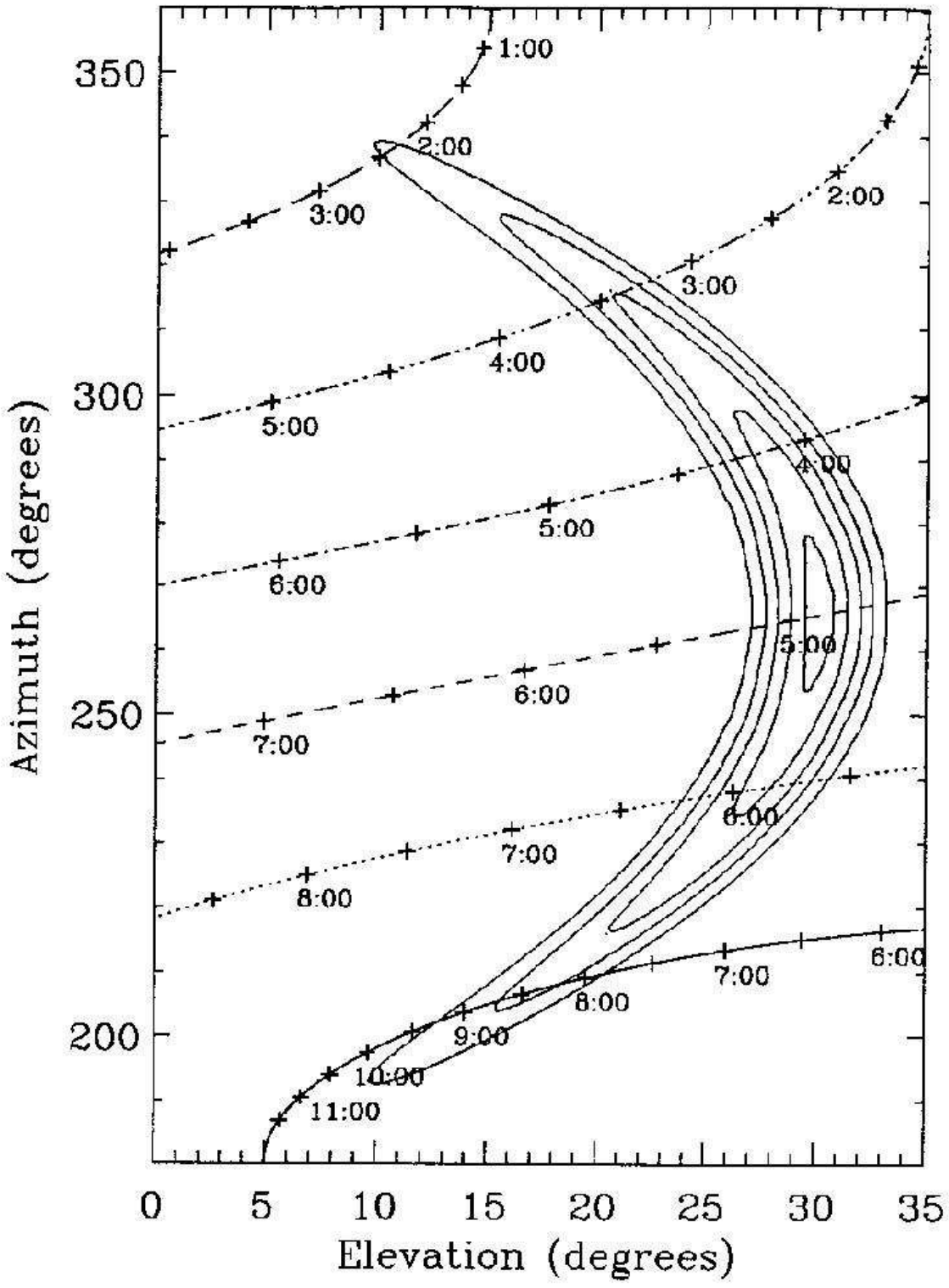

Figure 7.1: The response function for the Buckland Park VHF radar at 30km s^{-1} plotted with six fictitious meteor radiants. The radar is tilted to the East (azimuth 86°, altitude 60°). The contours shown are at levels of 20%(outermost contour), 40%, 60%, 80% and 95%(innermost contour). See text for details. (After (Cervera 1996))

shape of the response of the main beam is unaffected, and as this is most important for the radiant determination, it will be assumed to be the same for all meteoroid speeds. Plotted with the response function are the paths of six fictitious radiants with declinations varying from $-60°$ (solid line) to $+40°$ (long dashed line) in steps of $20°$. The radiants have identical right ascensions and occur on the same date. The crosses mark the time that the radiants pass through the plot in half hour intervals, and every hour is labelled. If we assume that the radiant is a point source of meteoroids, then the expected count rates for each radiant can be determined. Figure 7.2 shows the expected count rates for the six radiants shown in Figure 7.1 with the declinations varying from $-60°$ to $+40°$ shown in panels (a) to (f) respectively. The structure shown in these plots beside the main peak is due to the sidelobes of the response function, which are not shown in Figure 7.1 as the response is smaller than the 20% contour. The radiants take unique paths through the response function but it is not possible to distinguish them unless the beam is directed at two different portions of the sky as the radiant passes through the response function. For example, radiants with declinations of $+20°$ and $-20°$ will have peak rates at the same time if the azimuth of the second is advanced by $22.3°$ with respect to the first.

7.2.3 Statistics of meteor rates

In order to detect increases in count rates due to meteor showers such as those depicted in Figure 7.2 against the sporadic background we must find a method which will highlight increases in the meteor count rate consistent with the detection of a shower without producing false results due to random meteors arriving close together in time. The conventional way of producing these count rates is to group the time of detection of the meteors into bins, and display these against time. Figure 7.3 shows a histogram of meteors detected on the 7^{th} of May 1999 during observations of the η-Aquarid meteor shower, sorted into bins of width one hour. This Figure is not particularly revealing, showing only that the rate varies from 2 to 18 meteors per hour, and possible increases in the rate at 5:00, 8:00, 10:00 and 12:00 LT. This data was taken with the

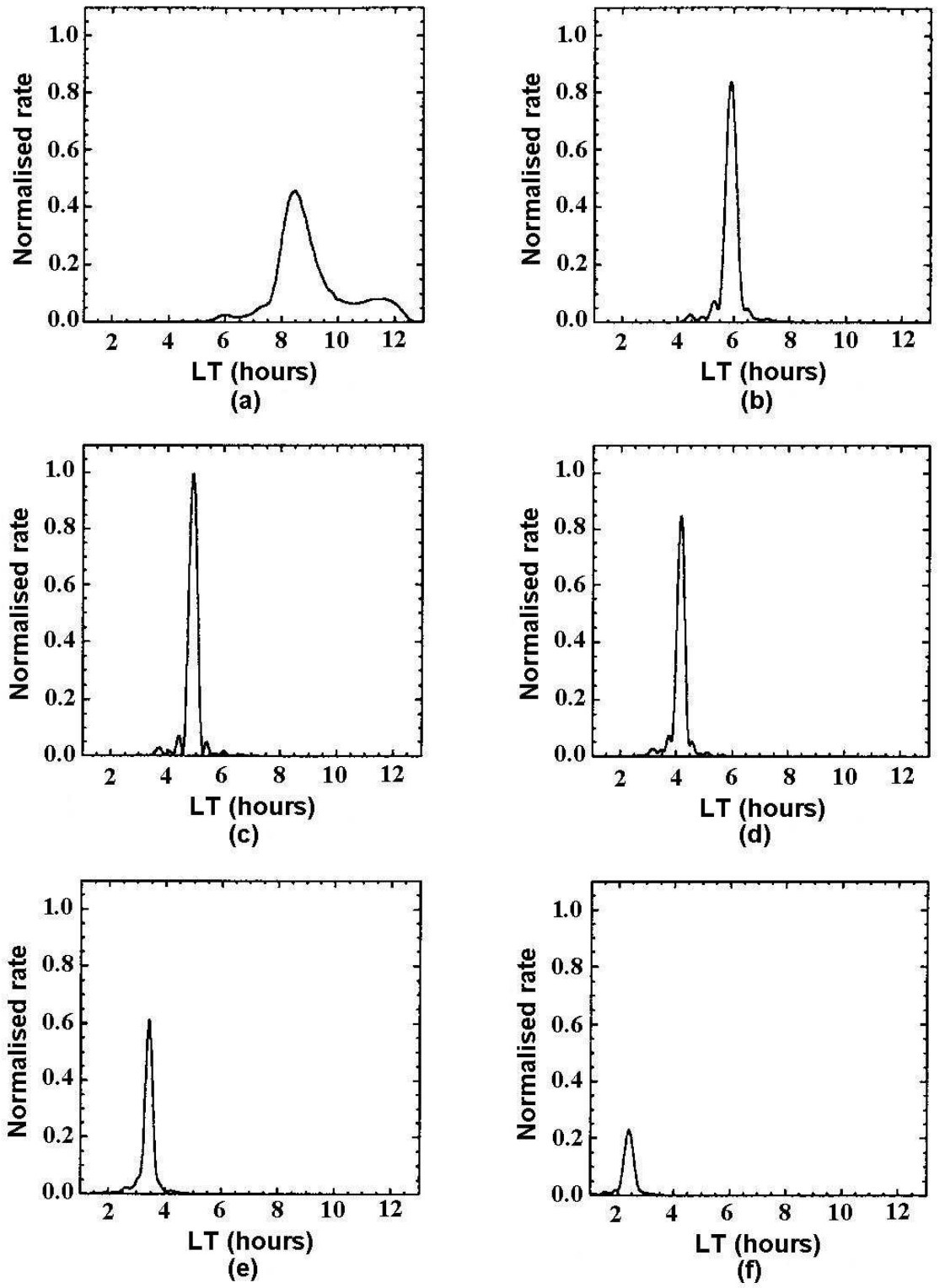

Figure 7.2: Expected normalised count rates for the fictitious radiants shown in Figure 7.1. The radiants have declinations varying from $-60°$ to $+40°$ in steps of $20°$ and are shown in panels (a) to (f) respectively. See text for details. (After (Cervera 1996))

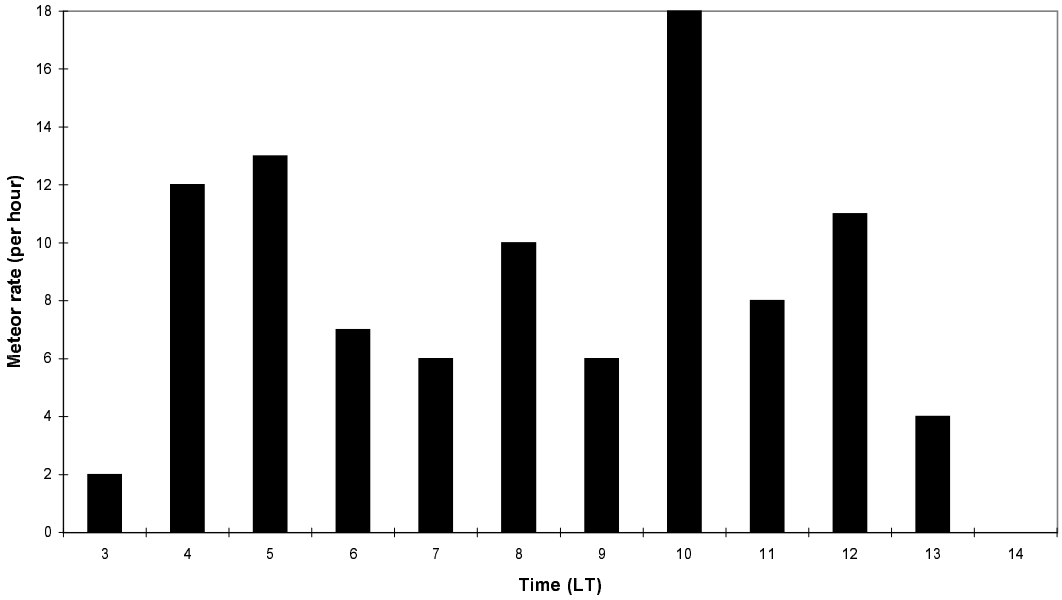

Figure 7.3: Histogram of meteor rates during observations taken on the 7^{th} of May 1999 using one hour bins.

radar pointing in three different directions, West 30° off zenith from 2:30 to 6:30 LT, East 30° off zenith from 9:00 to 13:00, and North 34.2° off zenith at all other times. The North beam, having a larger off zenith angle would have a larger collecting area and should give slightly higher backgound rates. The shower would be expected to be present in the centre of the observations with the East and West beams, and armed with this knowledge we could guess that the peaks at 5:00, 10:00 and 12:00 are due to the shower, but this is a rather tenuous association.

The η-Aquarid meteor shower, with a declination of $-1°$ should produce a peak similar to that shown in Figure 7.2 (d), with a width of about half an hour. Narrowing the bins to half an hour produces the histogram shown in Figure 7.4. The peaks at around 5:00, 10:00 and 11:30 are better defined, but there are a number of other peaks which are just as significant at other times in the day. It seems that the number of extra meteors due to the shower is not sufficient to show up in this method.

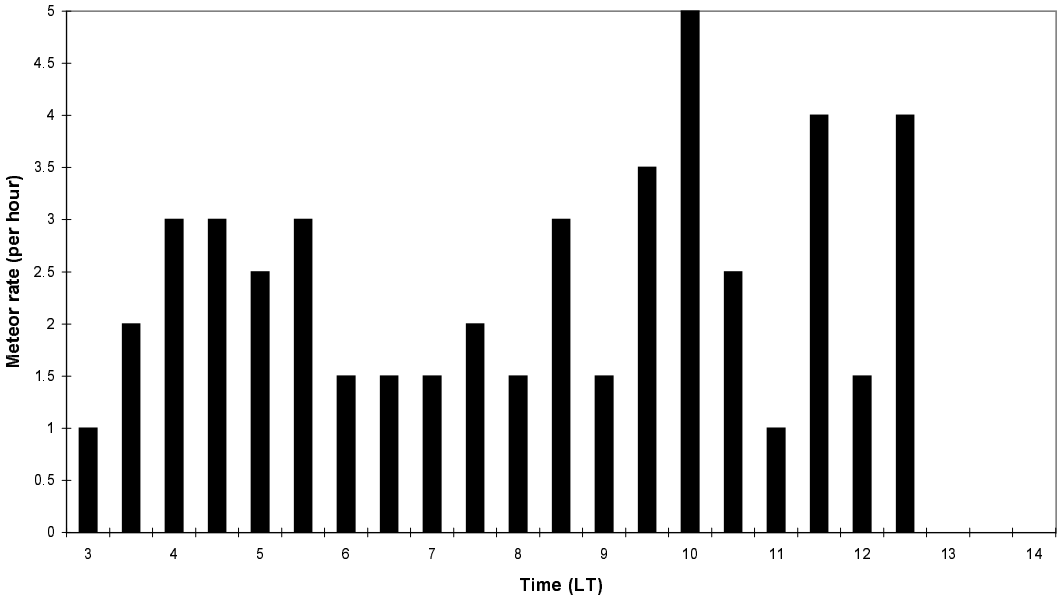

Figure 7.4: Histogram of meteor rates during observations taken on the 7^{th} of May 1999 using half hour bins.

Since we expect that there will be an increase in the meteor rate over a short time period, we need to be able to calculate an instantaneous meteor rate. We can use the time between successive meteors to give a measure of the rate. The rate is the inverse of the time between the meteors, but random variations can easily produce very small gaps, leading to huge spikes in the rate. This effect can be reduced by calculating the rate based on the time for several meteors to occur. Figure 7.5 shows instantaneous meteor rates for the 7^{th} of May 1999, smoothed over 9 echoes. For the n^{th} meteor detected the rate, R_n, is calculated as follows:

$$R_n = \frac{8}{t_{n+4} - t_{n-4}} \tag{7.1}$$

where t_n is the time of detection of the n^{th} meteor. R_n is plotted against t_n to produce Figure 7.5. This means that a point is plotted for each meteor detected. The gaps in the plots at 6:30 and 9:00 correspond to a change in the beam direction. At each of these gaps there are eight meteors not plotted since rates cannot be calculated across

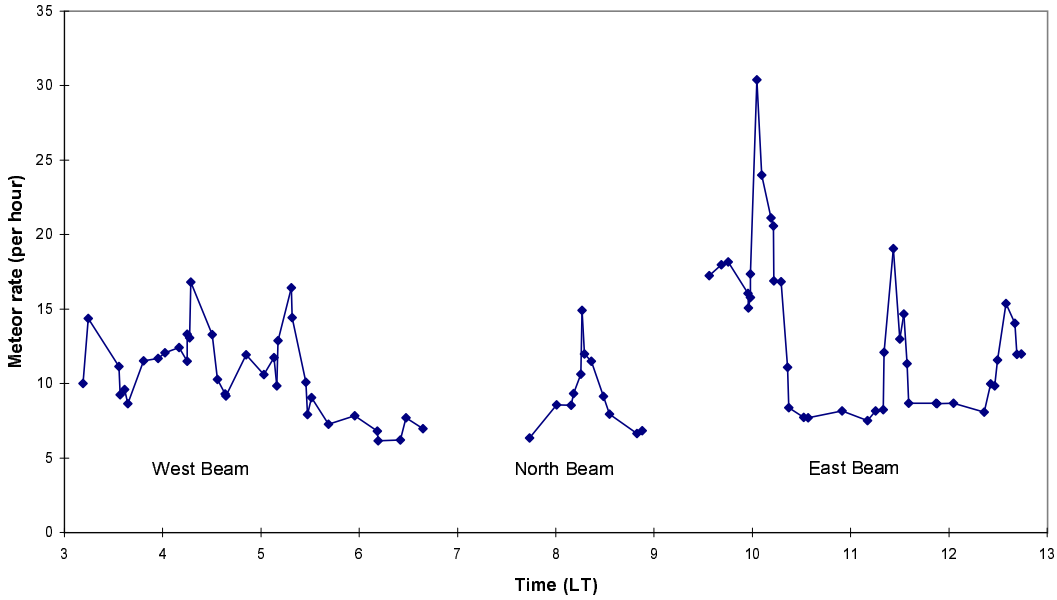

Figure 7.5: Instantaneous meteor rates for the 7^{th} of May 1999, smoothed over 9 echoes.

beam changes. There are now plainly visible strong peaks in the meteor rate in the East and West beams at 4:30, 5:15, 10:10, 11:30 and 12:40. There is also a strong peak in the North beam at about 8:20.

The question arises whether these peaks could be produced by random variation of the meteor arrival times. In order to determine the probability of these peaks occurring by chance, we must model the event spacing distribution. The Number distribution of the spacing, t, of random events is:

$$N(t) = N_0 e^{\frac{-t}{\tau}} \tag{7.2}$$

where τ is the mean spacing of the data (Dawson 1980). If we equate the integral of the spacing probability distribution with the integral of the probability distribution of a uniform random variable we obtain:

$$\int_0^\infty e^{\frac{-t}{\tau}} dt = C \int_0^1 dK = C \tag{7.3}$$

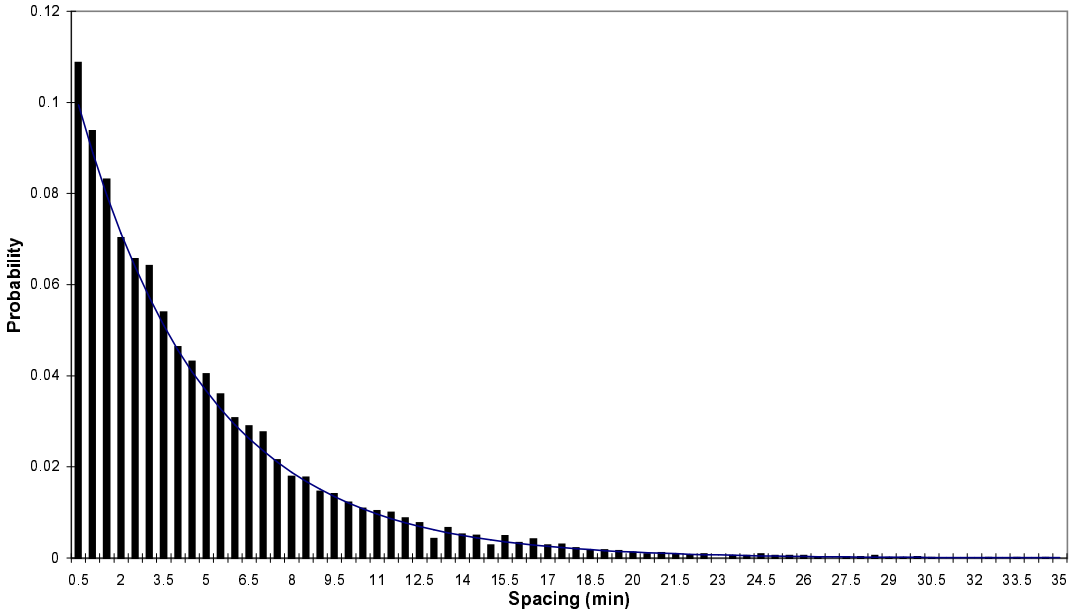

Figure 7.6: Spacing distribution of meteor echoes from the 1998 η-Aquarids campaign. Data from the East and West beams is shown. The solid line is an exponential distribution with mean = 4.8 minutes.

where C is a constant and K is the uniform random variable (Tocher 1963)

Thus

$$C = \tau \tag{7.4}$$

For a given spacing t and a random number, ϵ, lying between 0 and 1, we obtain (Tocher 1963):

$$\int_0^t e^{\frac{-t}{\tau}} dt = \tau \int_0^\epsilon dK \tag{7.5}$$

Therefore:

$$t = -\frac{\ln(1-\epsilon)}{\tau} \tag{7.6}$$

Thus using a series of random numbers between 0 and 1 we can generate a series of random spacings with a mean spacing of τ. Figure 7.6 shows the spacing distribution of meteors detected during the 1998 η-Aquarids campaign in the East and West beams. The mean spacing was 4.802 minutes. Also shown is an exponential distribution with

	Mean (minutes)	Standard Deviation
Before Shower	6.773	6.882
During Shower	4.007	4.134

Table 7.1: Mean of the spacing of meteors detected in the East and West beams before and during the 1998 η-Aquarids shower

a mean of 4.802 minutes.

The central limit theorem tells us that although the spacing distribution of meteor arrival times is not normal, for a large number of samples the sampling distribution of the mean, $\bar{x}$ is normal (Moore & McCabe 1993). For large sampling size n we can regard $\bar{x}$ as having the $N(\mu, \sigma/\sqrt{n})$ distribution. This means we can perform a test of significance on the mean of the spacing during the expected shower to see if it is significantly smaller than the mean when the shower is not present. Table 7.1 shows the mean of the spacing of meteors detected in the East and West beams before and during the shower. Note that the standard deviation of the data is very close to the mean, as expected for the exponential distribution.

We want to find the probability that the much smaller mean spacing during the shower could occur by chance. From the values in the table, the distribution of $\bar{x}$ is $N(6.773, 6.882/\sqrt{n})$, so in n observations the probability of getting $\bar{x} < 4.007$ is:

$$P(\bar{x} < 4.007) = P\left(\frac{\bar{x} - 6.773}{\frac{6.882}{\sqrt{n}}} < \frac{4.007 - 6.773}{\frac{6.882}{\sqrt{n}}}\right)$$

For the 786 meteors detected in the East and West beams during the shower period the probability that their mean spacing was equal to 4.007 by chance is so small as to be unmeasurable. Even for a mean of 6.0 the chances are 1 in 1220.

This test can also be used on the instantaneous meteor rates shown in Figure 7.5, as each point on the graph is the inverse of the mean over 8 values. The background mean spacing is 15.85 minutes for the 1999 data. The mean spacing is much larger in 1999 than 1998 as the meteor detection rate was much lower for this year's data. Table 7.2 shows a list of probabilities of obtaining different rates calculated over eight meteors with random mean spacing of 15.85 minutes.

Rate (per hour)	Probability
1000	0.0024
500	0.0025
100	0.0032
75	0.0036
50	0.0045
40	0.0052
30	0.0067
20	0.011
15	0.017
10	0.039

Table 7.2: Probability of obtaining meteor rates from random spacing with a mean spacing of 15.85 minutes

The chance of getting a rate of 15 or greater is about 1.7 %. The chance of this happening five or more times in the 105 meteors detected in the East and West beams on the 7^{th} of May 1999 (as depicted in Figure 7.5) is less than one in six billion. This strongly suggests that these peaks represent significant shower activity.

Further certainty can be obtained by reducing the background count rate by filtering the data. If the speed of the shower is known then those meteoroids which have speeds near the shower speed can be used to generate count rates. Figure 7.7 shows filtered count rates for the 7^{th} of May 1999. The η-Aquarids shower has a geocentric speed of about 66km s^{-1}. The data has been filtered by removing all meteors with measured speeds lower than 45km s^{-1}. The peaks at 2:00, 5:00, 10:00 and 11:30 are readily apparent.

7.3 Fine structure in meteor showers

The first observations of meteor showers by visual observers produced an apparent position of the source of the meteoroids, the radiant. These were quite uncertain as they relied on the observer seeing the meteor trail and identifying the background stars, then marking the path of the meteor on a star map. The trails of a number of meteors when extended back meet at the radiant. With the introduction of photographic and

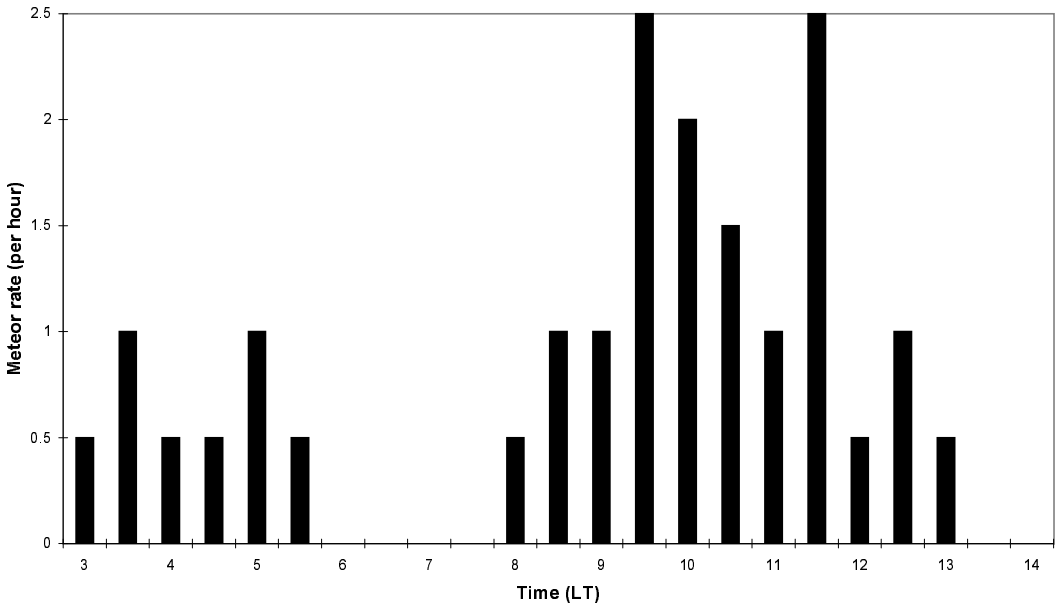

Figure 7.7: Meteor count rates for the 7^{th} of May 1999 where the data has been filtered by the speed of the meteor and is in half hour bins

radio meteor observation the radiant could be described more accurately, but different meteors were found to have slightly different radiants, and so "average radiants" and "radiant areas" or "radiant spread" were used to describe the source positions of meteor showers. On many occasion researchers have noted that there appeared to be two or more distinct radiants observed during the duration of a shower and also great discrepancies in the day to day count rates of the shower. These properties of meteor showers suggest that the particles in the stream are not randomly distributed throughout the orbit, but are separated into a large number of smaller streams or filaments. This conclusion is supported by the results of numerical integration of the orbits of test particles ejected from a comet at various dates throughout history (Asher 1999, Göckel & Jehn 2000).

The Buckland Park VHF radar is a useful tool for observing the structure of meteor showers. This structure is quite difficult to see, as the flux of particles into the earth is

extremely variable, and the earth's rotation means that the shower is only observable at a particular point on the earth for a short period. In addition the shower is only present when the orbit of the meteoroid stream intersects that of the earth, which depends on the width of the stream, but is usually from a few days to a couple of weeks in duration.

A radar system with a narrow beam will give good time resolution as the radiant of the shower crosses the sky. For the Buckland Park VHF radar, with a 3° beam, the time resolution is 12 minutes (*ie* the earth rotates 3° in 12 minutes). By making use of the vastly increased reflection coefficient of meteor trails incident perpendicular to the beam, the exact time when the shower crosses the beam, and therefore its position in the sky can be determined. In addition, the ability to swing the beam means that observations can be made of the shower at several times during a day. Of course a radar system has an advantage over optical systems in that observations can be made regardless of sunlight, moon, or weather conditions.

The experimental setup for a shower observation depends on the expected position of the radiant, but usually the beam would be set to 30° west of the zenith as the radiant rises in the east. This should give specular reflection when the radiant is at 30° elevation, if the radiant passes through the zenith. Of course this is rarely the case, but the peak will occur when the radiant is 90° away from the beam direction. Next the beam would be changed to point toward the position of maximum elevation of the radiant (usually to the north from Buckland Park) to obtain down-the-beam observations as the radiant passes its highest point in the sky, or it can be directed to the south to give transverse observations. The radiant is in the response function for some time when the south beam is used, as the path of the radiant follows the shape of the response function. Lastly the beam would be changed to 30° east of zenith to give transverse observations as the radiant sets. The geometric properties of meteor showers means that the radiant changes position each day with respect to the stars but stays in roughly the same place with respect to the observer for a given time of day, since the stream of particles are in the near solar system and our time system is

based on the rotation of the Earth.

7.4 Observations of meteor showers with the Buckland Park VHF radar

The Buckland Park VHF radar has been used for meteor observation during the years 1997-2000, and observations include the η-Aquarids, Orionids, Geminids, Leonids, Southern δ-Aquarids, Lyrids, Phoenicids, Pegasids, Pisces Austrinids, α-Capricornids, Taurids,

7.4.1 η Aquarid meteor shower

The η Aquarid meteor shower is visible during the period of April 21 to May 12, and reaches maximum around May 5. It appears to originate from the constellation of Aquarius (hence the name) from an average radiant of 336° in Right Ascension and $-1°$ in Declination. In 1863, Professor Hubert A. Newton examined the dates of ancient showers and suggested a series of periods which deserved the attention of observers. One of those periods was April 28-30, and included observed showers in 401 AD, 839 AD, 927 AD, 934 AD and 1009 AD. The Eta Aquarids were officially discovered in 1870, by Lieutenant-Colonel G. L. Tupman who observed 15 η-Aquarid meteors on April 30 and 13 on May 2-3. The shower was shown to have a spread of about 5° and also to have multiple dates for the maximum count rate, making the shower an ideal candidate for observation of possible fine structure. The geocentric speed of these meteoroids has been measured at 66km s^{-1}, and the shower (and also the Orionids in October) has been associated with Comet Halley (McIntosh & Hajduk 1983).

7.4.1.1 Review of η-Aquarids observations and analysis

Olivier (1912) collected visual observations of the η Aquarids from 1910-1912 and produced a table of observed radiants for the shower. This data is reproduced in Table

Date (UT)	Right Ascension (deg)	Declination (deg)
1910 May 4.97	334.0	-3.4
6.85	337.7	-0.6
11.99	342.0	-0.6
1911 May 2.82	331.7	+0.2
4.87	332.4	-0.8
5.87	336.0	+0.0

Table 7.3: Observed radiants of the η-Aquarid meteor shower (Olivier 1912)

7.3, where it can be seen that there were a number of different observed radiants for η-Aquarids meteors, although these radiants were produced with only a few observed meteors each, ranging from only 3 for the May 4 1911 radiant, to 25 for the May 6 1910 radiant. Olivier made many more observations of the shower, in 1914-18, 21, 22, 24 and 25. In 1935 McIntosh (1935) reported that observers of the New Zealand Astronomical Society had reported over 31 radiants for their observations of the η-Aquarids. McKinley (1955) used the meteor radar at Ottawa to produce a mean observed speed for the η-Aquarids of 64.4km s^{-1}, and a radiant of $330 \pm 4^{\circ}$ in Right Ascension and $0 \pm 2^{\circ}$ in Declination. Weiss commented on observations made with the Adelaide radar during the period 1952-6 that the η-Aquarids were detected for a considerable time before the expected rise time of the radiant and for some time after the expected set time. This implied either a diffuse radiant or a compact radiant surrounded by diffuse activity (Weiss 1957). Keay and Ellyett's radar surveys of meteor activity from New Zealand also showed extended activity for the shower (Ellyett & Keay 1963, Keay & Ellyett 1969). Hajduk performed a number of analyses of shower activity from 1910 to 1978 from various sources, both visual and radar observations (Hajduk 1973, Hajduk 1980, Hajduk & Buhagiar 1982). The shower showed variations in activity throughout each apparition, as well as a displacement of the date of peak activity. A double peak in the activity was observed along with a central zone of increased density. The small differences in the rates of the η-Aquarids when compared to the Orionids, and the durations of the showers, could not be satisfactorily explained

while labouring under the assumption that meteoroid streams were centred on the current orbit of the associated comet.

McIntosh & Hajduk (1983) developed a shell model for the meteoroid streams produced by Comet Halley, which postulated that the meteoroids were in orbits where the comet has been in all previous revolutions. The libration of the orbit of the comet then produces a segment of a shell, which as the meteoroids disperse becomes a belt of meteoroid orbits. Over many cycles of libration, there would be several such belts formed, producing the observed multiple peaks in activity. Observations by Hajduk & Váňa (1985) confirmed the existence of at least two belts of particles as did observations by Hajdukova et al. (1987) and Hajduk (1987). Chebotarev et al. (1988) also confirmed the double peak in the activity of the shower, and produced radiants for a number of radar meteors observed in 1969. This radiant plot showed two separate diffuse radiants for the shower, each with approximately the same flux throughout the shower period. The area of the radiants covered 6° and was centred at 338° in Right Ascension and +1° in Declination. Thomas (1989), using the Jindalee Over-the Horizon radar in central Australia, observed the shower and recorded a radiant centred at 339° in Right Ascension and 0° in Declination, with a spread of at least 6°.

Modelling of up to 500 test particles by McIntosh & Jones (1988) verified the shell hypothesis of McIntosh and Hajduk quantitatively, including the effects of planetary perturbations, solar radiation pressure and Poynting-Robertson drag on the particles. They found that the stream cross-section becomes highly elongated in a few thousand years and suggested that the particles which produce the Orionids were released from Comet Halley less than a few thousand years ago, and those in the η-Aquarids stream are even more recent.

After the return of Comet Halley in 1986, when three spacecraft closely approached the comet, Hughes produced a comparison between the dust collected by these spacecraft and the meteoroids observed on Earth as meteors (Hughes 1987). He compared the mass distribution and particle fluxes, although non-overlapping mass ranges

and collection locations made comparison difficult. Further observations of the η-Aquarids include orbit determinations from photographic and TV system double station observations (Lindblad et al. 1994, Shigeno et al. 1997), and visual observations (Baldacchino 1995, Cooper 1996, Rendtel 1997).

7.4.1.2 Radar observations of the η-Aquarids at Buckland Park

Observations of the η Aquarids were made in the years 1997-2000 using slightly different radar configurations, and the data recorded were analysed using the processes outlined in earlier chapters. The observations were made at a PRF of 1024 Hz in 1997, 2000 Hz in 1998 and 1650 Hz in 1999 and 2000. The general experimental setup involved observing with the beam tilted 30° off zenith to the West for two to three hours around the time maximum rates were expected. This was determined according to the response function for that particular beam orientation and the radiant as described above, and was at about 0450 local time (1920 UT). This was followed by an observation with the beam tilted 30° off zenith to the East under the same conditions, at around 1040 local time (0110 UT). At all other times, the beam was directed to the North or the South, to allow the observation of down-the-beam echoes or transverse echoes respectively, while the radiant was at its highest point. The detection and analysis of the η Aquarids shower in 1997 has been previously published (Badger 1997, Badger & Elford 1999) and the paper by Badger and Elford is reproduced in Appendix B.

7.4.1.3 Meteor rates during the Buckland Park η- Aquarids campaigns

The first analysis performed was to determine the meteor rates during the observations. This was done by using the instantaneous meteor rates as described in Section 7.2.3. Figure 7.8 shows this instantaneous meteor rate for three days in 1998. Of note is the existence of not just one, but two or more significant peaks in each beam direction on many of the days of observation. In Figure 7.8 there are two peaks in each beam on the 6^{th} and the 8^{th}, and on the 7^{th} there are three peaks visible in each beam direction.

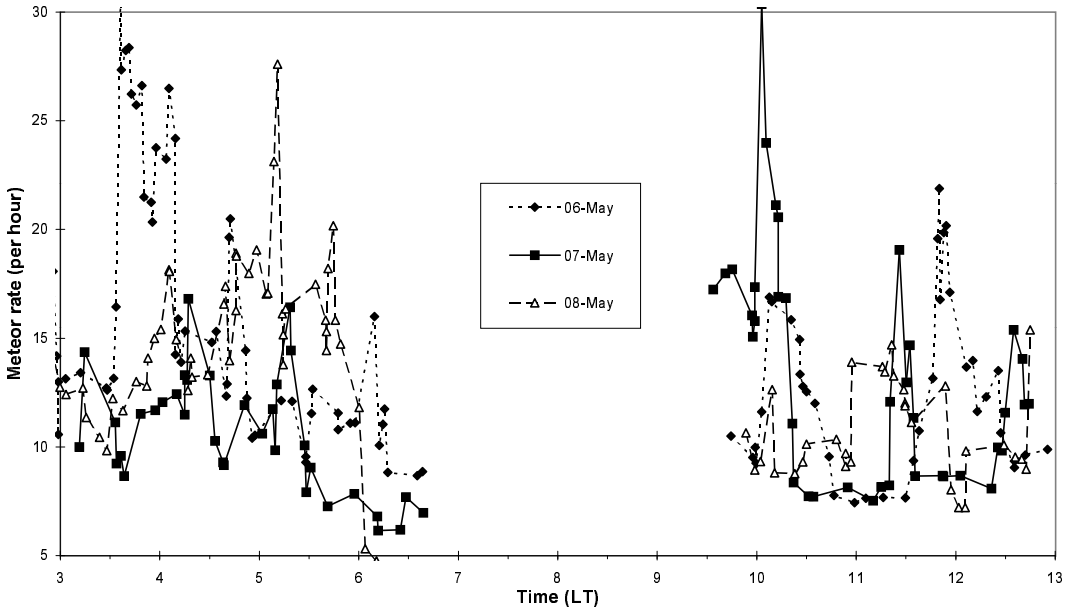

Figure 7.8: Instantaneous meteor rates during the η-Aquarid meteor shower in 1999.

When the records had been analysed and speeds obtained, the peaks could be further resolved by producing instantaneous meteor rates for only those meteors which had measured speeds between 50 and 70km s^{-1}. Figure 7.9 shows the instantaneous rate for meteors with speeds between 50 and 70km s^{-1} for three days in 1999. Although the peaks are smaller than those in Figure 7.8, they are even more significant, as the rate of sporadic meteors with speeds between 50 and 70km s^{-1} was measured at 1.25 per hour, which is much lower than the rate for all speeds (8.86 per hour). The probability of obtaining instantaneous rates of seven meteors per hour is about 2.5 % from random meteors with a mean rate of 1.25 per hour, about the same as getting an instantaneous rate of thirty per hour if all meteors were used (see Section 7.2.3.

Table 7.4 shows the times when the instantaneous meteor rate showed a statistically significant peak for each of the days of observations, to the nearest five minutes. The data in the table shows the changeability in the meteor rate from day to day as has been previously observed, suggesting that the distribution of particles in the stream is

Day of observation	Time of peak - West beam (LT)	Time of peak - East beam (LT)
May 01 1998	0415	-
May 02 1998	-	1215
May 04 1998	0610	-
May 05 1998	0450, 0630	0950, 1120
May 06 1998	0335, 0420	1135
May 07 1998	0425, 0520	0950, 1135
May 08 1998	0420, 0505, 0610	1000, 1105, 1210
May 09 1998	0320, 0610 (double)	1020, 1135
May 10 1998	0240, 0355, 0620	1055, 1110
May 11 1998	0410, 0610	-
Apr 29 1999		-
Apr 30 1999	-	1035
May 01 1999	0555, 0610	-
May 02 1999	-	0950, 1010, 1050, 1150
May 03 1999	0520	1245
May 04 1999	0545	1020, 1035
May 05 1999	-	0945
May 06 1999	0255, 0335, 0410, 0415, 0440, 0610	1010, 1155
May 07 1999	0415, 0520	1005, 1125, 1235
May 08 1999	0250, 0405, 0440, 0510, 0535, 0545	0920, 1245
May 09 1999	0255, 0425, 0500	1030
May 10 1999	0350, 0420, 0630	0950, 1125
May 11 1999	0445, 0515 (double)	1050 (double), 1110
May 12 1999	0240, 0555, 0625	1120 (double), 1150, 1220
Apr 29 2000	-	-
Apr 30 2000	-	1145
May 01 2000	-	-
May 02 2000	-	-
May 03 2000	-	1050
May 04 2000	0405, 0555	1010, 1020, 1150
May 05 2000	0245, 0400, 0610	1115
May 06 2000	0420, 0620	-
May 07 2000	0340, 0450	0910
May 08 2000	0355	-
May 09 2000	0615 (double)	1045 (double)
May 10 2000	0400	-
May 11 2000	0305 (double)	1030, 1120
May 12 2000	-	-

Table 7.4: Peaks in the instantaneous meteor rate

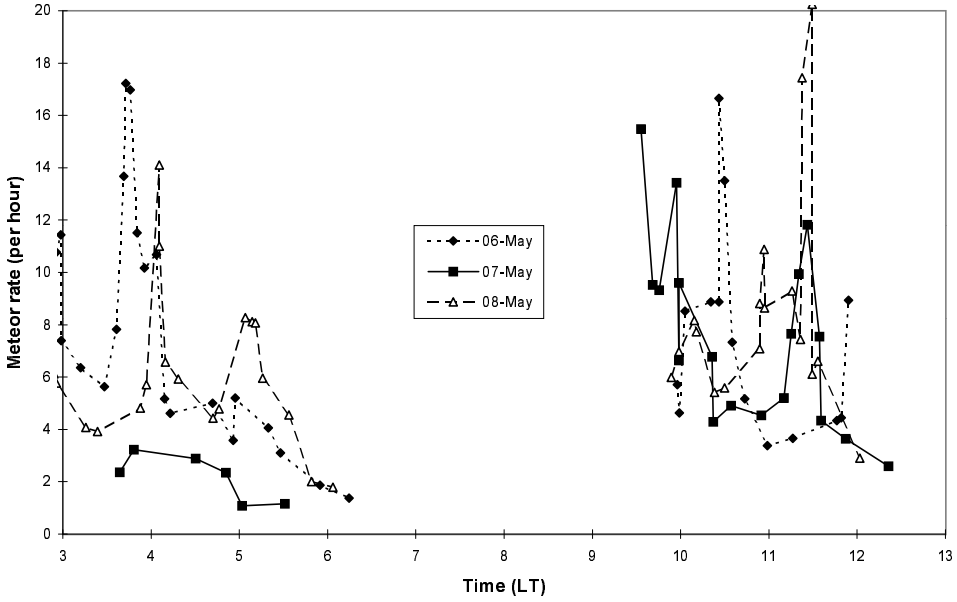

Figure 7.9: Instantaneous rates of meteors with measured speeds between 50 and 70km s^{-1} during the η-Aquarid meteor shower in 1999.

not even, but that there are "belts" of particles throughout the stream. These "belts" are generally observed in the West and in the East beam observations. However most previous radar observations utilised wide beam radars which did not allow the resolution of individual peaks in activity, but rather averaged the activity over a wide angle (typically $> 30°$).

Another important feature is that the time of the individual peaks changes from day to day, and peaks can occur twice or even three times during the observation with a single beam direction in a day.

The IMO meteor shower chart lists several minor showers which may be active during the period of observation. Jenniskens (1994) lists other showers which were observed around this time, the only one commonly listed being the η-Aquarids and possibly the (γ) Sagittarids. Table 7.5 shows these showers and lists the period of activity, day of peak activity, radiant position, speed and the expected time of rate

Shower	Activity	Peak	R. A. deg	Decl deg	Spd km/s	West LT	East LT
η-Aquarids	Apr 19-May 28	May 06	338	-01	66	0410	1120
ϵ-Arietids #	Apr 24-May 27	May 08	044	+21		0715	1655
Arietids (May) #	May 04-Jun 06	May 16	037	+18		0620	1600
o-Cetids #	May 05-Jun 02	May 20	028	-4		0640	1400
Sagittarids #	Apr 15-Jul 15	May 20	247	-22	30	2025	0520
α-Scorpiids*	May 06-May 26	May 16	240	-25	35	2005	0525
β-Corona Australids*	May 13-May 20	May 17	284	-40	45	2210	0855
γ-Sagittarids*	May 16-Jul 15	Jun 06	271	-26	29	2040	0615
μ-Virginids*	Apr 13-May 16	Apr 26	227	-7	30	2125	0505

Table 7.5: Showers present during the Observation period ("#" from IMO meteor shower list and "*" Jenniskens (1994)) Listed are the dates of possible activity and the date of peak activity (the η-Aquarids is well known to have two peaks, the average is shown). Next the average radiant in degrees of Right Ascension and Declination, the measured geocentric speed in km s^{-1} and the estimated time of peak rates in the West and East beams.

peaks in the West and the East beams of the radar. The radiant positions are those for the date of peak activity, but the expected rate peaks are for May 6. Any recorded radiant drift[1] has been taken into account.

Since observations were typically made with the West beam from 0230 to 0630 (LT) and with the East beam from 0900 to 1300 (LT)[2], these minor showers would not have been observed if their radiants were those listed and point sources of meteors. However, there is no reason to assume that these minor showers would not exhibit behaviour similar to the η-Aquarids, and have diffuse or multiple radiants.

The o-Cetids is likely to be observed in the last minutes of the observation in the West beam. Table 7.4 shows an increase in the rates at times around 0600 to 0630

[1]The radiant drift occurs because the radiant is a position relative to the background stars, and these have an apparent movement in the sky each day. The Earth spins about 365.25 times a year, but as it moves around the sun it rotates one extra time per year, this extra spin moves the apparent star positions by $360/365.25 \approx 0.99°$ each day. The meteor radiant is dependent on the orientation of the Earth with the orbit of the stream, and is in nearly the same place in the sky every night, therefore the radiant drifts by nearly 1° each day with respect to the sky. This drift is compounded by the observation of different filaments, which has slightly different radiants.

[2]There was some variation in these times due to dead time in recording the RDAS data and clocks drifting out of sync, but the maximum variation was of the order of 15 minutes. The average variation was about 2 minutes.

Peak	Mean peak '98	Mean Peak '99	Mean Peak '00	Activity '98	Activity '99	Activity '00	Speed km/s
1-W	2:56 ±11	2:53 ±2	2:58 ±7	5,9,10	6,8,9	5,11	62.2
2-W	3:40 ±6	3:41 ±7	3:35 ±11	2,4,5,10	6,9,11	7,8,11	62.5
3-W	4:27 ±5	4:19 ±4	4:13 ±9	5-8,11	8-10,12	4-7,10	63.5
4-W	5:10 ±7	5:03 ±7	-	4,8	4,8	-	61.5
1-E	-	9:23 ±4	9:11 ±12	-	6,8,9	7	60.8
2-E	10:03 ±5	10:09 ±3	10:19 ±3	1,5,7-9	2,6-11	4,11	61.8
3-E	11:01 ±3	10:55 ±4	11:02 ±7	2,7-10	3,8-11	3,5,9,11	62.1
4-E	11:43 ±5	11:32 ±8	11:39 ±7	30,2,5-9	6-8,10	30,4,5	61.1

Table 7.6: Mean peak activity time for the η-Aquarids 1998-2000. The peaks are labelled in chronological order, and the "W" or "E" denotes the West or East beam respectively. The times are all local times, and the dates of activity are all May, except for "30" which denotes April 30. The "Speed" column denotes the mean speed of meteors with speeds between 50 and 70 km s^{-1} in each of the peaks

(LT) for May 4,5,8,9,10 and 11 in 1998, May 1,6,10, and 12 in 1999, and May 4,5,6,and 9 in 2000. This increase in activity could be due to the May Arietids or the o-Cetids. It is worth noting that there does not seem to be a significant increase in the rates in the East beam at times around 1300 (LT) on these days. If the rate increase on these days was due to the η-Aquarids, it would be reasonable to see peaks late in the East beam as well as the West beam. Due to the radiant position of the Arietids and o-Cetids, there would be no activity from these showers in the East beam for another hour or more, even if it was diffuse enough to produce activity late in the West beam observations.

An investigation of the instantaneous rates for meteors with measured speeds between 50 and 70km s^{-1} for the above mentioned dates where increased rates were observed was performed. This revealed that the peaks from 0600 to 0630 are not due to meteors with measured speeds in this range, and thus are likely to be due to the May Arietids or the o-Cetids, and not the η-Aquarids. These instantaneous rates were used as the basis for more accurate determination of the time of the peaks in the data, and these peaks were used to determine the radiants of the shower.

Peak (West)	Mean time (LT)	Peak (East)	Mean (LT)	R A (deg)	Decl (deg)	Speed km/s	Activity
1-W	2:53 ±3	2-E	10:09 ±3	316.5	-0.75	61.9	Strong
2-W	3:40 ±4	1-E	9:20 ±4	316.0	19	61.7	Medium
3-W	4:12 ±3	3-E	11:03 ±4	332.5	4.8	62.9	V. Strong
4-W	5:58 ±5	4-E	11:44 ±4	344	5.2	61.2	Strong

Table 7.7: Mean peak activity and radiants for the η-Aquarids 1998-2000. The peaks in the West beam observations and their matching East beam peaks are shown, with the mean time of peak activity. The corresponding radiants are shown in degrees of Right Ascension and Declination. The mean speed of the meteors in the peaks is given and the activity of each radiant

7.4.1.4 Radiants of the η-Aquarids

The peaks obtained from the instantaneous meteor rates for meteors with speeds between 50 and 70km s^{-1} were examined, and it was found that there were four distinct peaks in the meteor rate in each of the two beam directions during observations. Table 7.6 shows the mean time of occurrence of these peaks for each of the years 1998-2000, the dates when these peaks were observed, and the mean speed of the meteors with speeds between 50 and 70km s^{-1} in the peaks. The error given in the mean time of occurrence is the sample standard deviation divided by the square root of the number of observations of each peak (commonly referred to as the standard error in the mean).

The mean speed should be lower than the expected entry speed of the η-Aquarids (66 km s^{-1}), since some sporadic meteors are included, and since many of the shower meteors will have decelerated before (and during) observation. It is of interest to note that the mean speed of the earlier observations (West beam) is about 1 km s^{-1} larger than that of the later observations (East beam). This may be due to the increased ionisation in the atmosphere after the sun has risen, increasing the effect of Faraday rotation attenuation.

With such a large number of the peaks in the instantaneous meteor rate, it is difficult to match the earlier peaks with peaks in the later observations to produce radiants. The simplest way is to look for a number of consecutive days when there

are peaks at around the same time each day, and find the mean time of the peak, then match peaks from the early to the late observation to give a mean radiant. The relative strength of the activity is also taken into account. This can be useful, but still leaves some ambiguity. By using the speed distribution of the meteors detected around each of the peaks, we find that the groups of peaks have different speed distributions, which assists us in matching them to each other (see (Badger & Elford 1999)). Once the peaks have been matched, the radiants can be determined.

By use of the radar response function, the declination of the radiant as a function of the gap between the peaks in the West and the East beam observations is determined. Once the declination is established, the Right Ascension is determined from time of peak activity in either the West or the East beam observations.

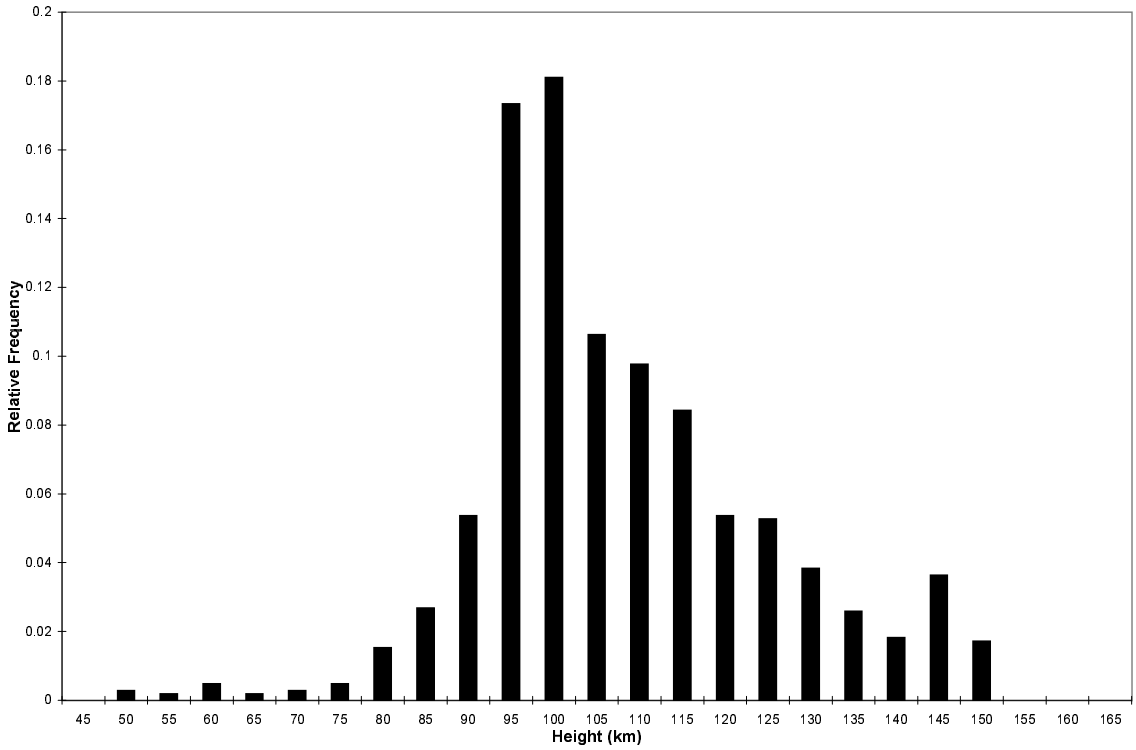

Figure 7.10: Height distribution of meteors observed during the period of η-Aquarid activity. The bin size is 5 km, centred on the labelled values.

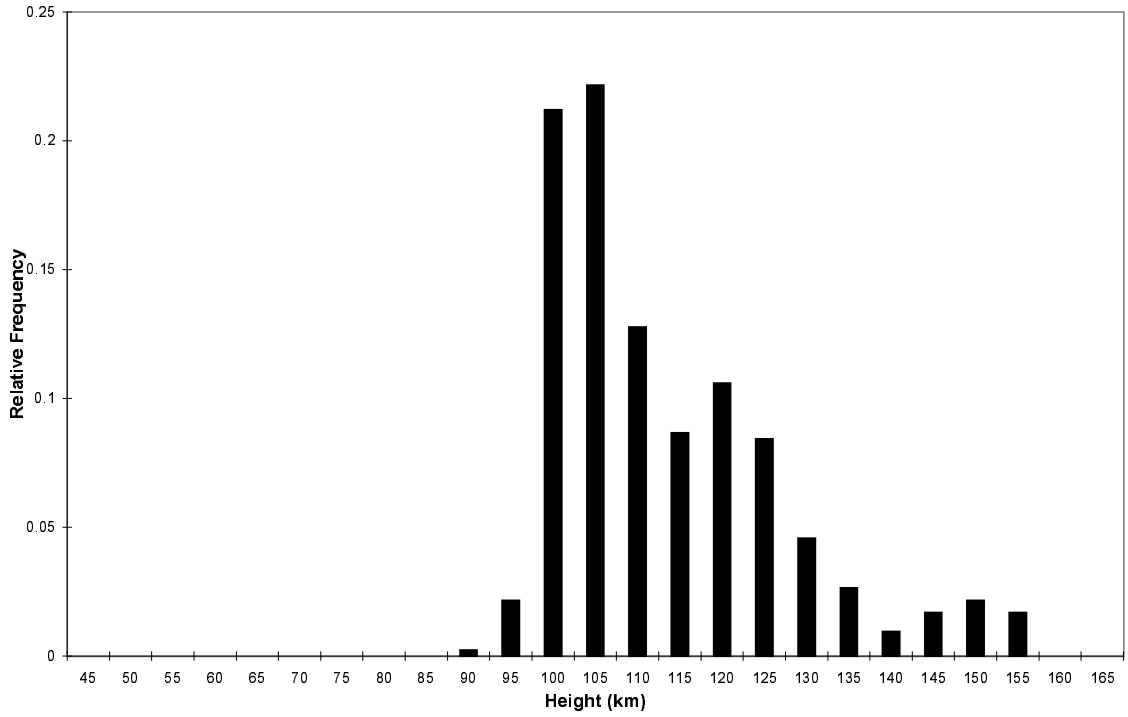

Figure 7.11: Height distribution of meteors observed during the period of η-Aquarid activity with measured speeds between 50 and 70 km s^{-1}. The bin size is 5 km, centred on the labelled values.

Table 7.7 shows the matched peaks, averaged over all observations, and the radiants determined from these peaks. The peaks in the West beam observations are listed first, along with the mean time of peak activity over all three years. These are matched to peaks in the East beam, and their mean time of peak activity. The radiants corresponding to the matching of peaks are shown in degrees of Right Ascension and Declination. The maximum error of 5 minutes in the time of peak activity leads to a maximum error in the Declination of $\pm 0.5^\circ$ and this error and the error in the time combined gives a maximum error of 1.5° in Right Ascension. The speed of the radiants was the mean calculated from all meteors with speeds between 50 and 70 km s^{-1} present in the peaks. Also shown is the activity of each radiant, based on the total number of meteors detected for each radiant.

The radiants determined here differ from those obtained previously with the Buckland Park VHF Radar (Badger & Elford 1999). The previous work was based on a much smaller subset of data recorded in 1997, and highlights the variability of the structure of the meteoroid stream. The radiants presented here are representative of the major structure of the stream, averaged over three years of observation.

7.4.1.5 Height and speed distribution of the η-Aquarids

In order to look at the characteristics of the η-Aquarids, we want to separate out the shower meteors from the sporadic background. The first step in this is to collect all meteors which occurred within half an hour of each of the peaks listed in table 7.4, except those which were identified as belonging to the May Arietids or the o-Cetids. This should increase the proportion of shower meteors in the sample significantly.

Figure 7.10 shows the distribution of the range/angle heights of the meteor echoes collected in this way. The bin size is 5 km, centred on the labelled values. There is a strong peak in the distribution around 95-100 km, superimposed on a smaller, broader distribution centred at around 105 km. There is also a suggestion of a peak at 125 km and one at 145 km. This distribution still contains meteors from the sporadic background. There are two ways to remove this background, by subtracting the height distribution of the sporadic background (see later in the chapter), or by sorting the meteors in Figure 7.10 by their speeds.

When only those meteors with speeds between 50 and 70 km s^{-1} are included in the height distribution, we obtain Figure 7.11 which shows distinct peaks, at 100, 115 and possibly 145 km. These suggest that these meteors are from two populations of meteoroids with different physical properties (see Section 5.6). Subtracting the sporadic background from the height distribution in Figure 7.10 produced results which were not significantly different from Figure 7.11, so this distribution is not reproduced here.

Those meteors collected during the periods of η-Aquarid activity for which the speed could be determined are shown as a histogram in Figure 7.12. The bins are

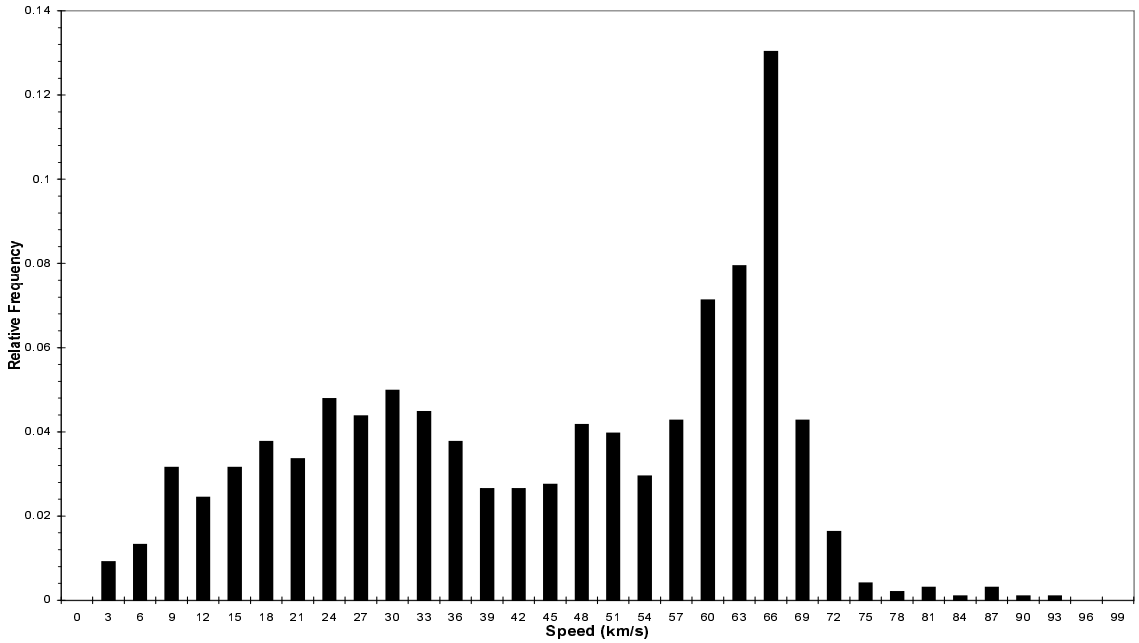

Figure 7.12: Speed distribution of meteors observed during the period of η-Aquarid activity. The bins are 3km s^{-1} wide, centred on the labelled values.

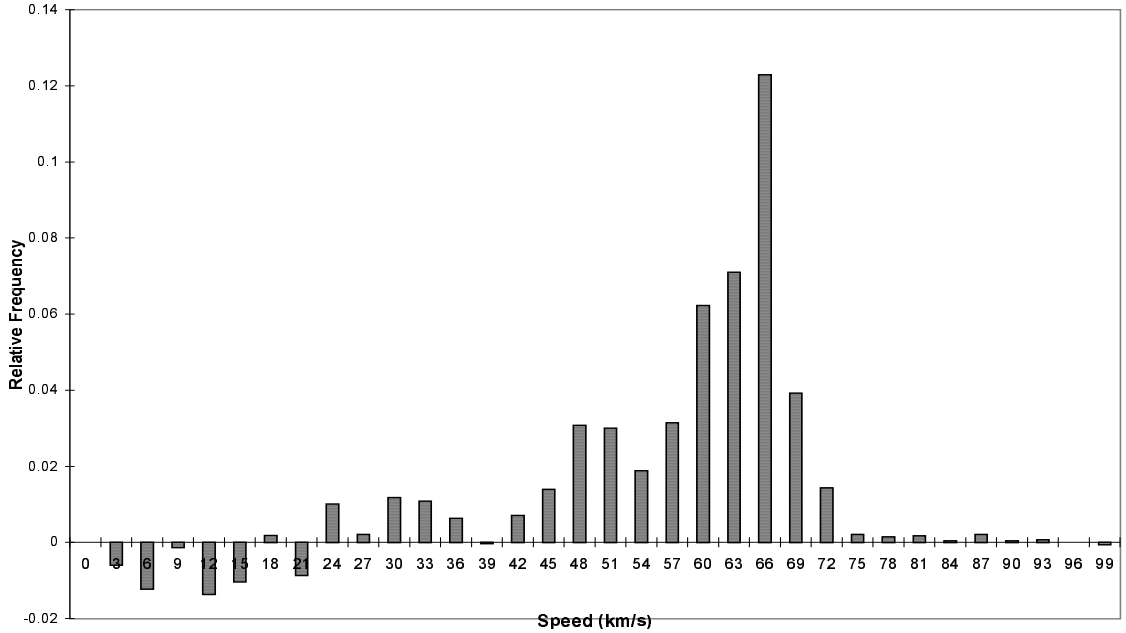

Figure 7.13: Speed distribution of η-Aquarids meteors with the sporadic background removed. The bins are 3km s^{-1} wide, centred on the labelled values.

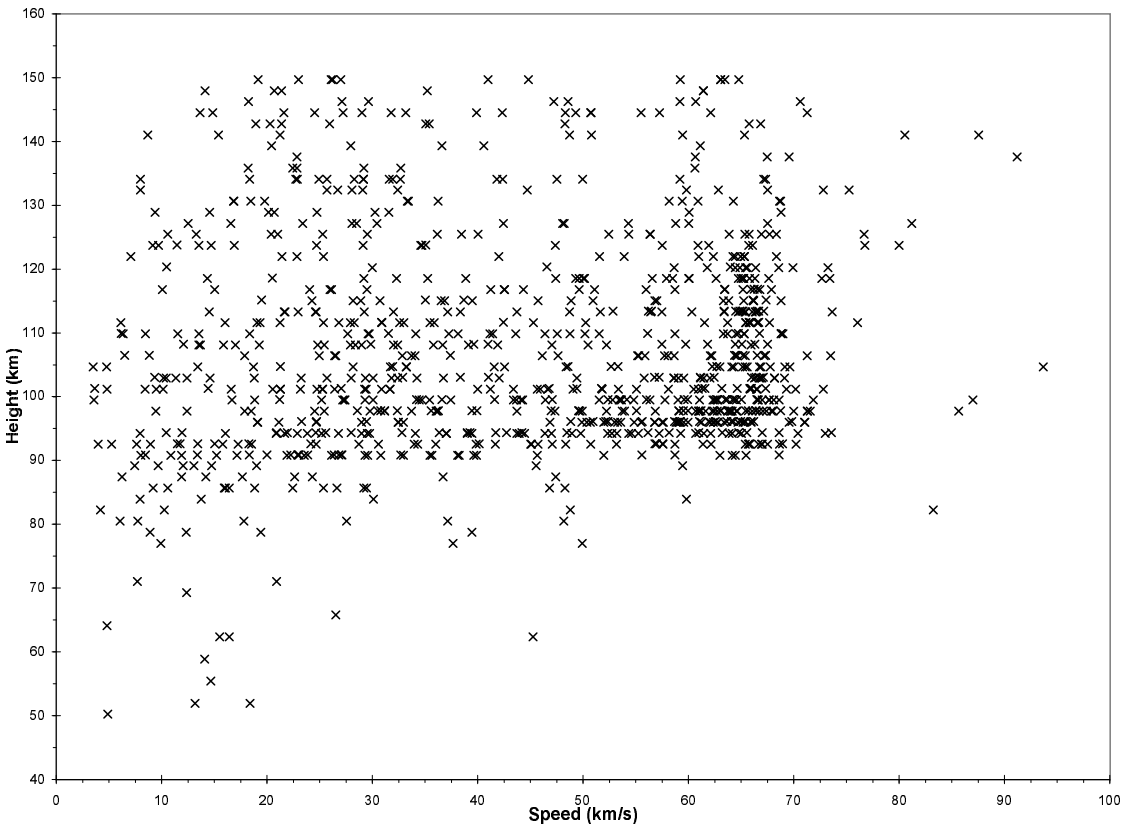

Figure 7.14: Speed-height scatterplot of η-Aquarids meteors

3km s^{-1} wide, centred on the labelled values. There is a strong peak in the distribution at 66km s^{-1}, which shows a sharp cut-off for higher speeds, but a decay into lower speeds. Such behaviour is to be expected due to retardation of meteoroids in the atmosphere. It is clear from the plot that other meteors besides the shower meteors are present, as the sporadic background shows up with a peak at about 30km s^{-1}. There is also a small peak at about 50km s^{-1}. We cannot remove the sporadic background from this distribution by sorting by speed, instead we must subtract the sporadic speed distribution from Figure 7.12.

Once the sporadic background (see Section 7.4.3) is removed from the data, we are left with Figure 7.13. The large peak at 66km s^{-1} is even more apparent, and also there is still a peak at about 50km s^{-1}. This would seem to be due to the minor showers which are present at the same time.

Figure 7.14 shows the selected meteors from Figures 7.10, 7.12 and 7.13 as a speed *versus* height scatterplot. We can see that there are shower meteors at 95 to 125 km, and as expected, those which are detected at lower heights have generally been decelerated from their pre-atmospheric speed of 66km s^{-1}.

7.4.2 Other showers

Observations were made when a number of other annual showers are active. Full analysis of this data has not yet been performed, but the preliminary results are as follows.

7.4.2.1 Orionids

The Orionid meteor shower, like the η-Aquarids, is associated with comet Halley. It is active from October 2 to November 7 with a maximum on October 22. The mean radiant of the shower is at 94° in Right Ascension, and 16° in Declination. The observed geocentric speed is 67km s^{-1}. The Orionids are the more frequently observed of the pair of showers, as the radiant rises higher in the sky when viewed from the Northern Hemisphere, where the bulk of observations have been made.

Figure 7.15 shows the height distribution of all of the meteors recorded during the Orionid meteor shower, 15-22 October 1999[3]. The PRF was 1650 Hz, producing restrictions in the possible range detected, allowing only 16-84 km (or 107-175 km when aliased once). Two different off-zenith angles were used for observations to allow transverse meteors from the shower to be observed over a long period of time. These were 38.7° for the East and West beams, and 22° for the South beam, which allowed observations while the radiant was passing to the North of the radar. Roughly equal numbers of meteors were detected with each off-zenith angle. The height distribution shows an artificial cut-off below 85 km, the shaded columns are produced by unaliased ranges, and could actually be at heights from 150-165 km not 65-80km as shown. This

[3]These meteors have not been selected by peaks in the meteor rates and thus a large number of sporadics are also depicted.

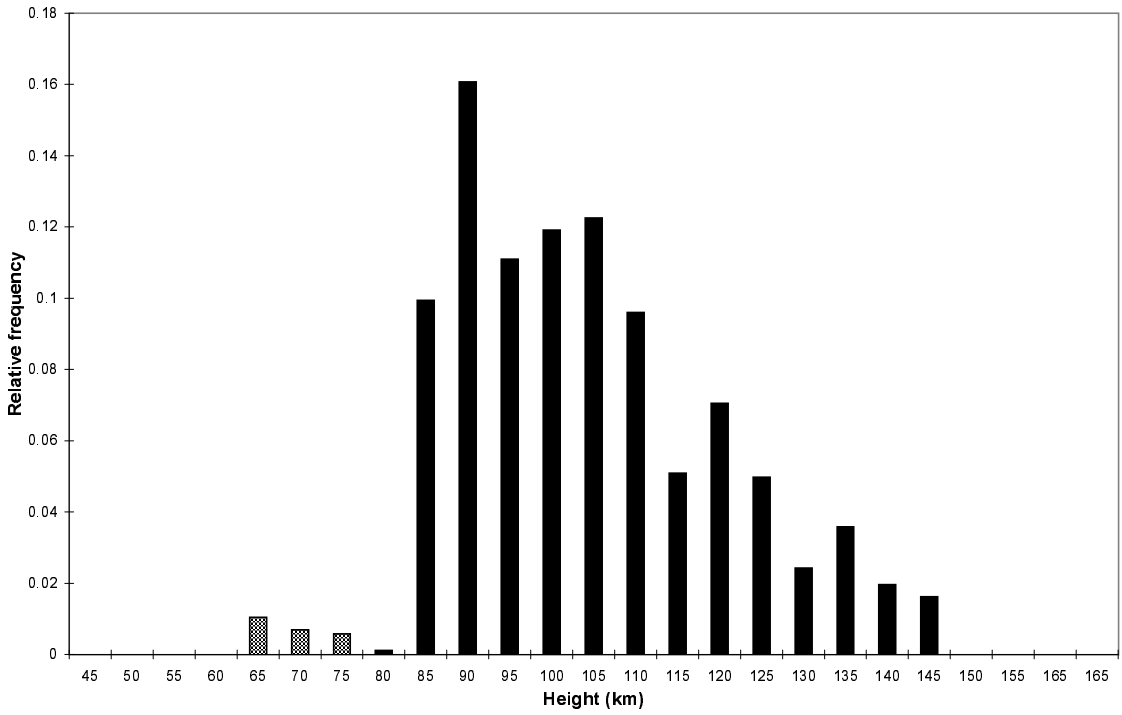

Figure 7.15: Height distribution of meteors observed during the Orionids, 15-22 Oct 1999. The bins are 5 km wide, centred on the labelled values.

ambiguity could be resolved by measuring the diffusion coefficient for the echoes in question, but in view of the small number of echoes involved this was not done. The height distribution shows a peak height of about 95-100 km for these meteors.

When the height distribution of the sporadic background is removed, we obtain Figure 7.16. This reveals peaks in the height distribution at 90, 105, 120 and 135 km. The height distribution is similar to that of the η-Aquarids, which is not unexpected as the two showers are produced by meteoroids from the same comet (Halley) and should have similar physical properties and geocentric speeds.

Figure 7.17 shows the instantaneous meteor rates for one day of observations of the Orionids. There are several peaks in the East and the West beam observations, suggestive of filamentary structure in the Orionids, as seen in the η-Aquarids, but the interesting feature is the widely varying rates seen with the South beam. The radar response to a radiant in the position of the Orionids is nearly constant for several

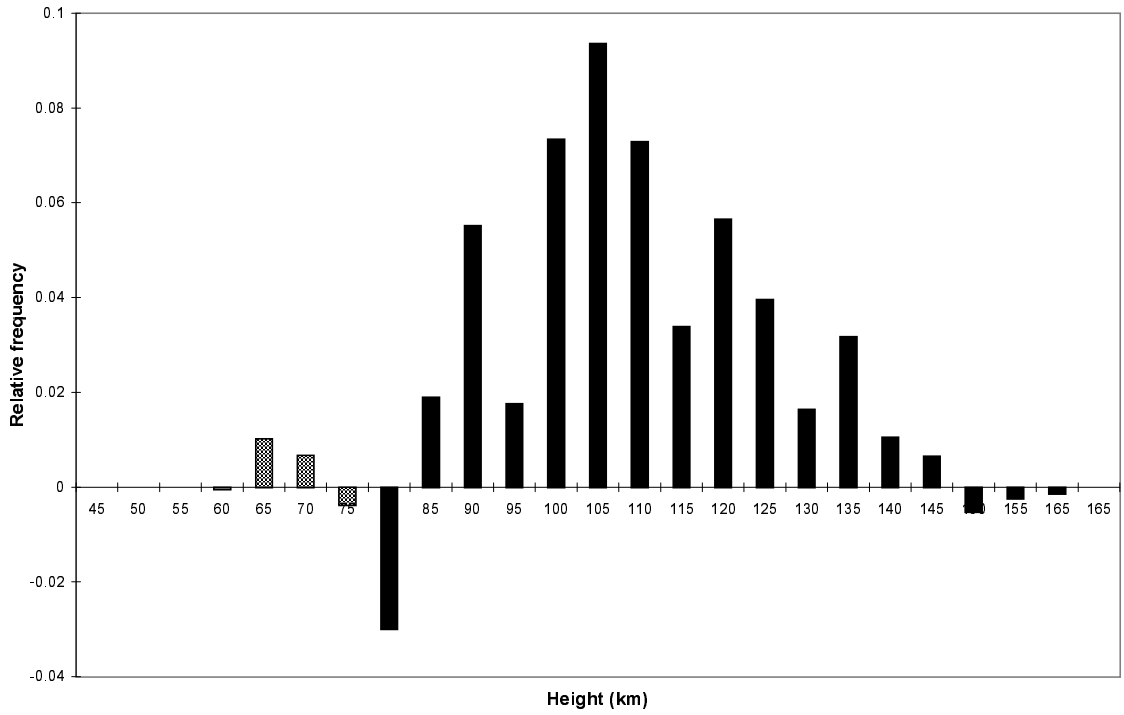

Figure 7.16: Height distribution of meteors observed during the Orionids, 15-22 Oct 1999, with the sporadic background removed. The bins are 5 km wide, centred on the labelled values.

hours for the South beam observations, as the response function "follows" the radiant during this time, *ie*, the antenna beam is perpendicular to the radiant for some time. Thus we would expect a gradual increase and decrease in the rate for a steady stream of meteors. Instead, what we see is sudden increases and decreases in the meteor rate. This suggests that the stream is arriving as "clumps" of particles.

7.4.2.2 Leonids

The Leonids have been the subject of intense observation and discussion in the years leading up to 2001, as the return of comet P/Tempel-Tuttle heralded the meteor storms associated with the Leonids, possibly a repeat of the spectacular displays of 1833 and 1966. For the first time, these storms would be a serious threat to space vehicles, not just because of their greatly increased numbers over the last 33 years, but also through

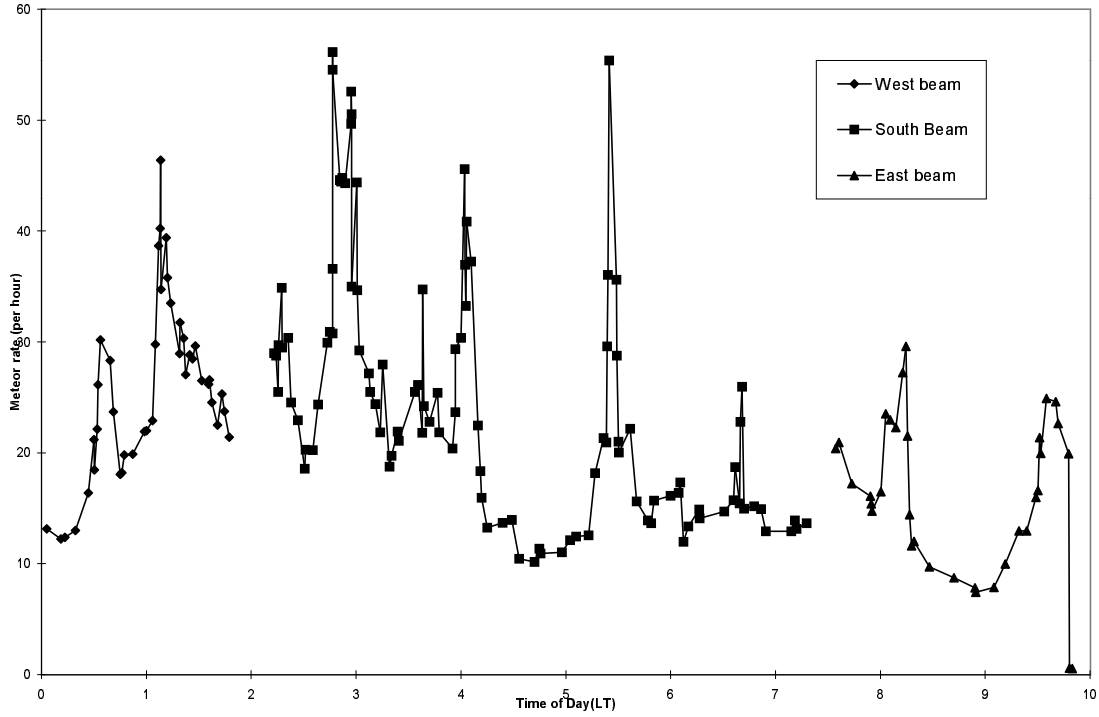

Figure 7.17: Instantaneous meteor rates for the Orionids on October 22 1999. The West and East beams were at an off zenith angle of 38.7° and the South beam was at an off zenith angle of 22°.

our dependence on them. The annual shower is active from November 14 to 21, with a maximum on November 17. The shower radiant is located at 153° in Right Ascension and 22° in Declination, and the observed geocentric speed is 71km s^{-1}. This high speed means that the Leonids produce bright visual trails which implies strong radar returns. The shower is also characterised by long enduring trails, lasting for many seconds, observed both visually and by radar. The meteor storms had previously coincided with the return of the comet every 33 years, and were expected to return in 1998 or 1999. There had already been some observations of increased activity in 1994 (Jenniskens 1996a, Jenniskens 1996b). The long-term activity of the shower has been observed by meteor radar (Brown et al. 1997), and a number of models to explain the 33 year cycle of storms have been put forward and tested against observations (Arlt et al. 1999, Asher 1999, Lyttinen 1999, McNaught & Asher 1999, Arlt & Gyssens 2000,

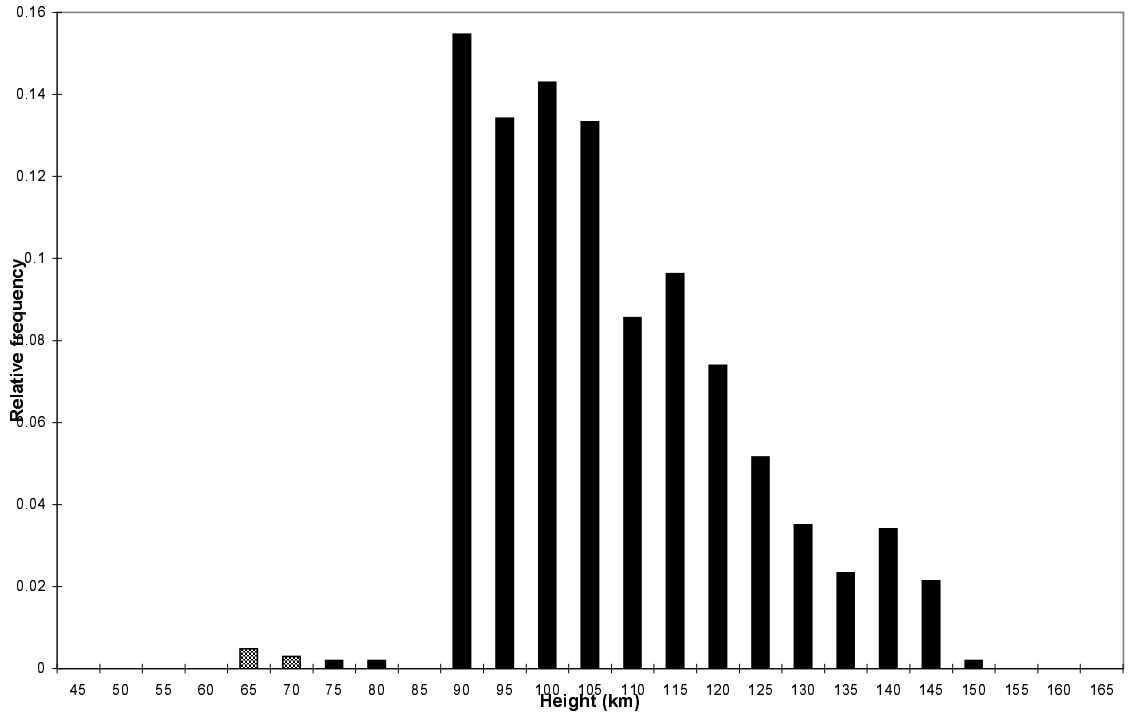

Figure 7.18: Height distribution of meteors observed during the Leonids, 10-20 November 1999. The bins are 5 km wide, centred on the labelled values.

Asher & McNaught 2000, Göckel & Jehn 2000, Singer et al. 2000).

The Buckland Park VHF radar seems to have an objection to observing the Leonids, as when preparations were being made for the shower, the radar always had problems! For example, about a week before the planned observations in 1998, a lightning strike near the radar destroyed all the receivers. A hasty repair was made, and observations began, but only the North-South array could be used. Again in 2000, the beam steering equipment developed a fault, and changed the off-zenith angle of the beam randomly during observations, especially when using the East-West array. Other problems include reduced power due to damage to the power amplifiers, and the transmitter failing completely for the 2001 observations.

Observations made in 1999 seemed to have relatively few problems, and Figure 7.18 shows the height distribution of all of the meteors observed in the period 8-20

November 1999[4]. The PRF was 1650 Hz, producing restrictions in the possible range detected, allowing only 16-84 km (or 107-175 km when aliased once). Two different off-zenith angles were used for observations to allow transverse meteors from the shower to be observed over a long period of time. These were 34.2° for the East and West beams, and 22° for the South beam, which allowed observations while the radiant was passing to the North of the radar. Roughly equal numbers of meteors were detected with each off-zenith angle. The height distribution shows an artificial cut-off below 90 km, the shaded columns are produced by unaliased ranges, and could actually be at heights from 150-165 km not 65-80km as shown. This ambiguity could be resolved by measuring the diffusion coefficient for the echoes in question, but in view of the small number of echoes affected, this was not done. The height distribution shows a peak in the height of these meteors at about 90-100 km.

When the height distribution of the sporadic background is removed, we obtain Figure 7.19. This reveals peaks in the height distribution at 100, 115 and 140km. The height distribution is similar to that of the other shower meteors, with the different peaks probably corresponding to meteors with different physical properties.

While the observations did not allow for the determination of a radiant for the shower, the daily activity could be determined, and this is shown in Figure 7.20. There is a clear increase in the number of meteors detected leading up to the expected maximum on November 17. The overall numbers of meteors was low as the radar was running with reduced power for these observations.

7.4.3 Sporadics

Sporadic meteors make up the largest proportion of observed meteors. Only about a quarter of visually observed meteors are associated with showers, the rest are from the general random, or sporadic background. These meteors are not recognisable as belonging to any known shower, but it seems likely that at least some of the sporadic

[4]These meteors have not been selected by peaks in meteor rates, and thus the distribution contains numbers of sporadics.

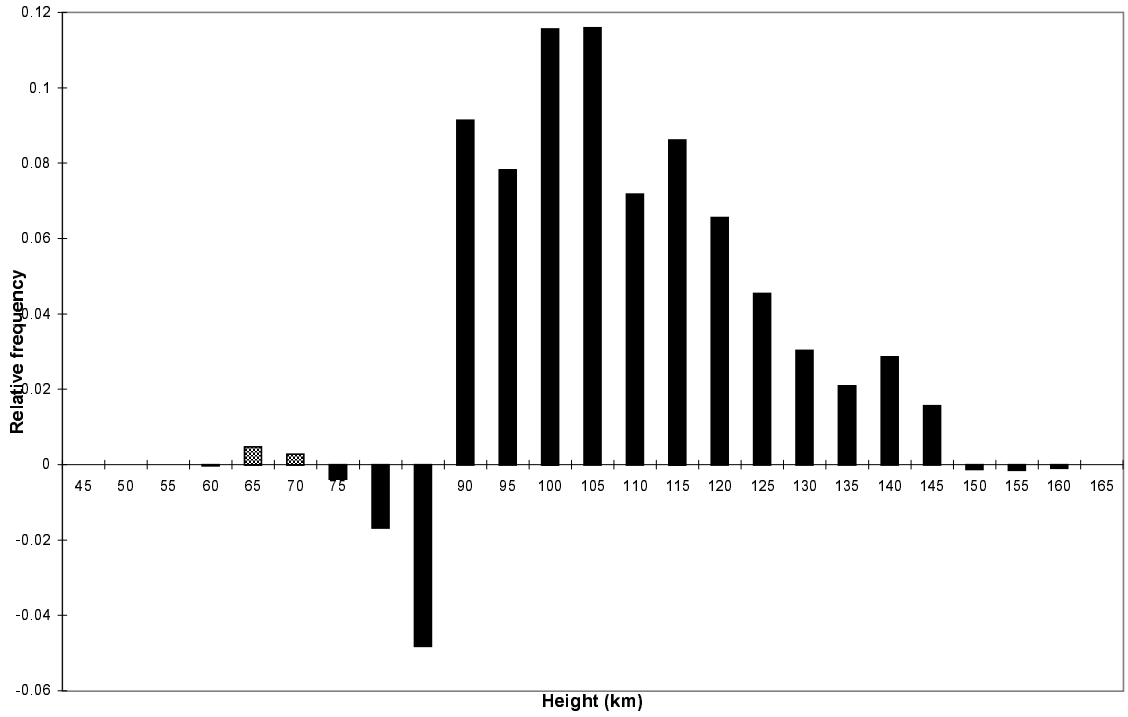

Figure 7.19: Height distribution of meteors observed during the Leonids, 10-20 November 1999, with the sporadic background removed. The bins are 5 km wide, centred on the labelled values.

population of meteors are (or were) members of meteor showers. The smaller particles in meteoroid streams are most affected by the perturbations which change meteoroid orbits, and these are the most likely to be "randomised". Medium sizes dominate the meteors associated with showers, and this is to be expected, as the smaller particles are quickly moved into different orbits and larger particles cannot escape the gravity of the parent comet.

It became apparent that sporadics have a seasonal and diurnal variation from the first serious observations. The diurnal variation was first explained as a geometric effect. If we assume that the meteoroids have an isotropic distribution, then the meteors will appear to be concentrated about the apex of the Earth because of the Earth's orbital motion. This will result in a maximum in the number of meteors observed in the morning and a minimum in the evening. We would expect the largest

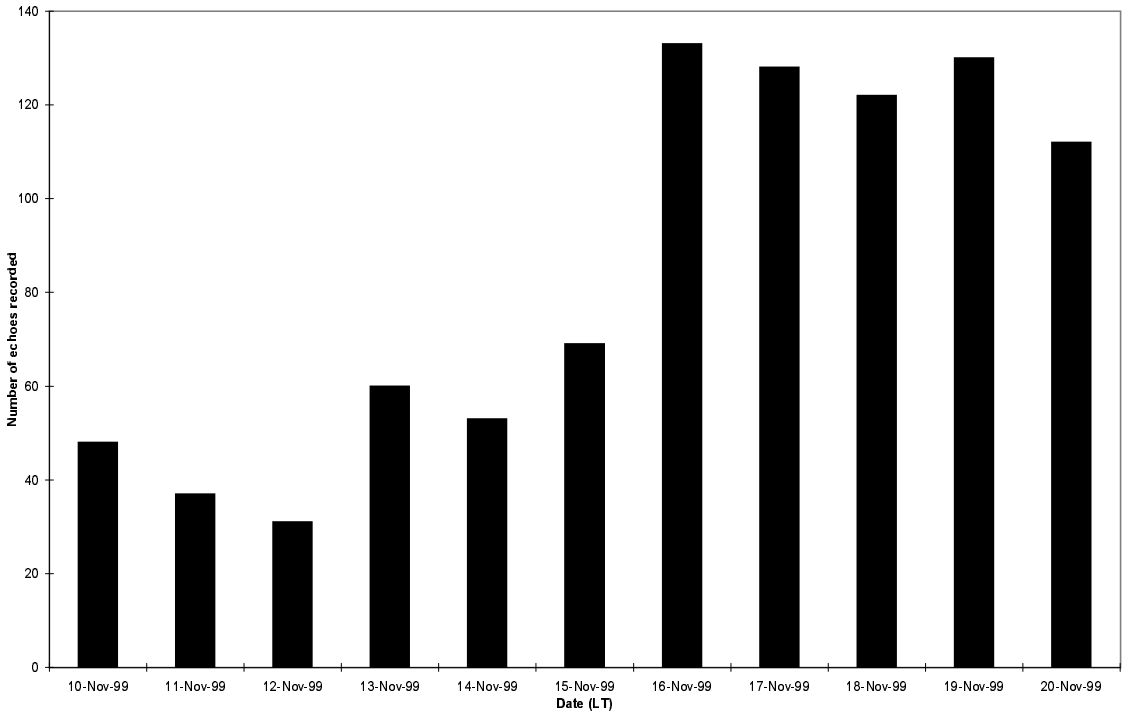

Figure 7.20: Daily activity of the Leonids. The meteors were detected between 0300 and 1100 (LT), and observations were made from November 10 to November 20.

daily variation at the Equator and the smallest near the Poles. The ratio of maximum to minimum is generally in the range 3 to 5 (McKinley 1961). As the seasons change, the apex moves from the Northern Hemisphere to the Southern, and then back again, so we would expect a yearly variation, with more meteors observed in autumn when compared to spring. When radar observations commenced, reliable results of the sporadic rate were available for the first time and the simple picture just described was shown to be incorrect. The diurnal change in the sporadic rate shows three maxima, about 0200, 0600, and 1000 LT (Štohl 1986). These correspond to three sources in the ecliptic; the *apex* source, in the direction of the Earth's motion, the *helion* source, in the direction of the sun, and the *antihelion* source, located in the opposite direction to the sun (Hawkins 1956). In addition there are two others, known as the *toroidal* sources, which are located at ecliptical latitudes of about $\pm 60°$. The apex source appears to be separated into northern and southern components (Elford &

Source	Longitude (deg)	Latitude (deg)	Radius (deg)
Antihelion	198	0	18
Helion	342	1	16
North Toroidal	271	58	19
South Toroidal	274	-60	16
North Apex	271	19	21
South Apex	273	-11	?

Table 7.8: Location and size (to half maximum) of the Sporadic sources (Jones & Brown 1994)

Hawkins 1964, Jones & Brown 1993, Brown & Jones 1994, Jones & Brown 1994, Jones et al. 1994, Taylor 1997, Taylor & Elford 1998). Table 7.8 shows the location and sizes of the sources as given by Jones and Brown.

The seasonal activity of the various sources shows an asymmetry during part of the year. Radar data of meteor rates revealed a strong maximum of the helion source in April-June, and maxima of the antihelion source in April-July and October-December. This activity can be interpreted as the activity of a very broad and diffuse meteoroid stream, and this may be related to several daytime (helion) and nighttime (antihelion) meteor showers associated with comet Encke (Štohl 1983, Štohl 1986). Since it is probable that many sporadics were originally associated with showers, this seems likely.

7.4.4 Observations of sporadic meteors

Since most of the observations made with the Buckland Park VHF radar were designed to detect shower meteors, care must be taken when selecting meteors in order to investigate the sporadic background, that the data is not contaminated with shower meteors. It would seem that observations made at a time of day, or on dates when no shower is active would ensure this. However, we have seen that showers do not always appear when expected. For the purposes of creating a sporadic background distribution, meteors were selected when instantaneous meteor rates showed that no significant shower activity was occurring, and these from periods before and after the

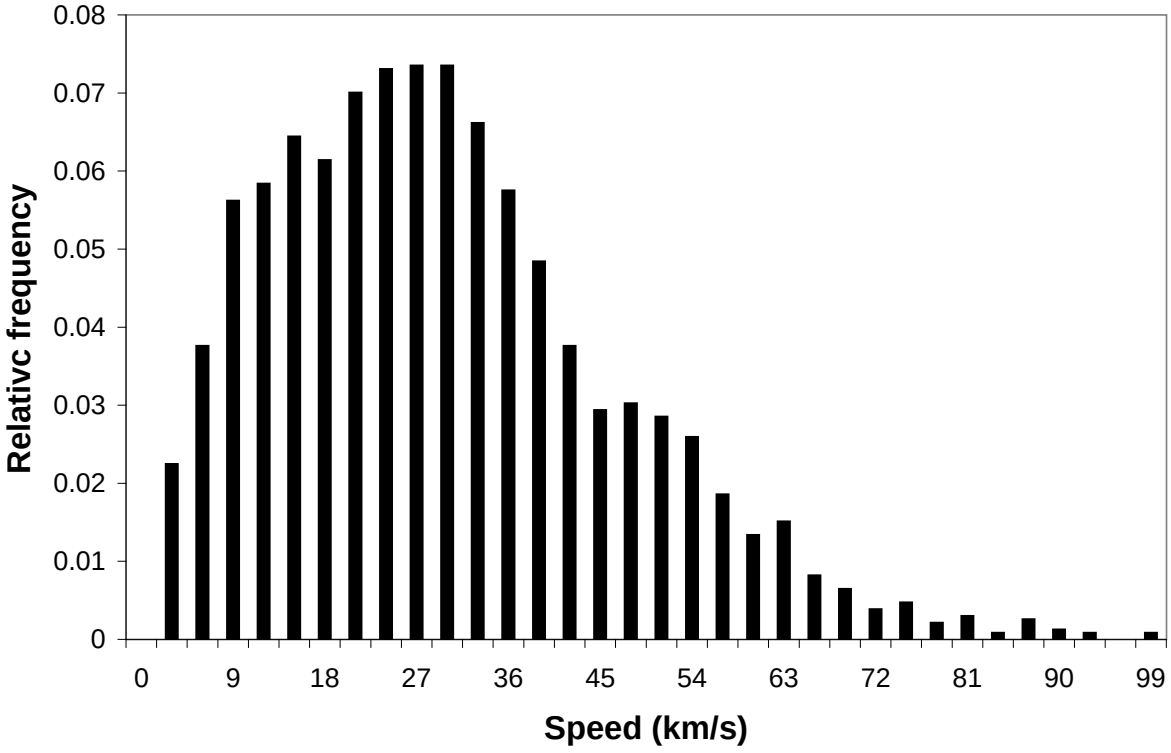

Figure 7.21: Speed distribution of sporadic meteors. The bins are 3km s^{-1} wide, centred on the labelled values.

expected activity of any showers which were active on or around those dates.

Figure 7.21 shows the speed distribution of the sporadic meteors in late April and early May of 1998 and 1999. The distribution shows a number of meteor speeds lower than 11km s^{-1}, although these may be explained by the effects of deceleration and the difficulty of measuring the speed of meteors slower than 15 km s^{-1} by the pre-t_0 phase method for measuring speeds (recent checks with the Fresnel transform method of speed determination by Campbell (private communication) confirm the unreliability of speeds slower than 15 km s^{-1}, see Section 6.5). There is a broad peak in the distribution centred at about 25km s^{-1} and another smaller peak centred at about 58km s^{-1}. It is interesting to note that a small but significant number of meteors have speeds which exceed the hyperbolic limit of 72km s^{-1}. This would imply that the meteoroids which caused these meteors were not in orbit around our sun, but were visitors from interstellar space. These amount to 1.4 % of detected meteors, which

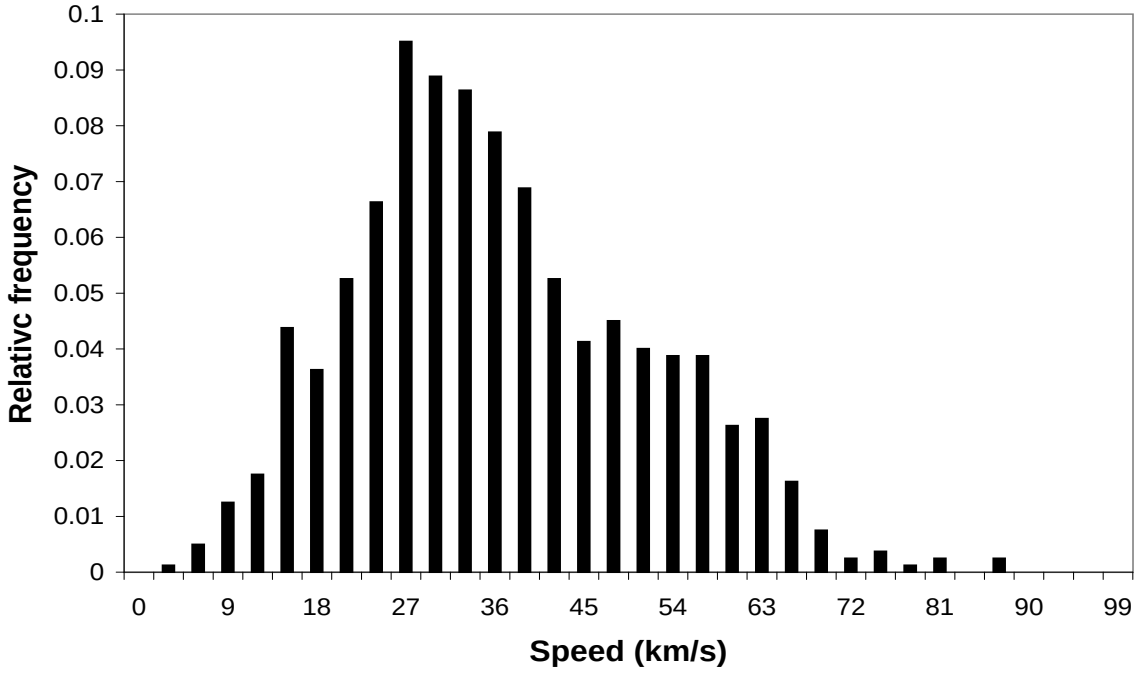

Figure 7.22: Speed distribution of Class A sporadic meteors. The bins are 3km s^{-1} wide, centred on the labelled values.

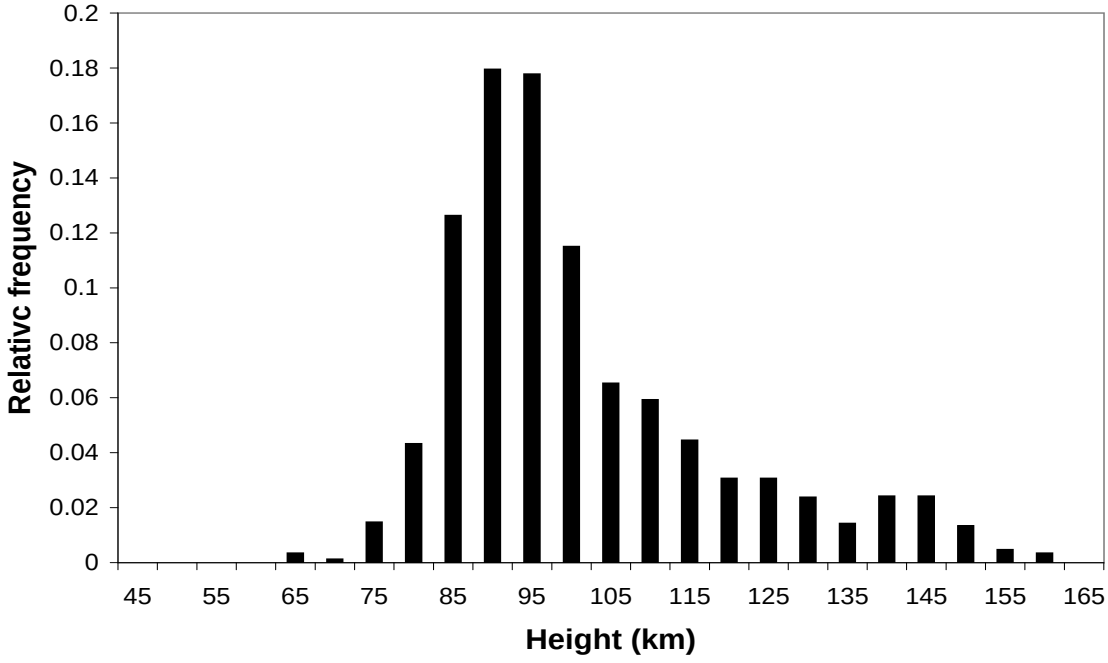

Figure 7.23: Height distribution of sporadic meteors. The bins are 5 km wide, centred on the labelled values.

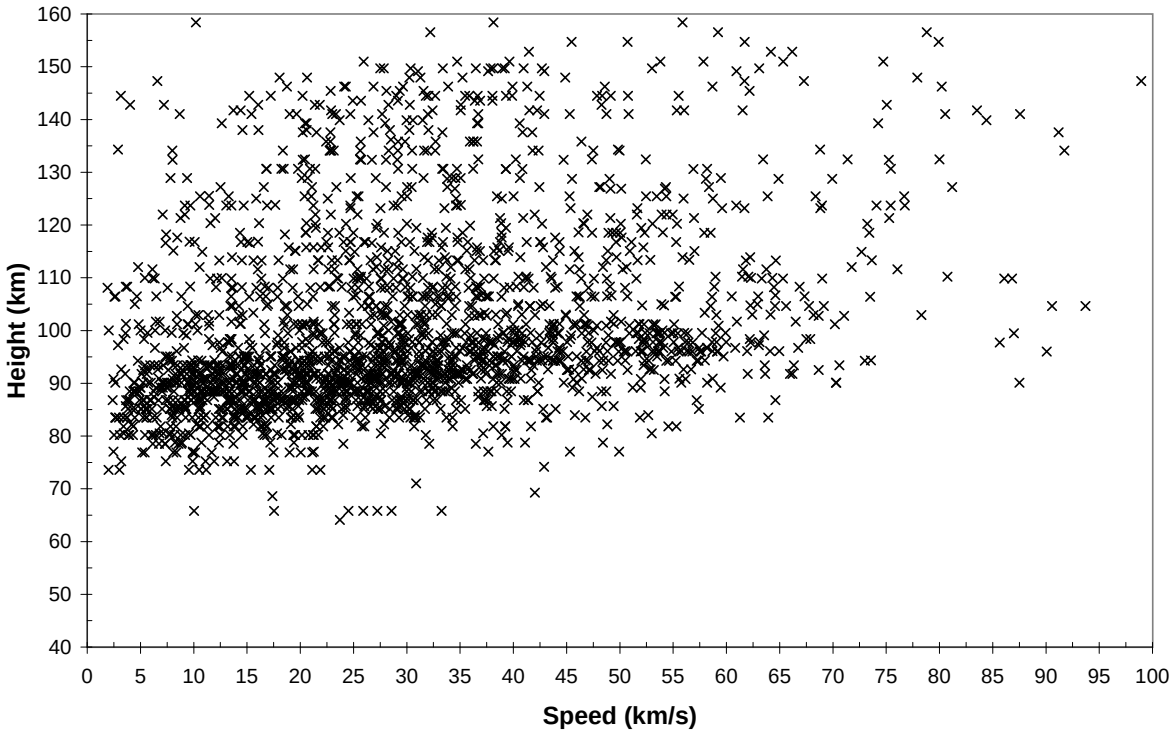

Figure 7.24: Speed-height distribution of sporadic meteors.

compares well to estimates that at most 2 % of meteors are hyperbolic (Baggaley 2000).

If only Class A meteors are included in the speed distribution, we obtain Figure 7.22, and we can see that the distribution has quite a different shape in the region between 3 and 30 km s^{-1}. This is due to the exclusion of many doubtful meteors in this region. In the other regions of the distribution the shape is nearly the same as Figure 7.21.

Figure 7.23 shows the distribution of the range/angle height for the same sporadic meteors as in Figure 7.21. This distribution shows a strong, narrow peak at 90 km, with a tail extending to 130 km. There is also a peak around 145 km. This is suggestive of two distinct populations of meteoroids with different mean values of ablation height. Figure 7.24 shows a scatterplot of speed *versus* height for these sporadic meteors, and again suggests two distinct populations, the strongest at heights between 75 and 100 km, and the second beginning at about 110 km and extending up to about 150 km.

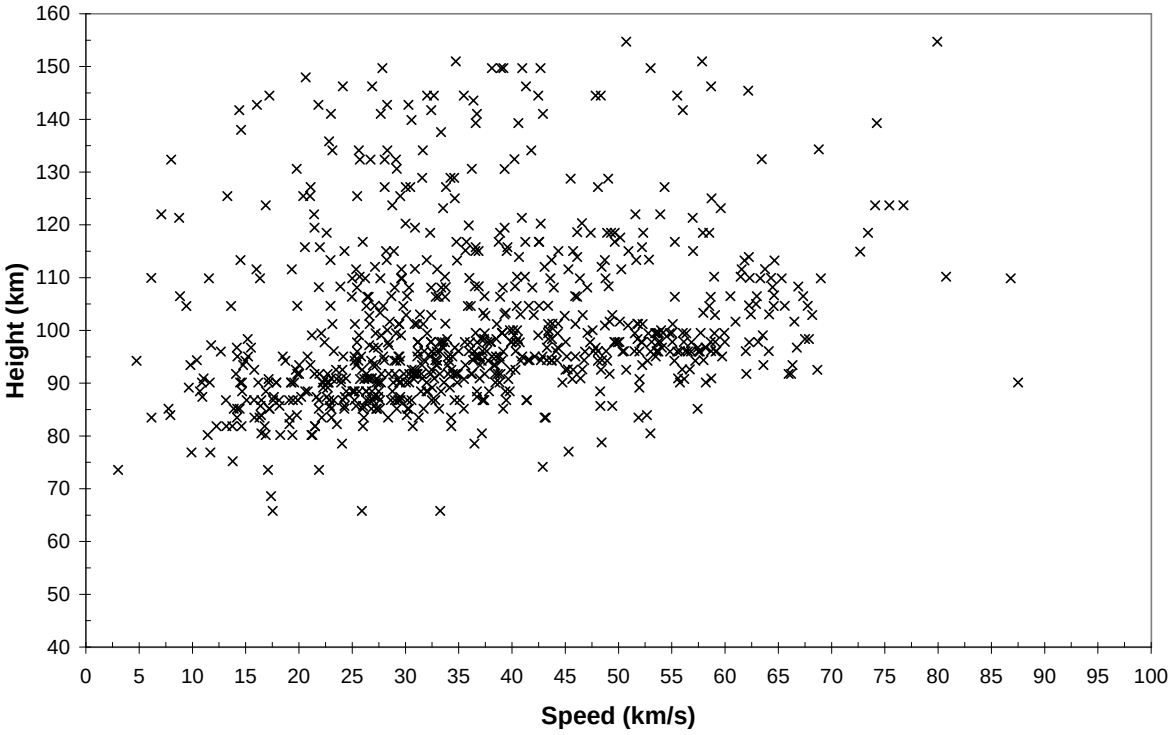

Figure 7.25: Speed-height distribution of Class A sporadic meteors.

Figure 7.25 shows only the Class A meteors, and is very similar to Figure 7.24, except for the omission of a number of the low speed meteors. Aside from this, the essential features of the speed-height distribution are the same.

7.5 Summary

This chapter was concerned with the observation of groups of meteors, known as meteor showers. The origin of these showers was discussed, and a review of the history of meteor shower discovery, their association with comets, and techniques used to observe meteor showers with radars is conducted. Next the technique used by the author was described, and this was followed by a discussion on the statistics of randomly spaced meteor and meteor rates. Next was a discussion on the structure of meteoroid streams, and how this related to the meteor showers they produce.

Observations of meteor showers with the BP VHF radar, in particular the η-Aquarid meteor shower, were analysed, and revealed that the η-Aquarids shows four distinct peaks in activity, from which four radiants were determined. The height and speed distributions of the shower were also discussed, and these confirmed previous measurements of the speed of the shower, but the height distribution showed many echoes which were higher than expected from ablation theory. Observations of the Leonids, and the Orionids were presented, with activity and height distributions shown. Lastly there was a short discussion on the sporadic background, and evidence provided for two different populations of meteoroids and a small interstellar component.

Chapter 8

Conclusion

8.1 Introduction

This thesis has been concerned with the observation and study of meteors with a narrow beam VHF radar operated by the University of Adelaide at the Buckland Park research station, in particular the study of the structure and characteristics of meteor showers and the geocentric speeds of meteors. There have been several observations of meteors made with the radar (Steel & Elford 1991, Cervera 1996, Taylor et al. 1996), but this is the first with a systematic study of the properties of meteor showers, automated data analysis and observations extended to heights above 110 km .

The Buckland Park VHF radar offers significant advantages over the wide beam radars traditionally used for meteor observation. The narrow beam, while reducing the collecting area of the radar, allows observations of much lower electron line densities than a wide beam radar of similar power. It also allows the determination of meteor shower radiants by the use of the radar response function. Pulse repetition frequencies of up to 2000 Hz allow excellent time resolution and the ability to record in-phase and quadrature data allows the phase information to be used to determine radial wind drifts and meteoroid speeds.

Three methods were used to determine meteoroid speeds using the phase data, each applying to a different type of meteor echo, and in combination, speeds were

determined for over 90 % of all meteor echoes.

The data presented in this thesis was collected in the period 1998-2000, and included annual observations of the η-Aquarids, the Orionids, and the Leonids. Observations of several other showers were made but remain to be analysed.

8.2 Summary and Conclusions

Meteors are an atmospheric phenomenon, caused by the entry of particles from space into the atmosphere. The particles heat up and evaporate, producing ionisation which can be detected by radar. Meteors have been observed visually for centuries, but serious observation began after the 1833 Leonids produced a spectacular display. Radio observation began after it was discovered in the 1930's that radio waves were scattered from meteor trails. Observations are also made photographically, spectroscopically, and using low light television systems.

The Buckland Park VHF radar operates at the frequency of 54.1 MHz, has a peak power of 24 kW, and a full width half at power of less than 3°. It can be steered off zenith in approximately 3° graduations to a maximum of 69.9°. The Pulse Repetition Frequency (PRF) can be varied, but values in the range 1500-2000 Hz are generally used for meteor observations.

A series of expressions can be derived to model the ablation of meteoroids in the atmosphere, taking into account the density of the atmosphere, the size, density and speed of the meteoroid, its ablation characteristics, radiation from the meteoroid, ionisation probability, fragmentation, and diffusion of the ionisation. The radar reflection coefficient of the meteor trail depends on the volume density of the ionisation, and the returned signal can be modelled based on Fresnel diffraction theory. The geomagnetic field has an effect on the diffusion of the ionisation at heights above 90 km, and there are a number of factors which attenuate the returned signal. The radar response function was developed, and calculated for the Buckland Park VHF radar, showing that the best results for observing transverse echoes are gained from a off-zenith tilt

of more than 20°.

The phase data must be unwrapped as recorded values of phase are limited to between $-\pi$ and π. The discovery of a design fault introducing a periodic signal into the data necessitated the development of Fourier transform method for removing this signal. The effects of coherent smoothing and receiver saturation were examined.

A survey of the different type of echoes detected by the radar was performed, and revealed that the underdense transverse echo was by far the most common, but the Fresnel oscillations expected in the post-t_0 amplitude of these echoes were usually missing. Other types of meteor echoes discussed were overdense, saturated, long enduring, and aliased head echoes. The down-the-beam echo was also discussed, as were sources of false triggers, aircraft and periodic noise.

The method of estimating the ambipolar diffusion coefficient from the rate of decay of the amplitude of the returned signal was discussed. Estimates of meteor ablation heights were made from the diffusion coefficient, and were found to be generally consistent with the heights calculated from the range and the beam angle, but showing significant numbers of echoes at heights above 90 km with much smaller diffusion coefficients than expected. The diffusion coefficient can be strongly affected by the geomagnetic field, depending on the orientation of the radar beam to the field. When echoes are detected in the sidelobes of the beam, it is expected that the change in the echo direction may affect the duration of echoes significantly, explaining the smaller than expected diffusion coefficients.

The ablation height of meteoroids was determined from the echo range and the beam angle. The PRF and the beam angle determine the range of heights in which meteors can be detected. A PRF of 2000 Hz and an off-zenith beam angle of 30° allows height coverage from 68 to 129 km, whereas a PRF of 1650, and a beam at the same angle, allows coverage below 74 km and between 91 and 151 km. The error in the heights depends on whether the meteor has been detected in a sidelobe or in the main beam of the antenna pattern. About 10 % of meteor echoes are detected in the sidelobes, depending on the off-zenith beam angle, and the maximum error in the

height of these is about 11 % if it is assumed that they are detected in the main lobe. This compares to an error of about 3 % for echoes which are detected in the main lobe. The vast majority of meteors detected in the sidelobes are in the first sidelobe with the greatest off-zenith angle, as this has the largest combination of collecting area and gain. This results in the overestimation of the heights of about 6 % of all meteors by about 11 % The errors due to meteor detection in the other sidelobes are negligible.

The meteor height distribution showed a significant number of meteors ablating above 100 km. This is surprising, because the theoretical initial radius attenuation factor is virtually zero at heights above 105 km for a radar frequency of 54.1 MHz, so very few underdense meteor trails should be detected at these heights. A survey of meteor echoes detected at heights greater than 110 km showed that over 60 % of these echoes are underdense. Jones (1995) suggested that meteor trails form with an inner core of ionisation which is much stronger than the average ionisation density of the trail, and would "appear" to the radar as a smaller trail. This would reduce the effect of the initial radius attenuation, and could explain observations of underdense meteor trails at greater heights than expected.

We know from observations at other frequencies (Steel & Elford 1991), that there are meteors ablating well above 110 km. These "high ablating" meteors are seldom detected, possibly because of the nature of previous observations. Many recent observations with powerful narrow beam radars have artificial height cut-offs, for example, Cervera had an equipment problem which limited heights to 110 km (Cervera 1996). Cervera's height distributions extended past his expected maximum of 105 km up to the artificial limit, but he attributed this to meteors detected in the sidelobes of the antenna pattern. The AMOR system can only be used for meteors at heights between 70 and 120 km (Taylor et al. 1994).

Often modern systems are designed on the assumption that there are no meteor trails to observe above 110 km. However, many of the great wide beam meteor survey radars had no such height limitations, and did not detect these very high ablating meteors, so why does this occur with the Buckland Park VHF radar? The answer

could lie in two properties of the radar, the narrow beam and the high pulse repetition frequency. The narrow beam allows the observation of much smaller ionisation densities than the wide beam systems, and we would expect that these high ablating meteors would be producing only small amounts of ionisation, as the atmospheric drag is much smaller at greater heights, and the ionisation would also diffuse more rapidly. This leads us to another advantage of the Buckland Park VHF radar, in that if the ionisation is diffusing rapidly, then there will be a very short time in which the meteor trail will produce detectable returns. Only a radar with a high PRF will be able to observe a sufficient number of data points to detect these short lived echoes.

The height distribution of the meteors shows at least two distinct populations of meteors, those which ablate in a region from 75 to 100 km and those which ablate in a region from 110 to 150 km. This second population cannot be composed of the stony material which is often used to model ablation, as the temperatures generated during the heating of particles at these heights are insufficient to ablate of this type of material. Speed-height distributions show that this population of "high ablating" meteoroids are not exclusively those with very high geocentric speeds (*ie* greater than 50 km s^{-1}) but have speeds as low as 15 km s^{-1}. This adds fuel to the fire, as lower speeds mean even the bodies are at even lower temperatures at these heights.

During and after a meteor trail has been formed the motion of the surrounding atmosphere causes movement of the trail. This produces a Doppler shift which can be determined from the rate of change of the phase of the signal returned after the meteoroid has passed the t_0-point. This in turn can be used, with an appropriate set of observations, to determine the local wind speed and direction. However there are a number of effects which must be taken into consideration, especially for trails above 90 km.

Radar observations of meteor trails are frequently different to predictions based on the modelling of ablation of a single body which maintains its integrity throughout its flight. Many features in these observations lead to the conclusion that fragmentation occurs in most detected meteors. The major feature is the lack of post-t_0 Fresnel

oscillations in nearly 90 % of the echoes analysed for this thesis. Modelling shows that this effect can be attributed to the combination of the returns from a number of closely spaced particles travelling together after fragmentation in the pre-ablation/heating phase of flight. Modelling of the heating of meteoroids shows that the stresses caused by the thermal gradient due to differential heating of an object as it travels through the atmosphere are greater than the tensile strength of many stony type materials tested.

Other characteristics of meteor echoes which suggest fragmentation are sudden increases in the amplitude of meteor returns, possibly corresponding to "flares" as small fragments rapidly burn up, and events with evidence of beating between two similar bodies travelling closely together. Use of a new "Fresnel Transform" technique to observe the structure of meteor trails as a function of distance from the body of the meteoroid reveals multiple ablation centres in some meteor trails.

There have been a number of different methods for determining the speed of meteoroids, most of which rely on the Fresnel diffraction pattern which sweeps over the radar station as the meteor trail is formed in the radar beam. Others use the geometry of meteor trails passing through the radar beam.

Elford showed that the pre-t_0 phase information is largely unaffected by the diffusion of the meteor ionisation (Elford et al. 1995), and by modelling the effects of ablation accurately, and comparing the modelled phase to the measured phase, the speed of the meteoroid can be obtained very accurately. The model used the measured diffusion coefficient, and an estimate of the meteoroid speed to give value of the phase as a function of x, a dimensionless variable. This method gives speeds which are accurate to slightly more than the uncertainty in the range when used with data from the Buckland Park VHF radar, and can determine the speed of nearly 90 % of transverse echoes, although when very few cycles of phase information are present (ie speeds less than 15 km s^{-1}), this technique can underestimate the speeds of these meteoroids. This is due to working with weak returns and short phase records, both characteristics of echoes from slow meteors. The underestimation can be eliminated,

at the expense of obtaining speeds from fewer meteor echoes, by comparing the speed obtained from the model with the preliminary estimate using the Cauchy approximations to the Fresnel integrals. The preliminary estimate is much more sensitive to the length of the available phase data. If the difference between these methods is less than 5 %, the meteor is designated a "Class A" meteor, with the others designated "Class B". About 40 % of meteors where speeds could be determined were of the Class A type.

Over 90 % of all echoes occur in only one range bin, and thus the trail must be perpendicular or nearly perpendicular to the boresight of the radar beam, but in nearly 10 % of these the t_0-point is not visible in the record. In these echoes, the combination of the sampling frequency (the PRF) and the rate of change of phase causes aliasing in the phase record, which precisely replicates the parabolic shape of the phase at the t_0-point. By applying the Cauchy approximation to the Fresnel integrals to these parabolae, the speed of the meteoroid can be determined. For the cases where the t_0-point is present, and enough phase signal is present for aliasing, the speed can be independently measured at two different times during the formation of the trail, and any deceleration can be estimated.

A further 8 % of meteor echoes are down-the-beam events. This type of event occurs when a meteor produces enough ionisation around the body of the meteoroid that it appears to the radar as a metallic object travelling through the beam at the position of the meteoroid body. With this type of echo, the line-of-sight speed is simply the rate of change of the phase. The difference between the line-of-sight speed and the true speed of the meteoroid is a function of the angle between the meteor trail and the line-of-sight from the radar station to the meteoroid body. As this angle changes as the meteoroid moves, this is a difficult problem to solve, and it is further complicated by any deceleration of the meteoroid. The deceleration is a function of the atmospheric drag, which depends on the local air density, and increases exponentially as the meteoroid travels into the atmosphere. The speed of the meteoroid is obtained by comparing the line-of-sight speed with a model which includes deceleration and the

change in angle. This method produces speeds accurate to about 1 % as well as an estimate of the average deceleration of the meteoroid.

Using these three techniques, speeds can be obtained reliably for some 85 % of all meteor echoes. The techniques were used to analyse about 6000 meteor echoes from observations made during the period of the η-Aquarid meteor shower (late April and early May) in 1998, 1999 and 2000.

Speed-height distributions of the analysed meteors show that the most probable height of a meteor increases with speed. In addition it is possible to separate the meteors detected into three groups. There is a main group, containing about 75 % of the meteors, which has a height range from 70 to 105 km, and the second group, with a height range from 105 to 135 km makes up about 20 %. The mean height of these groups increases with speed. The third group ranges from 135 to 155, and seems to have ablation heights independent of their speed. This is difficult to explain, and this "group" may in fact be composed of members of the second group which are "sandwiched" between the hardware height limit at 161 km and an attenuation effect at around 135 km. The speeds ranged from 3 to 94 km s^{-1}, with the most common speed being about 25 km s^{-1}. There was a "clump" of meteors with speeds at and slightly below 66 km s^{-1}, associated with η-Aquarids meteoroids. There was a larger number than expected of meteors with speeds below 11 km s^{-1}, the speed which an object would have from the effects of the Earth's gravitational field alone. This can be explained by a combination of underestimation of some speeds, the ablation of orbital debris, and detection of highly decelerated meteoroids in the last stages of ablation.

When the speed-height distribution of the Class A meteors was produced, its characteristics were extremely similar to those of the entire set of meteors, with the notable exception that most of the meteors with speeds below 15 km s^{-1} were absent. This is not unexpected, as these tend to be weak echoes which are not amenable to speed measurements, but notably, there are still a few meteors below the 11 km s^{-1} limit.

Observations of the η-Aquarids shower consisted of pointing the radar beam to the West to obtain specular reflections as the assumed radiant rises in the East, and then

pointing the radar beam to the East as the assumed radiant sets. For a point source of meteors this would produce an increase in the meteor rate at times determined by the radar response function and the radiant position of the source. However, the instantaneous meteor rates showed that several peaks of activity were present in each beam direction, suggesting more than one radiant. Observations were also made while the assumed radiant was at its maximum elevation by pointing the beam into an appropriate North or South direction.

Filtering the echoes by only including meteors where the speed was measured and lay between 50 and 70 km s^{-1} removed some of the peaks, which were attributed to other meteor showers, and increased the signal to noise ratio of the remaining peaks. There were still several peaks remaining, and these were matched between the West and East beam observations by comparing their speed distributions and relative strengths and durations. Once the peaks were matched in the West and East beams, the radiants corresponding to the sets of peaks were calculated. These four radiants reveal that there is substantial fine structure in the η-Aquarids. The variability of the peaks in the meteor rates from day to day also shows structure in the meteoroid stream, in that not only is the stream made up of a number of different "sub streams" or filaments, but these filaments are made up of "clumps" of particles of the size that can be detected by the Buckland Park VHF radar as meteors, so that one day the filament is detected, and the next there is no detectable increase in the activity. The average position of the measured radiants corresponded to previously measured radiants for the shower.

The height distribution of the meteors detected during the presence of the activity peaks shows a strong peak in the height of ablation around 95 km, which is consistent with the sporadic background, superimposed on a broader distribution with a peak at 105 km, and a suggestion of a smaller distribution peaking at 125 km. When only meteors with a measured speed lying between 50 and 70km s^{-1} are included in the height distribution, peaks at 100 km and 115 km show up strongly, and there is the suggestion of a peak at 145 km.

The speed distribution of the meteors detected during the presence of the activity

peaks shows several peaks, one peaking at 25 km s^{-1}, consistent with the sporadic background, and the another at 50 km s^{-1}. Of note is a very strong peak at 66 km s^{-1}, which is the previously measured geocentric speed of η-Aquarids meteoroids. If the speed distribution of the sporadic background is subtracted, the peaks at 50 and 66 km s^{-1} remain, and are decidedly skewed, showing few meteors with speeds higher than the peak value, and many with speeds smaller than the peak value, consistent with deceleration of meteoroids in the atmosphere. The peak at 50 km s^{-1} is probably due to a minor shower (the daytime Arietids or the o-Cetids).

A scatterplot of the speed *versus* the height of these meteors shows that a large proportion of the tail of the 66 km s^{-1} peak in the speed distribution (*ie* those which have been decelerated) are detected at heights between 90 and 105 km, while the meteors which were detected higher (from 105 to 125 km) show little deceleration. Above this height there is a sharp cutoff of meteors associated with the η-Aquarids.

Preliminary analysis of observations of the Orionids and Leonids meteor showers show that these showers were detected in 1999, and also have fine structure. Height distributions of meteors detected during the period of the shower extend up to 150 km and show suggestions of different populations of meteors.

Observations of sporadic meteors were made for the purpose of determining the characteristics of the sporadic background in shower observations. The speed distribution shows a strong broad peak at 25 km s^{-1} and a smaller peak at 58 km s^{-1}. This distribution is consistent with previous observations (McCrosky & Posen 1961, Nilsson 1962, Elford et al. 1995, Cervera 1996) with the exception of the number of meteors with speeds below 11 km s^{-1}, which are due to underestimation of the speeds of meteors in the region 11 to 20 km s^{-1}. The speed distribution reveals a significant number of meteors with measured speeds in excess of the hyperbolic limit of 72 km s^{-1} (about 1.4 %). This is consistent with observations with AMOR which suggest that about 2 % of meteors have speeds this high, which means they cannot be in orbit around our sun, but must be of interstellar origin.

The height distribution of the sporadic background shows a strong peak at 90 km,

with a tail out to 130 km. There is also a peak at 145 km, and it appears that there are two populations of meteors with overlapping height distributions. It should be noted that Cervera (1996), although he had an artificial range cutoff at 110 km, saw the distribution extending past his expected maximum of 105 km up to 110 km, but attributed this to observations in the sidelobes of the antenna pattern.

Highlights of the work described in this thesis are:

- The pre-t_0 phase method of measuring the speeds of meteoroids has been shown to be robust, accurate, capable of a high degree of automation, and has a yield of 85 % of all meteors detected by a VHF radar.

- The combination of meteoroid speed measurements and the application of the response function can reveal the fine structure in meteor streams, and make possible the measurement of the radiants, speeds, and strengths of filaments within the stream.

- Extension of the possible detection of meteors to a height of 160 km with a VHF radar has revealed a population of meteors distributed from 110 to 150 km in height and from 10 to 70 km/s in speeds.

- The estimate of meteor heights using the rate of decay of meteor echoes has shown that the most probable diffusion height is close to the actual height, but the standard error in the diffusion height is about 5 km.

8.3 Further work

The techniques described in this thesis to determine the speeds of detected meteors have, as the major source of error, the uncertainty in the range of the detected meteor trail. The system as described uses a 2 km pulse size, and a corresponding 2 km range bins, leading to an error in the range of about 1 %. If the range resolution could be increased, then there would be improvements in the accuracy of speed measurements using the pre-t_0 phase technique and its adaptation to aliased head echoes, the down

the beam technique and also the Fresnel transform technique. In addition it would be useful to be able to determine the range absolutely, both for speed measuring and determining the range/angle height of a meteor trail. While better range resolution can be achieved by reducing the pulse length to (say) 0.5 km, this will have the effect of reducing the mean power emitted by the radar. In any case the number of rangebins required to cover ranges from 4 to 90 km would quadruple, and this was beyond the processing power of the Meteor PC (a 166 MHz Pentium) which has to check each rangebin with the detection algorithm. While current advances in processor technology have solved the latter problem the only solution to the former would be to increase the peak power of the transmitter. Another, more elegant solution, would be to use a coded pulse, which could also be used to eliminate the range aliasing ambiguity. The newly installed transmitter has a pulse coding capability.

A number of meteor showers have already been observed with the Buckland Park VHF radar, and the data is yet to be analysed. Considering the revelations which resulted from the detailed analysis of only one shower (the η-Aquarids) it seems likely that much valuable information can be obtained by processing this other data. It seems probable that other meteor showers will share some the characteristics of the η-Aquarids; the temporal and spacial variation of the meteoroids in the stream. In addition there is scope for improved observation techniques, such as using the south beam to observe a northern radiant (such as the η-Aquarids), which gives several hours of strong radar response to shower meteors, while still allowing the high sensitivity of narrow beam radars. It is likely that temporal variation will be observed, similar to that seen in the Orionids observations discussed in this work.

Other significant areas to be investigated are the different types of meteors observed, especially the aliased head echo and down-the-beam meteors. It is of great interest to see if these meteors, which are much brighter than the average transverse meteor observed with the Buckland Park VHF radar, are from a different population than the transverse meteors, and possibly have different physical properties.

The capability to use the radar for interferometric observations was discussed

briefly in this thesis. This capability is important, as it allows the direction of arrival of a particular echo to be determined. In combination with the possibility to determine the speed of the meteor accurately for most echoes, this would allow the determination of individual orbits for a vast number of meteoroids, of all sizes and compositions. This would certainly give a broad view of the populations of particle which visit us from space. Determining the direction of arrival of meteors would also allow accurate measurements of the effect of the geomagnetic field on diffusion, as the angle between the direction to the trail and the magnetic field could be determined without ambiguity.

It is a strange coincidence, that just as work on this thesis was being completed in late 2001, the new Fresnel Transform technique was shown to be capable of giving precise meteor speeds without many of the complications associated with the pre-t_0 phase technique.

Undoubtedly, in the future the Fresenel transform will be the technique of choice for analysing radar meteor echoes, as it gives a comprehensive outcomes as regards speed and deceleration of meteoroids, and the structure of the trail.

This may well be the last work to use the pre-t_0 phase technique, which in itself was a revolutionary step forward in the measurement of meteor speeds.

Appendix A

Radio Scattering from a Meteor Trail with application to the measurement of the speed of Meteoroids

This is a reprint of the paper:

Elford W. G., *Radio Scattering from a Meteor Trail with application to the measurement of the speed of Meteoroids*, Internal Departmental Report.

Appendix B

New radar studies of the velocity distribution within meteor showers and implications for stream structure

This is a reprint of the paper:

Badger D. P. & Elford W. G.(1999), *New radar studies of the velocity distribution within meteor showers and implications for stream structure*, in "Proceedings of Meteoroids 1998", Astronomical Institute of the Slovakian Academy of Science, pp. 195–198

References

Adolfsson, L. G., Gustafson, B. A. S. & Murray, C. D. (1996), 'The Martian atmosphere as a meteoroid detector', *Icarus* **119**, 144–152.

Alvarez, H., Aparici, J., May, J. & Olmos, F. (1997), 'A 45 MHz continuum survey of the southern hemisphere', *Astronomy and Astrophysics Supplement Ser.* **124**, 315–328.

Arlt, R. & Gyssens, M. (2000), 'Bulletin 16 of the International Leonid Watch: Results of the 2000 Leonid meteor shower', *WGN* **28**, 195–208.

Arlt, R., Rubio, L. B., Brown, P. & Gyssens, M. (1999), 'Bulletin 15 of the International Leonid Watch: First global analysis of the 1999 Leonid storm', *WGN* **27**, 286–295.

Asher, D. J. (1999), 'The Leonid meteor storms of 1833 and 1966', *Monthly Notices of the Royal Astronomical Society* **307**, 919–924.

Asher, D. J. & McNaught, R. H. (2000), 'Expectations for the 2000 Leonids', *WGN* **28**, 138–143.

Aspinall, A., Clegg, J. A. & Hawkings, G. S. (1951), 'A radio echo apparatus for the delineatio of meteor radiants', *Phil. Mag.* **42**, 504–514.

Babadzhanov, P. B. (1993), Densities of meteoroids, *in* 'Meteoroids and their parent bodies', Slovakian Academy of Science, pp. 295–302.

Babadzhanov, P. B., Wu, Z., Williams, I. P. & Hughes, D. W. (1991), 'The Leonids, comet Biela and Biela's associated meteoroid stream', *Monthly Notices of the Royal Astronomical Society* **253**, 69–74.

Badger, D. P. (1997), 'Meteor velocity measurments with a narrow beam VHF radar-the April/May η-Aquarids in 1997', Honours Thesis, University of Adelaide, Adel., Australia.

Badger, D. P. & Elford, W. G. (1999), New radar studies of the velocity distribution within meteor showers and implications for stream structure, *in* 'Proceedings of Meteoroids 1998', Astronomical Institute of the Slovakian Academy of Science, pp. 195–198.

Baggaley, W. J. (1970), 'The determination of the initial radii of meteor trains', *Monthly Notices of the Royal Astronomical Society* **147**, 231–243.

Baggaley, W. J. (1980), Solid particles in the solar system, *in* 'Meteors and atmospheres', D. Reidel Publishing Co., Dorecht, Holland, pp. 295–302.

Baggaley, W. J. (1981), 'Single wavelength measurements of the initial radii of radio meteor ionization columns', *Bulletin of the Astronomical Institute of Czechoslovakia* **32**, 345–348.

Baggaley, W. J. (2000), 'Advanced meteor orbit observations of interstellar meteoroids', *Journal of Geophysical Research - Space Physics* **105**, 10353–10361.

Baggaley, W. J., Bennet, R. G. T., Steel, D. I. & Taylor, A. D. (1994), 'The Advanced Meteor Orbit Radar facility: AMOR', *Quarterly Journal of the Royal Astronomical Society* **35**, 293–320.

Baggaley, W. J., Bennet, R. G. T. & Taylor, A. D. (1997), 'Radar meteor atmospheric speeds determined from echo profile measurements', *Planetary and Space Science* **45**, 577–583.

Baggaley, W. J. & Fisher, G. W. (1980), 'Measurements of the initial radii of the ionization columns of bright meteors', *Planetary Space Science* **28**, 575–580.

Baggaley, W. J. & Webb, T. H. (1977), 'The thermalization of meteoric ionization', *Journal of Atmospheric and Terrestrial Physics* **39**, 1399–1403.

Baldacchino, G. (1995), 'The 1994 eta-Aquarids: A Tentative Global Analysis', *WGN, Journal of the International Meteor Organization* **23**, 213–216.

Bayrachenko, I. V. (1965), 'Measurements of the initial radii of ionized trails from simultaneous observations of radio meteors on two wavelengths', *Geomagn. Aeronom.* **5**, 353–356.

Bosler, J. & Roure, H. (1937), 'La Comète de Bièla et l'Essaim des Leonides', *Journal des Observateurs* **XX**, 105.

Briggs, B. H., Elford, W. G., Felgate, D. G., Golley, M. G., Rossiter, D. E. & Smith, J. W. (1969), 'Buckland Park aerial array', *Nature* **223**, 1321–1325.

Bronshten, V. A. (1983), *Physics of meteor phenomena*, D. Reidel Publishing Co, Dordrecht, Holland.

Brown, P., Ceplecha, Z., Hawkes, R. L., Wetherill, G., Beech, M. & Mossman, K. (1994), 'The orbit and atmospheric flight of the Peerskill meteorite from video records', *Nature* **367**, 624–626.

Brown, P. & Jones, J. (1994), 'A determination of the strengths of the sporadic radiometeor sources', *Earth, Moon and Planets* **68**, 223–245.

Brown, P., Šimek, M. & Jones, J. (1997), 'Radar observations of the Leonids 1964-1995', *Astronomy and Astrophysics* **322**, 687–695.

Budden, K. G. (1985), *The propagation of radio waves*, Cambridge University Press, Cambridge.

Campbell, M. D., Hawkes, R. L. & Babcock, D. D. (1999), Light curves of faint shower meteors: implications for physical structure, *in* 'Proceedings of Meteoroids 1998', Astronomical Institute of the Slovakian Academy of Science, pp. 363–366.

Ceplecha, Z. (1957), 'Photographic Geminids 1955', *Bulletin of the Astronomical Institute of Czechoslovakia* **8**, 51–61.

Ceplecha, Z. (1958), 'On the composition of meteors', *Bulletin of the Astronomical Institute of Czechoslovakia* **9**, 154–159.

Ceplecha, Z. (1961), 'Multiple fall of Příbram meteorites photographed: Double station photographs of the fireball and their relations to the found meteorites', *Bulletin of the Astronomical Institute of Czechoslovakia* **12**, 21–47.

Ceplecha, Z. (1968), 'Discrete levels of meteor beginning heights', *Smithsonian Astrophysical Observations Special Report* **279**, 1–54.

Ceplecha, Z. (1988), 'Earth's influx of different populations of sporadic meteoroids from photgraphic and television data', *Bulletin of the Astronomical Institute of Czechoslovakia* **39**, 221–236.

Ceplecha, Z. (1993), Interactions of meteoroids with the atmosphere, *in* 'Meteoroids and their parent bodies', Slovakian Academy of Science, pp. 287–294.

Ceplecha, Z., Borovička, J., Elford, W. G., Revelle, D. O., Hawkes, R. L., Porubčan, V. & Šimek, M. (1998), 'Meteor phenomena and bodies', *Space Science Review* **84**, 327–471.

Ceplecha, Z., Spurný, P., Borovička, J. & Keclíková, J. (1993), 'Atmospheric fragmentation of meteoroids', *Astronomy and Astrophysics* **279**, 615–626.

Cervera, M. A. (1996), Meteor observations with a narrow beam VHF radar, PhD thesis, University of Adelaide, Adelaide, Australia.

Cervera, M. A., Elford, W. G. & Steel, D. I. (1993), Meteor observations with the Adelaide 54 MHz radar, *in* 'Meteoroids and their parent bodies', Slovakian Academy of Science, pp. 249–252.

Cervera, M. A., Elford, W. G. & Steel, D. I. (1997), 'A new method for the measurement of meteor speeds: The pre-t0 phase technique', *Radio Science* **32**, 805–916.

Cervera, M. A. & Reid, I. M. (1995), 'Comparison of simultaneous wind measurements using colocated VHF meteor and MF spaced antenna radar systems', *Radio Science* **30**, 1245–1261.

Chebotarev, R. P., Isamutdinov, S. O. & Hajduk, A. (1988), 'Radar observations of Eta Aquarids in 1981-1986 at Dushanbe and Ondřejov', *Bulletin of the Astronomical Institutes of Czechoslovakia* **39**, 82–85.

Clegg, J. A. (1948), 'Determination of meteor radiants by observation of radio echoes from meteor trails', *Phil. Mag.* **39**, 577–594.

Clifton, K. S. (1973), 'Television studies of faint meteors', *Journal of Geophysical Research* **78**, 6511–6521.

Close, S., Hunt, S. M., Minardi, M. J. & McKeen, F. M. (2000), 'Analysis of perseid meteor head echo data collected using the advanced research projects agency long-range tracking and instrumentation radar (altair)', *Radio Science* **35**, 1233–1240.

Cook, A. F. (1954), 'The physical theory of meteors. VI: The light curve', *The Astrophysical Journal* **120**, 572–577.

Coon, R., Dugan, J., Hallgren, D. & Hemenway, C. (1965), 'Balloon top collections of particles from meteor showers', *The Astronomical Journal* **70**, 671.

Cooper, T. (1996), 'A Decade of Visual eta-Aquarid Meteor Obsevations', *WGN, Journal of the International Meteor Organization* **24**, 157–161.

Davies, J. G. & Ellyett, C. D. (1949), 'The diffraction of radio waves trom meteor trails and the measurement of meteor velocities', *Phil. Mag.* **40**, 614–626.

Davies, J. G. & Gill, J. C. (1960), 'Radio echo measurements of the orbits of faint sporadic meteors', *Monthly Notices of the Royal Astronomical Society* **121**, 437–462.

Davis, P. M. (1993), 'Meteoroid impacts as seismic sources on Mars', *Icarus* **105**, 469–478.

Dawson, B. R. (1980), 'The event spacing distribution of extensive air showers', Honours Thesis, University of Adelaide, Adel., Australia.

Denning, W. F. (1899), 'General catalog of the radiant points of meteoric showers and of fireball and shooting stars observed at more than one station.', *Memoirs of the Royal Astronomical Society* **53**, 203.

Djuth, F. T. & Elder, J. H. (1993), 'The VHF meteor radar system used during the Arecibo Initiative in Dynamics of the Atmosphere (AIDA) campaign '89', *Journal of Atmospheric and Terrestrial Physics* **55**, 229–239.

Drummond, J. D. (1982), 'Theoretical meteor radiants of Apollo, Amor and Aten asteroids', *Icarus* **49**, 143–153.

Dyrud, L. P., Oppenheim, M. M. & vom Endt, A. F. (2001), 'The anomalous diffusion of meteor trails', *Geophysical Research Letters* **28**, 2775–2778.

Elford, W. G. (1964), Calculation of the response function of the Harvard Radio Meteor Project Radar System, *in* 'Harvard Radar Meteor Project Report', Vol. 8, Harvard University, Cambridge, Mass.

Elford, W. G. (1999), Thermally induced stresses within ablating meteoroids, *in* 'Proceedings of Meteoroids 1998', Astronomical Institute of the Slovakian Academy of Science, pp. 67–70.

Elford, W. G. (2001a), 'Novel applications of MST radars in meteor studies', *Journal of Atmospheric and Terrestrial Physics* **63**, 143–153.

Elford, W. G. (2001b), Observations of the structure of meteor trails at radio wavelengths using Fresnel holography, *in* 'Proceedings of the Meteoroids 2001 Conference,Kiruna, Sweden', ESA Publications division, ESTEC, Noordwijk, The Netherlands, In Print.

Elford, W. G. & Campbell, L. (2001), Effects of fragmentation on radar observations of meteor trails, *in* 'Proceedings of the Meteoroids 2001 Conference, Kiruna, Sweden', ESA Publications division, ESTEC, Noordwijk, The Netherlands, In Print.

Elford, W. G., Cervera, M. A. & Steel, D. I. (1994), 'Single station identification of radar meteor shower activity: The June Librids in 1992', *Monthly Notices of the Royal Astronomical Society* **270**, 401–408.

Elford, W. G., Cervera, M. A. & Steel, D. I. (1995), 'Meteor velocities: A new look at an old problem', *Earth, Moon and Planets* **68**, 257–266.

Elford, W. G. & Elford, M. T. (1999), The effect of the Earth's magnetic field on the lifetime of radar meteor echoes, *in* 'Proceedings of Meteoroids 1998', Astronomical Institute of the Slovakian Academy of Science, pp. 71–74.

Elford, W. G. & Elford, M. T. (2001), The effective diffusion coefficient of meteor trails above 100 km, *in* 'Proceedings of the Meteoroids 2001 Conference, Kiruna, Sweden', ESA Publications division, ESTEC, Noordwijk, The Netherlands, In Print.

Elford, W. G. & Hawkins, G. S. (1964), Meteor echo rates and the flux of sporadic meteors, *in* 'Harvard Radar Meteor Project Report', Vol. 9, Harvard University, Cambridge, Mass.

Elford, W. G. & Olsson-Steel, D. (1988), 'The height distribution of radio meteors: observations at 6 MHz', *Journal of Atmospheric and Terrestrial Physics* **50**, 811–818.

Elford, W. G. & Taylor, A. D. (1997), 'Measurement of Faraday rotation of radar meteor echoes for the modelling of electron densities in the lower ionosphere', *Journal of Atmospheric and Terrestrial Physics* **59**, 1021–1024.

Ellyett, C. D. & Davies, J. G. (1948), 'Velocity of meteors measured by diffraction of radio waves from trails during formation', *Nature* **161**, 596–597.

Ellyett, C. D. & Keay, C. S. L. (1963), 'Southern Hemisphere meteor rates', *Monthly Notices of the Royal Astronomical Society* **125**, 325–346.

Eshelman, V. R. (1955), 'Theory of radio reflections from electron-ion clouds', *Institute of Radio Engineers Trans. AP* **3**, 32–39.

Evans, J. V. (1966), 'Radar observation of meteor deceleration', *Journal of Geophysical Research* **71**, 171–188.

Evans, J. V. & Brockelman, R. A. (1963), Radio echo studies of meteors at 68 cm, part 1: Sporadic meteors, *in* 'Lincoln Lab Tech Report 332,DDC 439354', Massachusetts Institute of Technology, Lexington, Massachusetts, USA.

Evans, J. V. & Brockelman, R. A. (1964), Radio echo studies of meteors at 68 cm, part 2: Shower meteors, *in* 'Lincoln Lab Tech Report 341,DDC 601518', Massachusetts Institute of Technology, Lexington, Massachusetts, USA.

Fisher, A. A., Hawkes, R. L., Murray, I. S., Campbell, M. D. & LeBlanc, A. G. (2000), 'Are meteoroids really dustballs?', *Planetary and Space Science* **48**, 911–920.

Fleming, D. E. B., Hawkes, R. L. & Jones, J. (1993), Light curves of faint television meteors, *in* 'Meteoroids and their parent bodies', Slovakian Academy of Science, pp. 261–264.

Flynn, G. J. (1989), 'Atmospheric entry heating: A criterion to distinguish between asteroidal and cometary sources of interplanetary dust', *Icarus* **77**, 287–310.

Flynn, G. J. & McKay, D. S. (1990), 'An assessment of the meteoric contribution to the Martian soil', *Journal of Geophysical Research* **95**, 14497–14509.

Gill, J. C. & Davies, J. G. (1956), 'A radio echo method of meteor orbit determination', *Monthly Notices of the Royal Astronomical Society* **116**, 105–113.

Göckel, C. & Jehn, R. (2000), 'Testing cometary ejection models to fit the 1999 Leonids and to predict future showers', *Monthly Notices of the Royal Astronomical Society* **317**, L1–L5.

Grebowsky, J. M. (1981), 'Meteoric ion production near Jupiter', *Journal of Geophysical Research* **86**, 1537–1543.

Greenberg, . (1978), Interstellar dust, *in* 'Cosmic Dust', J A M McDonnell, Ed, p. ????

Hajduk, A. (1973), 'The Structure of the Eta Aquarid Meteor Stream', *Bulletin of the Astronomical Institutes of Czechoslovakia* **24**, 9–13.

Hajduk, A. (1980), The core of the meteor stream associated with Comet Halley, *in* 'IAU Symp. 90: Solid Particles in the Solar System', Vol. 90, pp. 149–152.

Hajduk, A. (1987), Results of observations of the Eta Aquarid and Orionid meteor showers in 1980-1984, *in* 'Middle Atmosphere Program, Volume 25', Vol. 25, pp. 329–335.

Hajduk, A. & Buhagiar, M. (1982), 'Southern and Northern Hemisphere observations of the ETA Aquarid meteor shower in 1969-1978', *Bulletin of the Astronomical Institutes of Czechoslovakia* **33**, 262–266.

Hajduk, A. & Váňa, J. (1985), 'Eta-Aquarids 1969-1977 from Ondřejov Meteor Radar Records', *Contributions of the Astronomical Observatory Skalnate Pleso* **13**, 61–73.

Hajdukova, M., Hajduk, A., Cevolani, G. & Formiggini, C. (1987), 'The p/ Halley Meteor Showers in 1985-1986', *Astronomy and Astrophysics* **187**, 919+.

Hasegawa, I. (1993), Historical records of meteor showers, *in* 'Meteoroids and their parent bodies', Slovakian Academy of Science, pp. 209–223.

Hawkes, R. L. & Jones, J. (1975), 'A quantitative model for the ablation of dustball meteors', *Monthly Notices of the Royal Astronomical Society* **173**, 339–356.

Hawkes, R. L. & Jones, J. (1986), 'Electro-optical meteor observation techniques and results', *Quarterly Journal of the Royal Astronomical Society* **27**, 569–589.

Hawkes, R. L., Jones, J. & Ceplecha, Z. (1984), 'The populations and orbits of double station TV meteors', *Bulletin of the Astronomical Institute of Czechoslovakia* **35**, 46–64.

Hawkes, R. L., Mason, K. I., Fleming, D. E. B. & Stultz, C. T. (1993), Analysis procedures for two station television meteors, *in* 'Proceedings International Meteor Conference 1992', IMO publications, pp. 28–43.

Hawkins, G. S. (1956), 'A radio echo survey of sporadic meteor radiants', *Monthly Notices of the Royal Astronomical Society* **116**, 92–104.

Herlofson, N. (1948), 'The theory of meteor ionization', *Repts. Prog. Phys.* **11**, 444–454.

Hey, J. S., Parsons, S. J. & Stewart, G. S. (1947), 'Radar observations of the Giancobinid meteor shower', *Monthly Notices of the Royal Astronomical Society* **107**, 176–183.

Hey, J. S. & Stewart, G. S. (1947), 'Radar observations of meteors', *Proc. Phys. Soc.* **59**, 858–883.

Hobbs, B. G. (1998), Measurements of tropospheric scatter with a new multibeam multireceiver VHF doppler radar, PhD thesis, University of Adelaide, Adelaide, Australia.

Hocking, W. K. (1999), 'Temperatures using radar-meteor decay times', *Geophysical Research Letters* **26**, 3297–3300.

Hocking, W. K. (2000), 'Real-time meteor entrance speed determinations made with interferometric meteor radars', *Radio Science* **35**, 1205–1220.

Hocking, W. K., Thayaparan, T. & Jones, J. (1997), 'Meteor decay times and their use in determining a diagnostic mesospheric temperature-pressure parameter: methodology and one year of data', *Geophysical Research Letters* **23**, 2977–2980.

Hoppe, J. (1937), 'Die physikalische Vorgänge beim Eindringen meteorischer Körper in die Erdatmosphäre', *Astronomische Nachrichten* **262**, 169–198.

Hughes, D. W. (1978), Meteors, *in* 'Cosmic Dust', J. A. M. McDonnell, Ed, pp. 123–185.

Hughes, D. W. (1987), 'P/Halley dust characteristics - A comparison between Orionid and Eta Aquarid meteor observations and those from the flyby spacecraft', *Astronomy and Astrophysics* **187**, 879–888.

Imoto, S. & Hasegawa, I. (1958), 'Historical records of meteor showers in China, Korea and Japan', *Smithsonian Contributions to Astrophysics* **2**, 131–144.

Ip, W. H. (1990), 'Meteoroid ablation processes in titan's atmosphere', *Nature* **345**, 511–512.

Jacchia, L. G. (1955), 'The physical theory of meteors VIII: fragmentation as cause of the faint meteor anomaly', *The Astrophysical Journal* **121**, 521–527.

Jacchia, L. G. (1958), 'On two parameters used in the physical theory of meteors', *Smithsonian Contributions to Astrophysics* **2**, 181–187.

Jacchia, L. G., Kopal, Z. & Millman, P. M. (1950), 'A photographic study of the Draconid (Giancobinid) meteor shower of 1946', *The Astrophysical Journal* **111**, 104–133.

Jacchia, L. G. & Whipple, F. L. (1961), 'Precision orbits of 413 photographic meteors', *Smithsonian Contributions to Astrophysics* **4**, 97–129.

Janches, D. (2000), Physical and orbital properties of micrometeors observed using the 430 Mhz Arecibo Observatory radar, PhD thesis, The Pennsylvania State University.

Janches, D., Mathews, J. D., Meisel, D. D., Getman, V. S. & Zhou, Q. H. (2000), 'Doppler studies of near antapex UHF radar micrometeors', *Icarus* **143**, 347–353.

Janches, D., Mathews, J. D., Meisel, D. D. & Zhou, Q. H. (2000), 'Micrometeor observations using the Arecibo 430 mhz radar, I. determination of ballistic parameter from measured Doppler velocity and deceleration results', *Icarus* **145**, 53–63.

Jenniskens, P. (1994), 'Meteor stream activity I. The annual streams', *Astronomy and Astrophysics* **287**, 990–1013.

Jenniskens, P. (1996a), 'Meteor stream activity III. Measurement of the first series of Leonid outbursts', *Meteorics and Planetary Science* **31**, 177–184.

Jenniskens, P. (1996b), 'The first in a new series of Leonid outbursts', *Astronomical Society of the Pacific Conference Series* **104**, 117–120.

Jessberger, E. K., Stephan, T., Rost, D., Arndt, P., Maetz, M., Staderman, F. J., Brownlee, D. E., Bradley, J. P. & Kurat, G. (2001), Properties of interplanetary dust: Information from collected samples, *in* 'Interplanetary Dust', E Grün, B A S Gustafson, S F Dermott and H Fechtig, Eds, pp. 253–294.

Jones, J. (1977), 'Meteor radiant distribution using spherical harmonic analysis', *Bulletin of the Astronomical Institute of Czechoslovakia* **28**, 272–277.

Jones, J. & Brown, P. (1993), 'Sporadic meteor radiant distributions: Orbital survey results', *Monthly Notices of the Royal Astronomical Society* **265**, 524–532.

Jones, J. & Brown, P. (1994), 'The radiant distribution of sporadic meteors', *Planetary and Space Science* **42**, 123–126.

Jones, J., Brown, P., Webster, A. R. & Ellis, K. (1994), 'A forwardscatter determination of the radiant distribution of sporadic meteors', *Planetary and Space Science* **42**, 127–134.

Jones, J. & Kaiser, T. R. (1966), 'The effects of thermal radiation, conduction and meteoroid heat capacity on meteoric ablation', *Monthly Notices of the Royal Astronomical Society* **133**, 411–420.

Jones, J., McIntosh, B. A. & Šimek, M. (1990), 'Ozone and the duration of overdense radio meteors', *Journal of Atmospheric and Terrestrial Physics* **52**, 253–258.

Jones, J. & Morton, J. D. (1977), 'The determination of meteor stream radiants from single station observations', *Bulletin of the Astronomical Institute of Czechoslovakia* **28**, 267–272.

Jones, J., Sarma, T. & Ceplecha, Z. (1985), 'Double station observations of 454 TV meteors III: Populations', *Bulletin of the Astronomical Institute of Czechoslovakia* **36**, 116–122.

Jones, J., Webster, A. R. & Hocking, W. K. (1998), 'An improved interferometer design for use with meteor radars', *Radio Science* **33**, 55–65.

Jones, W. (1991), 'Theory of diffusion of meteor trains in the geomagnetic field', *Planetary and Space Science* **39**, 1283–1288.

Jones, W. (1995), 'Theory of the initial radius of meteor trains', *Monthly Notices of the Royal Astronomical Society* **275**, 812–818.

Jones, W. (1997), 'Theoretical and observational determinations of the ionization coefficient of meteors', *Monthly Notices of the Royal Astronomical Society* **288**, 995–1003.

Kaiser, T. R. (1953), 'Radio echo studies of meteor ionization', *Phil. Mag. Suppl.* **2**, 495–544.

Kaiser, T. R. (1960), 'The determination of the incident flux of radio meteors', *Monthly Notices of the Royal Astronomical Society* **121**, 284–298.

Kaiser, T. R. (1961), 'The determination of the incident flux of radio meteors. II Sporadic meteors', *Monthly Notices of the Royal Astronomical Society* **123**, 265–271.

Kaiser, T. R. & Closs, R. L. (1952), 'Theory of radio reflections from meteor trails: I', *Phil. Mag.* **43**, 1–32.

Kaiser, T. R., Pickering, W. M. & Watkins, C. D. (1969), 'Ambipolar diffusion and motion of ion clouds in the Earth's magnetic field', *Planetary and Space Science* **17**, 519–552.

Kascheev, B. L. & Lebedinets, V. N. (1963), 'The initial radius of ionized meteor trails', *Smithsonian Contributions to Astrophysics* **11**, 183–199.

Keay, C. S. L. (1957), 'Meteor radiant determination from high echo-rate observations', *Australian Journal of Physics* **10**, 471–482.

Keay, C. S. L. & Ellyett, C. D. (1969), 'Southern Hemisphere meteor rates', *Memoirs of the Royal Astronomical Society* **75**, 185–232.

Kim, Y., Fox, J. L. & Grebowsky, J. M. (1998), 'Meteoric ions in the ionosphere of Jupiter', *EOS Trans. AGU, Fall Meet. Suppl.* **79(46)**, F671.

Klimov, M. P. & Lyatskaya, A. M. (1988), 'The diffusion of a plasma filament oriented at an angle with the magnetic field', *Geomagnetism and Aeronomy* **28**, 144–146.

Krinov, E. L. & Fonton, S. S. (1954), 'Meteoric dust from the place of the fall of the Sihkote-Aline iron meteorite shower', *Meteoritica* **11**, 122–131.

Lebedinets, V. N. (1991), 'Organic particles of cometary dust in space', *Advances in Space Research* **11**, 149–153.

Lebedinets, V. N., Manochina, A. V. & Shushkova, V. B. (1973), 'Interaction of the lower thermosphere with the solid component of the interplanetary medium', *Planetary and Space Science* **21**, 1317–1332.

LeBlanc, A. G., Murray, I. S., Hawkes, R. L., Worden, S. P., Campbell, M. D., Brown, P., Jenniskens, P., Correll, R. R., Montague, T. & Babcock, D. D. (2000), 'Evidence for transverse spread in Leonid meteors', *Monthly Notices of the Royal Astronomical Society* **313**, L9–L13.

Lindblad, B. A., Ohtsuka, K. & Shirakawa, K. (1994), 'The orbit of the Eta Aquarid meteor stream', *Planetary and Space Science* **42**, 113–116.

Love, S. G. & Brownlee, D. E. (1991), 'Heating and thermal transformation of micrometeoroids entering the earth's atmosphere', *Icarus* **89**, 26–43.

Lovell, A. C. B. (1954), *Meteor Astronomy*, Clarendon Press, Oxford.

Lovell, A. C. B. & Clegg, J. A. (1948), 'Characteristics of radio echoes from meteor trails. I: The intensity of radio reflections and electron density in the trail', *Proc. Phys. Soc.* **60**, 491–498.

Lyons, J. R. (1995), 'Metal ions in the atmosphere of Neptune', *Science* **267**, 648–651.

Lyttinen, E. J. (1999), 'Meteor predictions for the years 1999-2007 with the satellite model of comets', *Meta Res. Bull.* **8**, 33–40.

Mason, B. (1971), *Handbook of elemental abundances in meteorites*, Gordon and Breach, Newark, NJ.

Mason, E. A. & Daniel, E. W. M. (1988), *Transport Properties of Ions in Gases*, Wiley, London.

Massey, H. S. W. & Sida, D. W. (1955), 'Collision processes in meteor trails', *Phil. Mag.* **46**, 190–198.

Mathews, J. D., Meisel, D. D., Hunter, K. P., Getman, V. S. & Zhou, Q. H. (1997), 'Very high resolution studies of micrometeors using Arecibo 430 MHz radar', *Icarus* **126**, 157–169.

Mathews, J. D., Sulzer, M. P., Tepley, C. A., Barnard, R., Fellous, J. L., Glass, M., Massebuf, M., Ganguly, S., Harper, R. M., Behnke, R. A. & Walker, J. C. G. (1981), 'A comparison between Thompson scatter and meteor radar wind measurements in the 65-105 km altitude region at Arecibo', *Planetary and Space Science* **29**, 341–348.

McCrosky, R. E. & Posen, A. (1961), 'Orbital elements of photographic meteors', *Smithsonian Contributions to Astrophysics* **4**, 15–84.

McDonnell, J. A. M., Bride, N. M., beard, R., Bussoletti, E., Colangeli, L., Eberhardt, P., Firth, J. G., Grard, R., Green, S. F., Greenberg, J. M., Grün, E., Hughes, D. W., Keller, H. U., Kissel, J., Lindblad, B. A., Mandeville, J. C., Perry, C. H., Rembor, K., Rickman, H., Schwehm, G. H., Turner, R. F., Wallis, M. K. & Zarnecki, J. C. (1993), 'Dust particle impacts during the Giotto encounter with comet Grigg-Skjellerup', *Nature* **362**, 732–734.

McIntosh, B. A. & Hajduk, A. (1983), 'Comet Halley meteor stream: a new model', *Monthly Notices of the Royal Astronomical Society* **205**, 931–943.

McIntosh, B. A. & Jones, J. (1988), 'The Halley comet meteor stream - Numerical modelling of its dynamic evolution', *Monthly Notices of the Royal Astronomical Society* **235**, 673–693.

McIntosh, R. A. (1935), 'Ephemeris of the radiant-point of the Eta Aquarid meteor stream', *Monthly Notices of the Royal Astronomical Society* **95**, 601.

McKinley, D. W. R. (1951a), 'Variation of meteor echo rates with radar system parameters', *Canadian Journal of Physics* **29**, 403–426.

McKinley, D. W. R. (1951b), 'Meteor velocities determined by radio observations', *The Astrophysical Journal* **113**, 225–267.

McKinley, D. W. R. (1955), 'Radio Determination of the Orbit of the Eta Aquarid Meteors.', *The Astrophysical Journal* **122**, 513+.

McKinley, D. W. R. (1961), *Meteor Science and Engineering*, McGraw Hill, Toronto and New York.

McKinley, D. W. R. & Millman, P. M. (1949), 'Determination of the elements of meteor paths from radar observations', *Canadian J. Res.* **A27**, 53–67.

McNaught, R. H. & Asher, D. J. (1999), 'Leonid dust trails and meteor storms', *WGN* **27**, 85–102.

Molina-Cuberos, G. J., Lammer, H., Stumptner, W., Schwingenschuh, K., Rucker, H. O., López-Moreno, J. J., Rodrigo, R. & Takano, T. (2001), 'Ionospheric layer induced by meteoric ionisation in Titan's atmosphere', *Planetary and Space Science* **49**, 143–153.

Moore, D. S. & McCabe, G. P. (1993), *Introduction to the Practice of Statistics*, W H Freeman and Company, New York.

Morton, J. D. & Jones, J. (1982), 'A method for imaging radio meteor radiant distributions', *Monthly Notices of the Royal Astronomical Society* **198**, 737–746.

Moses, J. I. (1992), 'Meteoroid ablation in Neptune's atmosphere', *Icarus* **99**, 368–383.

Nagoaka, H. (1929), 'Possibility of disturbance of radio transmissions by meteoric showers', *Proceedings of the Imperial Academy of Tokyo* **5**, 233.

Nemtchinov, I. V., Jacobs, C. & Tagliaferri, E. (1997), 'Analysis of satellite observations of large meteoroid impacts', *Annals of the New York Academy of Science* **822**, 303.

Nicol, E. J., MacFarlane, J. & Hawkes, R. L. (1985), 'Residual mass from atmospheric ablation of small meteoroids', *Planetary Space Science* **33**, 315–320.

Nilsson, C. S. (1962), A radio survey of the orbits of meteors, PhD thesis, University of Adelaide, Adelaide, Australia.

Olivier, C. P. (1912), 'The η aquarids meteors', *The Astronomical Journal* **27**, 129–130.

Olsson-Steel, D. I. (1988), 'Identification of meteoroid streams from Apollo asteroids in the radar orbit surveys', *Icarus* **75**, 64–94.

Olsson-Steel, D. I. & Elford, W. G. (1987), 'The height distribution of radio meteors: observations at 2 MHz', *Journal of Atmospheric and Terrestrial Physics* **49**, 243–258.

Öpik, E. J. (1922), 'A statistical method of counting shooting stars and its application to the Perseid shower of 1920', *Publ. Astron. Obs Tartu.* **25**(1).

Öpik, E. J. (1934), 'Result of the Arizona expedition for the study of meteors. III: Velocities of meteors observed visually', *Harvard Circular* (389).

Öpik, E. J. (1937), 'Researches on the physical theory of meteor phenomena. III: Basis of the physical theory of meteor phenomena', *Publ. Astron. Obs. Tartu* **29**(5).

Öpik, E. J. (1955), 'Meteors and the upper atmosphere', *Irish Astronomical Journal* **3**, 165–181.

Öpik, E. J. (1958), *Physics of Meteor Flight*, Interscience, New York.

Oppenheim, M. M., vom Endt, A. F. & Dyrud, L. P. (2000), 'Electrodynamics of meteor trail evolution in the equatorial e-region ionosphere', *Geophysical Research Letters* **27**, 3173–3176.

Pecina, P. & Ceplecha, Z. (1983), 'New aspects in single-body meteor physics', *Bulletin of the Astronomical Institute of Czechoslovakia* **34**, 102–121.

Pecina, P. & Ceplecha, Z. (1984), 'Importance of atmospheric models for interpretations fo photographic fireball data', *Bulletin of the Astronomical Institute of Czechoslovakia* **35**, 120–123.

Pellinen-Wannberg, A. & Wannberg, G. (1994), 'Meteor observations with the European incoherent scatter UHF radar', *Journal of Geophysical Research* **99**, 11379–11390.

Peregudov, F. I. (1958), 'On the effect of meteor velocities on the hour number in radio-echo detection of meteors', *Soviet Astronomy* **2**, 833–838.

Pesnell, W. D. & Grebowsky, J. (2000), 'Meteoric magnesium ions in the Martian atmosphere', *Journal of Geophysical Research* **105**, 1695–1707.

Pettengill, G. H. (1962), 'A new technique for investigation of meteor echoes at UHF', *Journal of Geophysical Research* **67**, 409–411.

Pettengill, G. H. & Pineo, V. C. (1960), A preliminary investigation of meteor echoes at UHF, *in* 'Lincoln Lab.,DDC 235669, H-67', Massachusetts Institute of Technology, Lexington, Massachusetts, USA.

Pierce, J. A. (1938), 'Abnormal ionisation in the E-region of the ionosphere', *Proceedings of the Institute of Radio Engineers* **26**, 892–902.

Poole, L. M. G. & Roux, D. G. (1989), 'Meteor radiant mapping with an all-sky radar', *Monthly Notices of the Royal Astronomical Society* **236**, 645–652.

Poulter, E. M. & Baggaley, W. J. (1977), 'Radiowave scattering from meteoric ionisation', *Journal of Atmospheric and Terrestrial Physics* **39**, 757–768.

Poulter, E. M. & Baggaley, W. J. (1978), 'The application of radio-wave scattering theory to radio-meteor observations', *Planetary and Space Science* **26**, 969–977.

Reid, G. C. (1983), 'The influence of electric field on radar measurements of winds in the upper atmosphere', *Radio Science* **18**, 1028–1034.

Rendtel, J. (1997), 'The eta-Aquarid Meteor Shower in 1997', *WGN, Journal of the International Meteor Organization* **25**, 153–156.

ReVelle, D. O. (1979), 'A quasi-simple ablation model for large meteorite entry: Theory versus observations', *Journal of Atmospheric and Terrestrial Physics* **41**, 453–473.

Robertson, M. C. & Hawkes, R. L. (1992), Wake in faint television meteors, *in* 'Asteroids Comets Meteors 1992', Lunar and Planetary institute, Houston, TX, pp. 517–520.

Robson, R. E. (2001), 'Dispersion of meteor trails in the geomagnetic field', *Physical Review E* **63**, 026404.

Sarma, T. & Jones, J. (1985), 'Double station observations of 454 TV meteors', *Bulletin of the Astronomical Institute of Czechoslovakia* **36**, 9–24.

Schafer, J. P. & Goodall, W. M. (1932), 'Observation of the Kennelly-Heaviside layer heights during the Leonid meteor shower of Nov. 1931', *Proceedings of the Institute of Radio Engineers* **20**, 1941–1945.

Schwieters, J., Cramer, H. G., Heller, T., Jürgens, U., Niehuis, E., Zehnpfenning, J. & Benninghoven, A. (1991), 'High mass resolution surface imaging with a time of flight secondary ion mass spectroscopy scanning microprobe', *Journal of Vacuum Science Technology* **A9**, 2864–2871.

Sekanina, Z. (1973*a*), 'Statistical model of meteor stream III', *Icarus* **18**, 253–284.

Sekanina, Z. (1973*b*), 'Statistical model of meteor stream IV', *Icarus* **27**, 265–321.

Shadbolt, L. & Hawkes, R. L. (1995), 'Absence of wake in faint television meteors', *Earth, Moon and Planets* **68**, 493–502.

Shafrir, U. (1967), 'The effective braking height for small interplanetary particles in the Martian upper atmosphere', *Icarus* **7**, 100–104.

Shigeno, Y., Toda, M. & Shioi, H. (1997), 'Double-Station Observations of the eta-Aquarids', *WGN, Journal of the International Meteor Organization* **25**, 217–221.

Šimek, M. (1966), 'The influence of diffusion on the radio determination of meteor velocities', *Bulletin of the Astronomical Institute of Czechoslovakia* **17**, 354–359.

Simonenko, A. N. (1968), 'The behavior of small particles detached from a meteoroid', *Soviet Astronomy* **12**, 341–348.

Singer, W., Molau, S., Rendtel, J., Asher, D. J., Mitchell, N. J. & von Zahn, U. (2000), 'The leonid 1999 meteor storm: Verification of rapid activity variations by observations at three sites', *Monthly Notices of the Royal Astronomical Society* **318**, L25–L29.

Skellett, A. M. (1935), 'The ionizing effects of meteors', *Proceedings of the Institute of Radio Engineers* **23**, 132–149.

Sorasio, G., Mendis, D. A. & Rosenberg, M. (2001), 'The role of thermionic emission in meteor physics', *Planetary and Space Science* **49**, 1257–1264.

Steel, D. I. (1995), *Rogue Asteroids and Doomsday Comets*, John Wiley and Sons Inc, New York.

Steel, D. I. (1998), 'The Leonids meteors: compositions and consequences', *A & G* **39**, 5.24–5.26.

Steel, D. I. & Elford, W. G. (1991), 'The height distribution of radio meteors: Comparison of observations at different frequencies on the basis of standard echo theory', *Journal of Atmospheric and Terrestrial Physics* **53**, 409–417.

Štohl, J. (1983), On the distribution of sporadic meteor orbits, *in* 'Asteroids Comets Meteors', Astron. Obs. University, Upsalla, pp. 419–424.

Štohl, J. (1986), The distribution of sporadic meteor radiants and orbits, *in* 'Asteroids Comets Meteors', Astron. Obs. University, Upsalla, pp. 565–574.

Stubbs, T. J. (1973), 'The measurement of winds in the D-region of the ionosphere by the use of partially reflected radio waves', *Journal of Atmospheric and Terrestrial Physics* **35**, 909–919.

Taylor, A. D. (1995), 'The Harvard Radio Meteor Project velocity distribution reappraised', *Icarus* **116**, 154–155.

Taylor, A. D. (1997), 'Radiant distribution of meteoroids encountering the Earth', *Advances in Space Research* **20**, 1505–1508.

Taylor, A. D., Baggaley, W. J., Bennett, R. G. T. & Steel, D. I. (1994), 'Radar measurements of very high velocity meteors with AMOR', *Planetary and Space Science* **42**, 135–140.

Taylor, A. D., Cervera, M. A., Elford, W. G. & Steel, D. I. (1996), A new technique for radio meteor speed determination: Inter-pulse phase changes from head echoes, *in* 'Proc. IAU Colloq. 150; Physics, Chemistry and Dynamics of Interplanetary Dust', Vol. 104, Astronomical Society of the Pacific Conference Series, pp. 75–78.

Taylor, A. D. & Elford, W. G. (1998), 'Meteoroid orbital element distributions at 1 AU deduced from the Harvard Radio Meteor Project observations', *Earth, Planets and Space* **50**, 569–575.

Thomas, R. M. (1989), 'Detection by HF radar of the Eta Aquarid meteor shower', *Planetary and Space Science* **37**, 837–846.

Thomas, R. M., Whitlam, P. S. & Elford, W. G. (1988), 'Response of high frequency radar to meteor backscatter', *Journal of Atmospheric and Terrestrial Physics* **50**, 703–724.

Tocher, K. D. (1963), *The Art of Simulation*, English University Press, London.

Verniani, F. (1965), 'On luminous efficiency of meteors', *Smithsonian Contributions to Astrophysics* **8**, 141–171.

Verniani, F. (1969), 'Structure and fragmentation of meteoroids', *Space Science Review* **10**, 230–261.

Verniani, F. (1973), 'An analysis of the physical parameters of 5759 faint radio meteors', *Journal of Geophysical Research* **78**, 8429–8462.

Vincent, R. A., Dullaway, S., MacKinnon, A., Reid, I. M. & Zink, F. (1998), 'A VHF boundary layer radar: First results', *Radio Science* **33**(4), 845–860.

Vincent., R. A., May, P. T., Hocking, W. K., Elford, W. G., Candy, B. H. & Briggs, B. H. (1987), 'First results with the Adelaide VHF radar: Spaced antenna studies of tropospheric winds', *Journal of Atmospheric and Terrestrial Physics* **49**, 353–366.

Vincent, R. A., Reid, I. M., Holdsworth, D. A. & Cervera, M. A. (1994), Spaced antenna wind measurments: the effects of signal saturation, *in* 'Wind observations in the middle atmosphere', CNES-HQ, Paris.

Weiss, A. A. (1955), 'Radio observations of meteors in the southern hemisphere', *Australian Journal of Physics* **8**, 148–166.

Weiss, A. A. (1957), 'Meteor activity in the Southern Hemisphere', *Australian Journal of Physics* **10**, 299–309.

Weiss, A. A. (1961), 'The distribution of meteor masses for sporadic meteors and three showers', *Australian Journal of Physics* **14**, 102–119.

Wheeler, H. A. (1956), 'A vertical antenna made of transposed sections of coaxial cable', *IRE Convention Record* **4**, 160–164.

Whipple, F. L. (1938), 'Photographic meteor studies I', *Proc. Amer. Phil. Soc.* **79**, 499–548.

Whipple, F. L. (1943), 'Meteors and the Earth's upper atmosphere', *Review of Modern Physics* **15**, 246–264.

Whipple, F. L. (1947), 'Photographic meteor studies. IV: the Geminid meteor shower', *Proc. Amer. Phil. Soc.* **91**, 189–200.

Whipple, F. L. (1949), 'The Harvard photographic meteor program', *Sky and Telescope* **8**(4).

Whipple, F. L. (1955), 'The physical theory of meteors. VII: On meteor luminosity and ionisation', *The Astrophysical Journal* **121**, 241–249.

Whipple, F. L. & Hughes, D. W. (1955), On the velocities and orbits of meteors, fireballs and meteorites, *in* 'Meteors', T R Kaiser, Ed, Pergamon Press, London, pp. 149–156.

Williams, I. P. (1993), The dynamics of meteoroid streams, *in* 'Meteoroids and their parent bodies', Slovakian Academy of Science, pp. 31–40.

Zhou, Q., Tepley, C. A. & Sulzer, M. P. (1995), 'Meteor observations by the Arecibo 430 MHz coherent scatter radar. I. detection, statistics and interpretation', *Journal of Atmospheric and Terrestrial Physics* **57**, 412–431.